

Quantifying Groundwater Recharge During Dynamic  
Seasonality in Cold Climates

by

Ehsan Pasha

A thesis  
presented to the University of Waterloo  
in fulfillment of the  
thesis requirement for the degree of  
Masters of Science  
in  
Earth Sciences

Waterloo, Ontario, Canada, 2018

©Ehsan Pasha 2018

## **AUTHOR'S DECLARATION**

I hereby declare that I am the sole author of this thesis. This is a true copy of the thesis including any final revisions, as accepted by my examiners.

I understand that my thesis may be made electronically available to the public.

## Abstract

Estimating groundwater recharge in cold climates during periods of dynamic seasonality such as winter melt periods and spring freshets is challenging due to subsurface heterogeneities and the complexity of vadose zone processes under partially frozen conditions. In order to obtain robust recharge estimates, numerical models simulating these complex processes need to be based on reliable parameter estimates and closely calibrated to field observations. This study focuses on quantifying recharge under an ephemeral stream that occasionally develops in the vicinity of a municipal well field during winter melts and spring freshets at a site in southern Ontario. Temperature and moisture content profiles in the vadose zone were obtained during the 2015 spring melt at three different locations (Stations), using a variety of hydrogeological instruments. Temperature thermistors were installed at 15-30 cm spacings from near ground surface to the depth of the water table in order to monitor transient heat migration during periods of rapid recharge. Similarly, transient soil water content data were collected through the vadose zone at each site with a neutron probe. Water table fluctuations were monitored both directly at the study Stations as well as in a network of monitoring wells located around the Site, and where applicable the water table fluctuation method was used to estimate localized recharge. A transducer was installed at the ground surface near a study station directly in the path of the ephemeral stream to monitor surface water levels. Relevant meteorological data such as air temperature and precipitation was collected at a meteorological station installed in close vicinity of the study site during previous studies at the site.

These combined data sets were used to document and quantify groundwater recharge magnitude and duration during the spring melt event and also provided the boundary conditions for the numerical model (Hydrus 1D) and allowed for its calibration and validation. Numerical models were developed at three stations to simulate water flow and heat transport in partially saturated media with transient boundary conditions based on the site-specific soil stratigraphy. Hydraulic and heat parameters were specified based on a combination of site-specific studies and literature values.

The cumulative infiltration estimates from the modelling exercise calculated in the Hydrus 1D package through water balance computations, showed a high variability in infiltration estimates at the three stations, demonstrating the extent of spatially variable recharge. Regions of rapid infiltration were observed at the site, as well as steep temperature gradients, which were used to help quantify recharge dynamics. The temperature and moisture content data provided support of surface water, groundwater interaction within event-based time periods predicted by the numerical models. The cumulative infiltration estimates at two of the stations over the brief spring melt period was higher than the average annual infiltration in the region, with one station being almost twice that amount (72 cm over 3 days), indicating that a significant pulse of water can infiltrate under relatively cold conditions in a very short period of time. Based on the subsurface temperature data, the transient nature of the frost layer appears to influence the timing of the recharge event and is therefore critical in accurate estimates of recharge under these cold climate conditions. Furthermore, Christie et al., 2009 found that surface water samples from the ephemeral stream at the study site had high concentrations of microbial indicator species, and therefore the intense recharge phenomena observed at the site has significant implications to groundwater vulnerability. An estimate of the total volume of recharge that can occur in the vicinity of the study site under transient conditions shows that a volume of water equal to the amount pumped per day (1 million Imperial gallons) by one of the downstream municipal wells can infiltrate within the brief spring melt period. The results of this study are important in managing the sustainability of groundwater resources from surface contaminants such as pathogens and for informing source water protection strategies in response to dynamic seasonality.

## **Acknowledgements**

I'd like to thank my supervisor Dr. David Rudolph for the opportunity and freedom to work on a challenging project that was relevant to my broader interests. I am grateful for your guidance, both technical and personal, during this experience and your encouragement through the obstacles and challenges. I have learned about more than just physical hydrogeology during this experience, for which you deserve significant credit.

I extend my thanks to my committee members Dr. Emil Frind and Dr. Neil Thomson, for their technical support over the course of the study and for holding me to their high standards. I'd also like to thank Dr. Brewster Conant for his help in the field study and in understanding the nuances of thermal transport. I owe a huge thanks to Paul Johnson and Robert Ingleton for their invaluable support and guidance throughout the field component of the study. Thank you both for your patience and concern, and for being friends and mentors. I'd also like to thank Sue Fischer for all of her help throughout the program, from admission to graduation you have been an ever present form of support.

I owe an infinite gratitude to my parents for supporting my decisions and academic pursuits, I couldn't have done this without you and am grateful for having you on my side. My sisters, thank you for setting the high standards to which I strive, for reassuring me on my goals and supporting me through my laboured pursuit of them. Finally, I'd like to thank my friends for being with me through the highs and lows of this endeavor.

## Table of Contents

AUTHOR'S DECLARATION.....	ii
Abstract.....	iii
Acknowledgements.....	v
List of Tables .....	viii
List of Figures.....	ix
1.0 Introduction.....	1
1.1 Research objectives.....	1
2.0 Background Section:.....	3
2.1 Groundwater Recharge Beneath Ephemeral Surface Water Bodies .....	3
2.2 Field-based Methods of Estimating Groundwater Recharge .....	3
2.3 Study Site Description and Previous Work.....	6
3.0 Methodology .....	11
3.1 Field Site characterization.....	11
3.2 Field Instrumentation .....	12
3.2.1 Heat monitoring instrumentation .....	13
3.2.2 Groundwater monitoring wells .....	13
3.2.3 Neutron Probe Access Tubes and TDR Installations .....	14
3.2.4 Pressure transducer network in the wells and surface water.....	14
3.2.5 Relevant Meteorology Data from the MET Station.....	15
3.3 Numerical Modelling tool.....	15
3.3.1 Hydraulic parameters .....	15
3.3.2 Heat Transport Parameters.....	16
3.3.3 Simulation Approach .....	17
3.3.4 Calibration.....	17
3.4 Recharge Estimates .....	18
3.4.1 Numerical Modelling .....	18
3.4.1 Water Table Fluctuation Method .....	18
4.0 Results and Discussion .....	19
4.1 Site characterization.....	19
4.2 Transient Meteorological and Subsurface Data .....	21
4.2.1 Climate Data and Formation of Ephemeral Stream .....	21
4.2.2 Hydraulic Head Data.....	24
4.2.3 Soil Water Content Data .....	26
4.2.4 Temperature Data.....	27
4.3 Numerical model (Hydrus 1D) .....	30

4.3.1 Transient Flow Simulations at Station 4 .....	30
4.3.2 Modeling Results for Station 3 and 5.....	37
4.4 Recharge Estimates .....	39
4.4.1 Water Table Fluctuation Method .....	39
4.4.2 Cumulative Infiltration Estimates from Numerical Modelling .....	40
4.4.3 Total Volume of Recharge at Study Site.....	41
5.0 Conclusions.....	45
References.....	47
Appendices.....	55
Appendix A: Soil Cores .....	56
Appendix B: Neutron Probe Calibration (Bekeris, 2007).....	62
Appendix C: Grain Size Distribution (Missori, 2015).....	68
Appendix D: Permeameter Tests (Missori, 2015) .....	95
Appendix E: Survey Data .....	97
Appendix F: Geochemistry Data (Christie, 2009) .....	117
Appendix G: Temperature Thermister Casing Design (Brook, 2012).....	119
Appendix H: Monitoring Well Details.....	121
Appendix I: Water flow equations (HYDRUS 1D Manual Chapter 7, Simunek et. al, 2013) .....	123
Appendix J: Temperature instrumentation calibration.....	133
Appendix K: Soil Moisture Content Data (Neutron Probe).....	135
Appendix L: Hydrus 1D parameters .....	138
Appendix M: Numerical Models Profile Discretization .....	140

## List of Tables

Table 1: Combined values for range of hydraulic parameters used for initial conditions simulation in Hydrus.....	31
Table 2: Hydraulic Parameters developed from trial and error variations of initial parameters used in Transient simulation .....	34



## List of Figures

Figure 1: Location of study site in Southern Ontario (adapted from Brook, 2012) .....	6
Figure 2: Topography and drainage at Study Site (Oxford County GIS, 2015).....	7
Figure 3: Cross section of hydrogeological setting through glacial outwash channel (Koch, 2009).....	8
Figure 4: Site pictures of ephemeral stream .....	9
Figure 5: Site location for detailed investigations .....	10
Figure 6: Location of topographic transect and drilling program.....	12
Figure 7: Location of regional monitoring wells used to monitor groundwater levels in the vicinity of the field stations located along the path of the ephemeral stream .....	14
Instrumentation network at each of the study Stations.....	15
Figure 8: Topographic survey cross sections. locations are shown on Figure 8 .....	19
Figure 9: Topographic contour map within study area based on the survey transect data.....	20
Figure 10: Geological Cross Section based on sediment core data .....	21
Figure 11: Daily cumulative precipitation and average daily air temperature .....	22
Figure 12: Picture of Snow Pack, March 9th, 2015 .....	23
Figure 13: Surface Water Pressure Head and Average daily air temperature (MET Station) during March 2015 .....	24
Figure 14: Picture of ephemeral stream (looking South of Curry Road) on March 17th, 2015.....	24
Figure 15: Average Daily Air Temperature and groundwater level fluctuations relative to March 1st levels in monitoring wells in the vicinity of the study site.....	25
Figure 16: Water Table fluctuations over the spring melt period at Station 3, 4 and .....	26
Figure 17: Moisture content profiles using the Neutron Probe for Core 3, 4 and 5 .....	27
Figure 18: Temperature data (Met Station); air, Station 4; surface water, soil surface and groundwater .....	28
Figure 19: Comparison of Temperature data at Station 3 and 4 measured with string thermistors .....	29
Figure 20: Soil profile used for initial Hydrus1D model domain simulation .....	30
Figure 21: Soil water content initial conditions and hydrostatic pressure head distribution in soil profile for Station 4 .....	32
Figure 22: Time variable boundary conditions used in transient simulation .....	34
Figure 23: Comparison of the simulated soil water content profiles (Sim) at Station 4 with the field data measured with the neutron probe (Obs).....	35
Figure 24: Initial conditions for soil temperature profile at Station 4.....	36
Figure 25: Comparison between simulated and observed soil temperature profiles at Station 4 .....	37
Figure 26: Comparison of the simulated soil water content profiles (Sim) at Station 3 with the field data measured with the neutron probe (NP) .....	38
Figure 27: Comparison of the simulated soil water content profiles (Sim) at Station 5 with the field data measured with the neutron probe (NP) .....	39
Figure 28: Magnitude of groundwater level fluctuation in surrounding unconfined monitoring wells relative to initial levels measure on March 1st.....	40
Figure 29: Cumulative infiltration estimates from numerical methods for Stations 3,4 and 5.....	41
Figure 30: Ephemeral stream dimensions for total recharge estimates .....	42
Figure 32: Picture of field site showing approximate width of ephemeral stream on March 17th, 2015 .	43

## 1.0 Introduction

Groundwater recharge represents a major component of the overall hydrologic cycle in most terrestrial environments. Recharge dynamics are influenced by many factors including surficial soil and subsurface conditions, topography, land use and climatic conditions. As such, its spatial and temporal quantification has proven to be challenging (Dripps and Bradbury, 2010; Fleckenstein et al., 2006; Jyrkama and Sykes, 2007; Cey et al., 1998). Both the timing and magnitude of recharge control annual groundwater storage replenishment and the introduction of surface-sourced contaminants to the subsurface, which in turn dictates sustainable aquifer yields, base flow and the quality of the groundwater resources.

Recharge processes in cold climatic regions such as Canada, the northern United States and northern Europe for example, are influenced by extreme seasonal variability, which include frozen soil conditions, temporary snow cover and highly variable cycles of evapotranspiration. Under these conditions, groundwater recharge is highly transient and seasonally dependent. This is especially evident during the spring melt period. Most of the areas in Canada are covered by glacial drift that vary spatially in both thickness and sediment characteristic. Conventional approaches to evaluating annual average groundwater recharge rates are often based on the monitoring of groundwater level fluctuations, catchment flows and inverse modelling (Batlle-Aguilar and Cook, 2012; Constantz et al., 2001; Healy and Cook, 2002a, 2002b; Nakhaei and Šimůnek, 2014; Twarakavi et al., 2008). Although average annual recharge rates are of interest in considering regional water balances and groundwater resource development, the seasonal variability of the recharge cycle dictates the spatial distribution of recharge flux and the timing of the recharge events. This transient nature of recharge, particularly in cold regions, can be a critical factor in determining the regional availability of the groundwater resource and the vulnerability of aquifer systems and public supply wells.

Identifying and quantifying transient recharge phenomena regionally, such as at the sub-watershed scale, has proven to be challenging due to the high degree of spatial and temporal variability and also as a result of the difficulty in field estimation (Iwata et al., 2010; Sophocleous, 2002; Winter et al., 1998). Numerical modeling tools that either couple or fully integrate surface water hydrology with the groundwater systems are routinely used to estimate regional recharge as the residual component of the water balance through a calibration process (Wiebe et al., 2015; Chung et al., 2010; Finch, 1998; Hornero et al., 2016; Okkonen and Kløve, 2011; Xu and Beekman, 2003). Direct field measurements of event-based recharge that could be used to ground truth the modeling results and identify vulnerable landscape settings, represents the focus of the current study.

### 1.1 Research objectives

This study focussed on quantifying infiltration and subsequent groundwater recharge within the vicinity of an ephemeral stream that develops due to large overland flow over partially frozen soils during spring freshet within glacial drift in southern Ontario during the winter 2015. The ephemeral stream temporarily flows in close proximity to several municipal supply wells. Due to the documented

occurrence of potential contaminants within the runoff waters, including microbial pathogen indicator species such as E-Coli (Christie et. al, 2009), infiltration along the streambed could be a significant source of contamination, thereby threatening the quality of the public supply wells. The occurrence of temporary or ephemeral surface waters is a common phenomenon during spring melt periods in cold regions. The main hypothesis of this work is that significant amounts of recharge flux from the perspective of contaminant loading can occur beneath ephemeral surface water features during the spring freshet. We propose that this type of event-based recharge phenomena may represent a threat to the drinking water quality of near-by public supply wells and should be considered when evaluating the long-term vulnerability of the municipal groundwater supply. The research involves two main components: 1). direct field measurement of infiltration in the vicinity of the ephemeral stream during the spring melt period and 2). numerical analysis of the combined field data sets to quantify the recharge flux.

The key research objectives are

- 1) to field monitor physical parameters such as soil moisture, heat and hydraulic head in the vicinity of the ephemeral stream through an integration of field instrumentation.
- 2) to apply a sophisticated vadose zone model to field data to get reliable estimates of infiltration in the vicinity of the ephemeral stream
- 3) to develop a case for public supply well vulnerability to snowmelt infiltration over agricultural fields which are known to contain pathogens.

The work is presented beginning with a Background section describing the context of the current study and previous investigations characterizing the climatic and geological conditions at the site. The text then describes the methodology employed to address the objectives, which included a more detailed characterization of the site and a description of the installation procedure for various instruments in order to monitor transient climatic and hydrogeological conditions. The methodology section also describes the numerical modelling tool used in the study to analyse the field data and quantify transient infiltration at the site. The study then discusses the results from the field observations and subsequent numerical modelling exercise, including some of the associated challenges. The work concludes with a consideration of the implications of the results on public supply well vulnerability and regional groundwater management.

## **2.0 Background Section:**

### **2.1 Groundwater Recharge Beneath Ephemeral Surface Water Bodies**

Due to the high seasonal variability in climatic conditions in cold regions including most of Canada, northern United States, Scandinavia and Europe, water movement within the main components of the hydrologic cycle is extremely dynamic and variable. This is particularly evident during the spring melt period when significant volumes of stored precipitation in the form of snow are released to the partially frozen terrestrial surface over a short time period (Berthold, 2004). Although the spring freshet is primarily characterized as a major surface runoff event, a significant amount of the melt-waters infiltrate and recharge the subsurface during this time period (Berthold, 2004; Iwata et al., 2010). In some locations, this infiltration period may be the most significant of the entire year (Shentsis and Rosenthal, 2003; Subyani, 2004; Niswonger et al., 2005). The processes controlling the spatial and temporal distribution of recharge during the spring melt and the quantification of its magnitude are poorly understood (Sophocleous, 2002; Winter et al., 1998), yet they may be influential to aquifer replenishment and aquifer/public supply well vulnerability (Frind et al., 2006; Van Der Kamp and Hayashi, 1998).

During the spring melt periods or following very high precipitation events, it is common for local temporary surface water bodies and ephemeral streams to develop as the land surface receives a large volume of surface runoff. As these features represent a concentration of the runoff waters, they may also be associated with locally high rates of recharge while they persist. For example, infiltration from ephemeral stream channels has been identified as an important source of aquifer recharge in arid and semiarid environments (Scanlon et al., 2006; Shanafield et al., 2014; Shanafield and Cook, 2014; Stewart-deaker et al., 2000). Numerous infiltration and recharge investigations have been conducted to quantify the contributions of streambed recharge to the water budget for resource planning (Baskaran et al., 2009; Callegary et al., 2007; Wilson et al., 1980). The majority of these studies of infiltration beneath ephemeral streams have focused on warm, semi-arid regions and often involving controlled infiltration experiments (Batlle-Aguilar and Cook, 2012; Scanlon et al., 2006; Stewart-deaker et al., 2000). Shanafield and Cook (2014), compiled and discussed various ways in which infiltration beneath an ephemeral stream could be quantified in the field, including controlled infiltration experiments, tracer based methods including heat, water table fluctuations and water balance approaches. They note that these approaches can often be misleading when used independently, and the use of numerical models to quantify physical processes by integrating multiple data sets, particularly in the vadose zone, can form an integral part of quantifying water and heat flow beneath ephemeral streams.

### **2.2 Field-based Methods of Estimating Groundwater Recharge**

Field studies of event-based recharge in cold regions are more limited (Iwata et al., 2010). Most reported studies have been based on the use of inverse parameter modelling to estimate recharge incorporating time variable boundary and physical conditions as opposed to direct field measurements (Batlle-Aguilar and Cook, 2012; Constantz et al., 2001; Yeh and Šimůnek, 2002). Although this approach

can provide valuable insight into the dynamic nature of transient recharge, local surface and subsurface heterogeneities are not easily accounted for and may result in significant uncertainties and non-uniqueness in the model estimates limiting the upscaling of the results for regional modelling analysis (Doherty, 2003; Hopmans and Simunek, 1997; Haws, 2004). Field scale studies of local recharge during the spring melt have provided additional critical understanding of these transient phenomena. In cold regions, near-surface soils may freeze during winter months, potentially resulting in conditions of lower hydraulic conductivity at ground surface. The influence of frost on soil permeability will depend on soil water content, grain size distribution and the nature of macroporosity (Flury et al., 1994; Hendrickx and Flury, 2001). During the spring melt, the influence of frost in the soil profile along with low intrinsic infiltration capacity of a portion of the near surface sediments can result in the transient generation of significant overland flow and the temporary collection of surface water in topographic lows (Woo and Winter, 1993). Derby and Knighton (2001), and Iwata et al. (2010), demonstrated that snowmelt water collecting in closed topographic lows can infiltrate fairly rapidly when the underlying soil thaws, providing a large input of groundwater recharge over a relatively short time period. A five-year study conducted by Iwata et al. (2008a), found that thin frozen layers did not impede snowmelt infiltration and a large amount of snowmelt water infiltrated to deeper soil horizons and possibly to the water table during the spring freshet period. Elsewhere, studies have shown that infiltration flux may be reduced as infiltrating melt water refreezes in the shallow soil profile temporarily reducing both the hydraulic conductivity and infiltration rate (Bayard et al., 2005). These studies demonstrate the transient and highly variable nature of spring recharge.

In addition to the formation of local water-filled depressions, ephemeral streams of runoff waters may also temporarily form on the landscape. Under these conditions, melt-water from a potentially large catchment area can focus in interconnected topographic lows resulting in the development of a temporary surface water drainage system. As in the case of the depression focused recharge features, transient and spatially variable groundwater recharge can occur beneath these ephemeral streams (Berthold, 2004; Shanafield and Cook, 2014). The magnitude and distribution of groundwater recharge related to spring melt ephemeral runoff is poorly understood, yet may impact the quality of groundwater resources at the local scale. For example, these ephemeral streams may transport runoff waters containing contaminants derived from the surficial environment over long distances to within close proximity of public supply wells where associated recharge waters may pose a risk to drinking water quality.

Direct field observations of groundwater recharge related to spring melt ephemeral streams are limited and are the focus of the current study. Various methods have been employed to estimate groundwater recharge using different field information and data analysis strategies (Healy and Cook, 2002a; Scanlon et al., 2002; Shanafield and Cook, 2014). Several of these approaches are specifically applicable to estimating event-based recharge and are dependent on the type and availability of the field data. The methods are selected to be appropriate to site-specific conditions and several of the most common approaches are briefly presented below with some example applications.

Where there is a significant contrast between the temperature of the surface water and the local groundwater, temperature is often used as a tracer to assess both the fate and transport of infiltrating

surface water. By monitoring the spatial and temporal changes of surface and soil water temperature with vertical strings of thermistors, groundwater infiltration rates can be estimated through the analysis of the transient temperature profiles with analytical and numerical models (Anderson, 2005; Constantz, 2010, 2002; Constantz et al., 2001; Stonestrom and Constantz, 2003). Infiltration rates can also be quantified by monitoring changes in soil water content through the shallow vadose zone during the course of a recharge event and quantifying changes in soil water storage over time. This approach requires sequential measurement of soil water content in a vertical profile using a neutron probe or other soil water monitoring method such as time domain reflectometry (TDR) and estimating increases in stored soil water by comparing consecutive profiles (Scott et al. 2000; Jackson, 2002; Vereecken et al., 2010). Recharge rates and total volumes are also estimated by monitoring vertical hydraulic gradients through the vadose zone with strings of tensiometers and combining these data with soil characteristic curve information specific to the local site for calculating infiltration based on Darcy's Law over the time period of the recharge event (Belan and Matlock, 1973; Brutsaert, 1982; Allen et. al. 1991; Young et. al., 1996). Where water tables are shallow, this approach is often combined with the direct monitoring of water table level rise beneath the monitoring location coincident with the infiltration event. These data can be used along with an estimate of the specific yield of subsurface material to quantify the recharge rate and total magnitude (Meinzer and Stearns 1929; Rasmussen and Andreasen, 1959; Gerhart, 1986). as described in detail by Healy and Cook (2002).

Although each of the methods mentioned above can provide point estimates of groundwater recharge independently, they are frequently used conjunctively so that more reliable estimations can be made. One approach that has gained increasing popularity has been the use of numerical models to analyze combinations of different data sets to calculate recharge rates and magnitudes (Batlle-Aguilar and Cook, 2012; Okkonen and Kløve, 2011; B R Scanlon et al., 2002; Singh, 1995; Kite, 1995). As an example, HYDRUS-1D, version 4.14 (Šimůnek et al., 2008) is a one dimensional finite element model that can simulate the movement of water, heat and solutes under variably saturated conditions. Amongst a range of capabilities, the model accommodates time-variant boundary conditions and transient flow conditions. By calibrating the model to the combined field measurements of soil water content, soil water tension, temperature and water table levels, and incorporating soil hydraulic properties determined in the laboratory, groundwater recharge rates can be calculated using a water balance approach i.e. the volume of water entering and leaving the model domain or soil profile. Where this approach is feasible, one of the distinct advantages is that by integrating several independent data sets in the overall analysis, some of the uncertainty in the recharge estimation may be reduced (Batlle-Aguilar and Cook, 2012; Constantz, 2010; Lu et al., 2011; Šimůnek et al., 2013; Twarakavi et al., 2008).

It should also be noted that where significant concentration contrasts exist, various geochemical, isotopic and microbial tracers can be used to provide additional insight into the fate and transport of infiltrating surface waters. Concentrations of these various tracers in the infiltrating surface water may be significantly different than those in the soil water and groundwater such that by monitoring their spatial and temporal distribution in the subsurface during an infiltration event can permit the observation of the downward mobility of the surface source water (Athavale and Rangarajan 1988; Sharma, 1985; Flury et al., 1994; Aeby, 1998). In some cases, the tracer information may also be used in

support of inverse modeling to estimate groundwater recharge rates (Liu et al., 2014; Turnadge and Smerdon, 2014; Yeh and Šimůnek, 2002)

### 2.3 Study Site Description and Previous Work

The study site is located near the City of Woodstock in southern Ontario, Canada (Figure 1) within an agricultural landscape. The area is characterized by a thick sequence of glacial drift overlying Silurian-Devonian carbonates and shales. The topography is gently rolling in nature with drumlins and low lying glacial outwash channel features. The ground elevations range from about 300 to 340 metres above sea level (masl) (Figure 2). The glacial overburden consists of a complex intermingling of till units and sand and gravel deposits and the surficial geology ranges from silty, stoney loams to coarse sands and gravels (Wicklund and Richards, 1961; Cowan, 1975; Padusenko, 2001). The region receives fairly uniform precipitation averaging 954 mm annually. The mean monthly temperatures range from -6.3 °C in January to 20.4 °C in July, with an annual average of 7.5 °C (Environment Canada, 2008). Surface water within the study site drains into Cedar Creek, a tributary of the Thames River (Haslauer, 2005) (Figure 2).

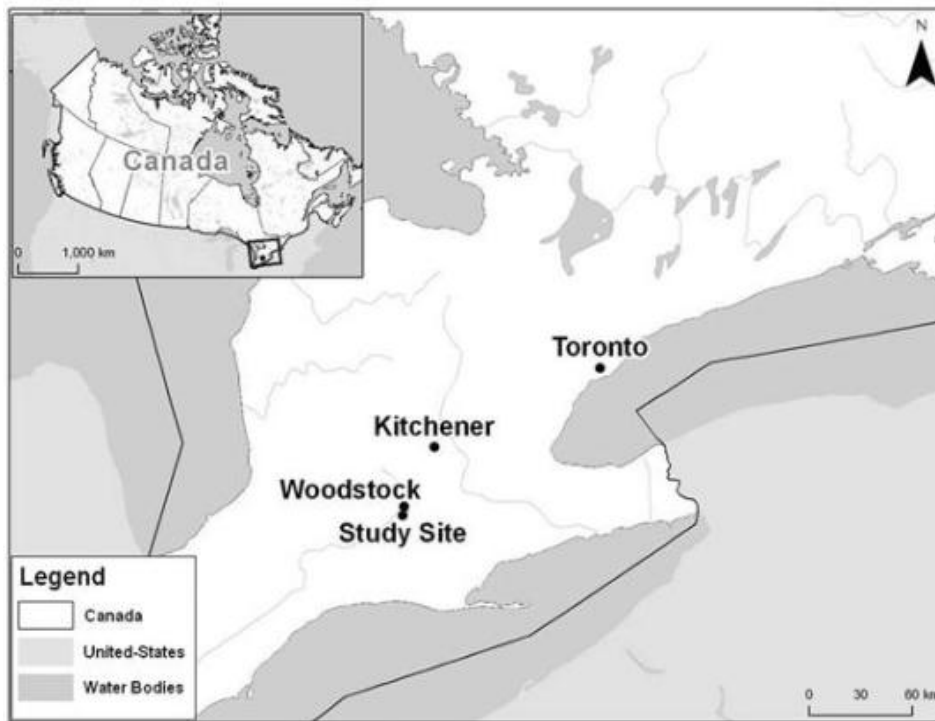
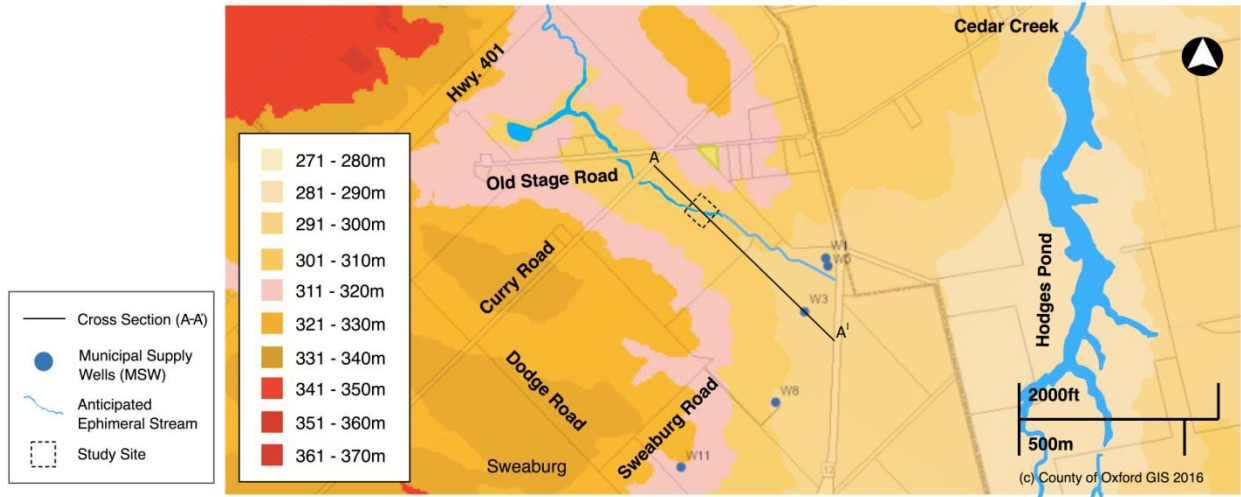


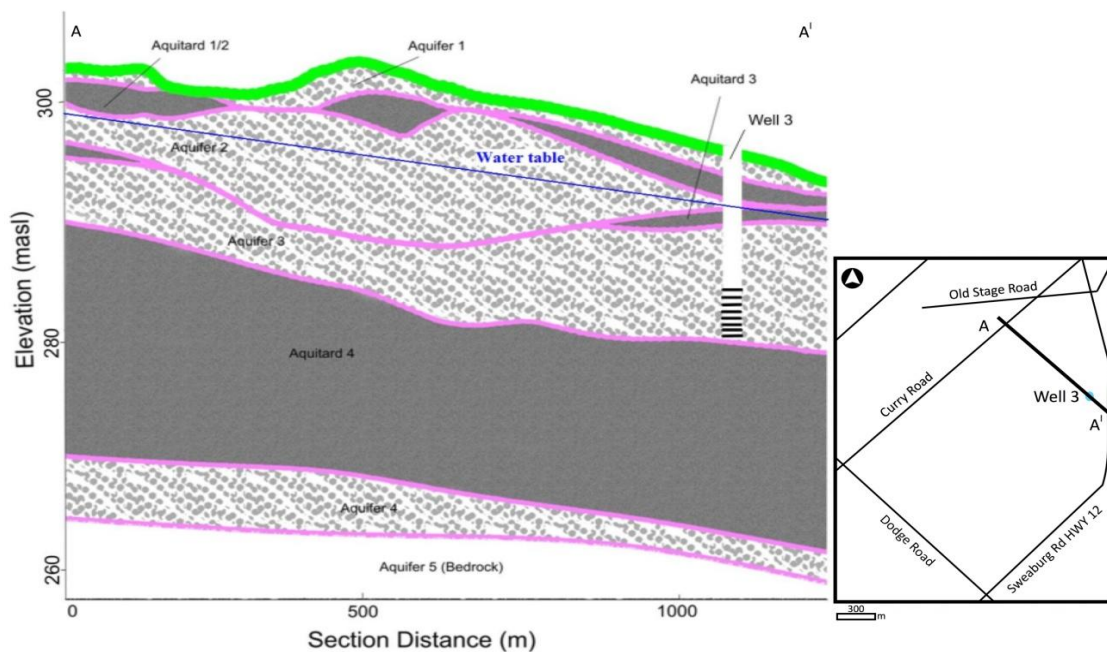
Figure 1: Location of study site in Southern Ontario (adapted from Brook, 2012)



**Figure 2: Topography and drainage at Study Site (Oxford County GIS, 2015)**

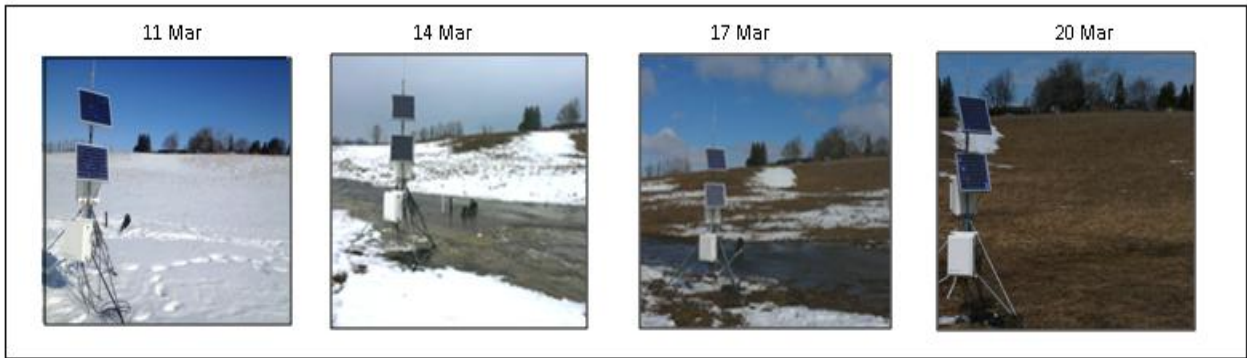
The City of Woodstock relies on aquifer units within the glacial overburden for domestic and industrial water supplies (Haslauer, 2005). The majority of the groundwater supply is derived from the Thornton Well Field situated in a low lying wooded area immediately adjacent to the project study site (Figure 2). Regional hydrogeologic investigations conducted by Padusenko (2001) and Haslauer (2005), presented a conceptual hydrogeologic model of the overburden sequence involving a 4 aquifer system consisting of discontinuous and interconnected sand and gravel units variably separated by till aquitards ranging in thicknesses from less than a metre up to tens of metres, shown below in Figure 3.





**Figure 3: Cross section of hydrogeological setting through glacial outwash channel (Koch, 2009). The location of the cross section is also shown on Figure 2.**

Historical monitoring of water quality in the Thornton public supply wells screened in Aquifer 3, revealed a chronic increase in nitrate concentrations over the course of several decades resulting in several of the wells exceeding the Ontario Drinking Water Guidelines of 10 mg/l in the mid-1990's (Padusenko, 2001; Haslauer, 2005; Rudolph et al., 2015). The source of the elevated nitrate concentrations is believed to be excess nutrients from the surrounding agricultural lands and the progressive increase in nitrate concentrations over time has illustrated the vulnerability of the wells to surface sources of contamination (Bekeris, 2007; Koch, 2006).



**Figure 4: Site pictures of ephemeral stream (2015)**

One unique aspect of the study area is the occasional formation of ephemeral stream features during winter and spring melt periods when sufficient snow coverage is present to contribute significant runoff water as shown in Figure 4. Due to the orientation of the drumlin features, the ephemeral streams tend to flow towards the low lying areas around the Thornton Well Field (Figure 2). One of the ephemeral streams flows over highly permeable surficial sediments near the public supply wells where previous hydrogeologic investigations have suggested direct hydraulic connections exist between the various overburden aquifer units as can be observed in Figure 3 (Brook, 2012; Koch, 2009). This local valley feature is classified as an outwash channel and the subsurface is characterized by thick, permeable sediments with shallow water table conditions. Previous hydrologic monitoring at this site has provided evidence of rapid infiltration in the vicinity of the ephemeral stream during the spring melt period. This was based on the monitoring of transient temperature and hydraulic head within a network of monitoring wells and observing a decrease in groundwater temperature during snow melt events (Brook, 2012; Haslauer, 2005). This suggested the presence of a rapid hydraulic connection between the surface and the water table in this region. Water samples from the ephemeral stream analyzed for microbial indicators by Christie et al. (2009), were found to have high concentrations of Total Coliform and Escherichia Coli. Furthermore, traces of the microbial indicators were detected both within the monitoring well network immediately following the runoff event and were also found in the nearby Thornton Wells several months after the melt event suggesting the surface water may represent a potential source of groundwater contamination and threat to the public supply wells (Christie et al., 2009). This is the area chosen for the current research work (Figure 5).



**Figure 5: Site location for detailed investigations**

Initial work to estimate groundwater recharge beneath the ephemeral stream at this site was conducted by Brook (2012). In this work, vertical profiles of soil water temperature were measured in conjunction with groundwater level monitoring in the vicinity of the ephemeral stream during the spring melt period. Using laboratory estimates of vadose zone hydraulic parameters and Chung and Horton, 1987 heat transport parameters, HYDRUS-1D was used to estimate transient groundwater recharge during the spring melt event. The results of the study by Brooke (2012), indicated that significant recharge is likely occurring beneath the ephemeral stream and that the near surface soil permeability plays a significant role in controlling the magnitude and timing of the recharge processes. The current research builds on the observations of the previous work completed at this site with the objective of quantifying groundwater recharge beneath the ephemeral stream in order to get a better understanding of the spatial distribution of recharge as well as the total volume of recharge that can occur within the capture zone of municipal wells during these dynamic events, in order to evaluate their potential impact on drinking water quality. The study site is located 110 meters south of the Brook (2012) site, in more permeable sediment, and several locations directly in the vicinity of the stream were chosen for further investigations.

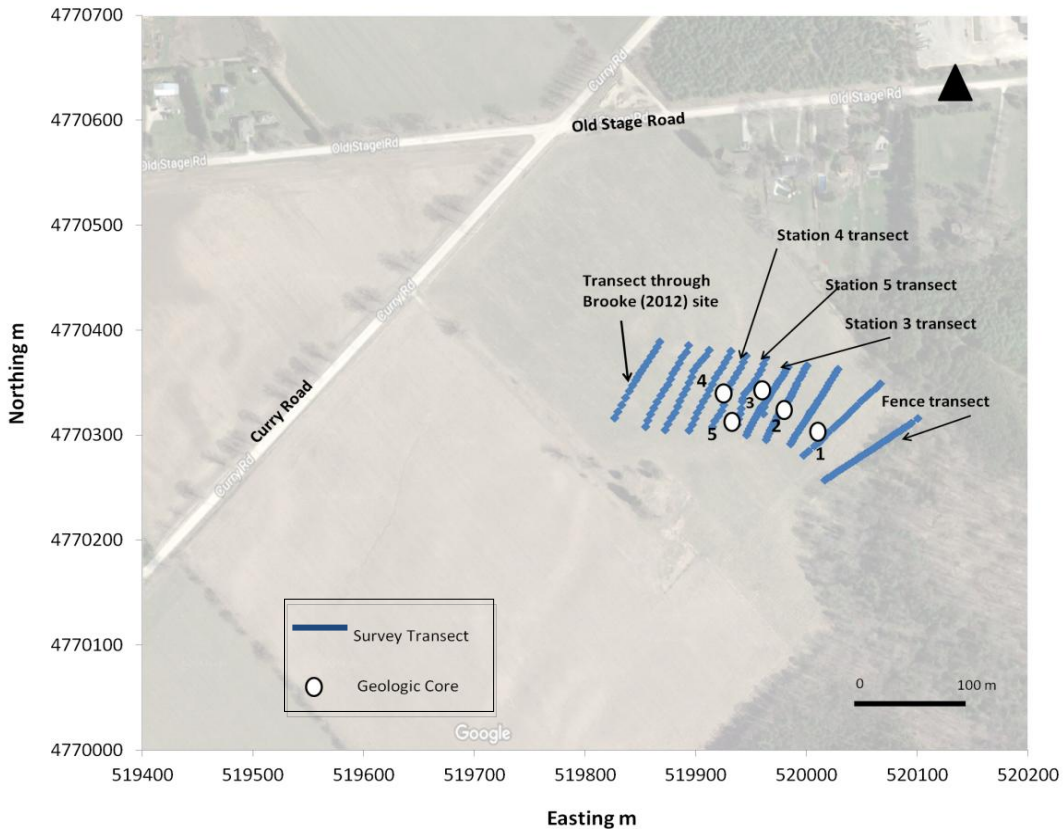
## 3.0 Methodology

### 3.1 Field Site characterization

Several studies at the site provided background information regarding the site characteristics. This included the topography around the study site as well as the general subsurface conditions. These studies were reviewed as a precursor to the field investigations undertaken during the current study between October 2014 and June 2015. In order to determine the probable flow path of seasonal ephemeral streams across the area, a detailed topographic survey was conducted at a much higher resolution in the immediate vicinity of the study site. The survey consisted of a series of transects mapped with a Thales survey system. Transects were surveyed in an east west direction in 15-20 meter intervals starting from the northern edge of the woodlot area (i.e. the northern edge of the subdivision containing the municipal wells shown in Figure 5). Each transect was at least 70 meters in length, and captured several meter fluctuations in topography on both sides of the lowest point in the transect, which also corresponded to the lowest point in the study site.

Once the anticipated drainage channel had been identified based on the lowest elevation contours, determined through the topographic data, a drilling and instrumentation program was conducted. The exploratory drilling and sediment coring campaign was conducted in the vicinity of the anticipated drainage channel location to identify potential monitoring locations. Drilling was performed with a Geoprobe® Model 7720DT direct push drill rig equipped with the Geoprobe sampling system used to advance a 1.5 m long and 5 cm diameter core barrel to collect a continuous geologic core in Lexan tubes. Cores were collected from ground surface to just below the water table (1.5 m to 3 m) at five locations spaced approximately 15-20 meter apart starting from the edge of a low lying wooded area adjacent to the study site and moving upstream through the lowest topographical contour lines. The location of the coring sites is shown in Figure 6 below. The core samples were opened in the field by splitting the plastic core liners down the middle. The basic stratigraphy of these geologic cores was visually logged in the field in order to further inform the drilling program on site. The core samples were then resealed for transport to the laboratory for further analysis. The field data were used to select candidate sites for detailed instrumentation.

A detailed log was completed in the lab on all cores based on the Unified Soil Classification System (ASTM, 2006) using a U.S.A. Standard Test Sieve analysis. Sediment samples from the cores were used for estimating hydraulic parameters through laboratory analysis as discussed below.



**Figure 6: Location of topographic transect and drilling program**

### 3.2 Field Instrumentation

Based on the results of the topographic survey and the core logging, a series of field monitoring locations were selected for detailed instrumentation. These are referenced to the numbered coring locations and are noted on Figure 6. The instrumentation configuration at each of the sites was different depending on the relative location of the Station with respect to its topographical position and the information desired at that site. The subsurface instruments included multilevel temperature thermistors, multilevel groundwater monitoring wells and a series of individual groundwater monitoring wells. The well network provided hydraulic head data and allowed for the collection of groundwater samples. Neutron probe access tubes and TDR probes were installed to track soil water content and a pressure transducer was installed at the surface to monitor the surface water pressure head. A Meteorological Station is located immediately adjacent to the field site and data from this set of instruments were relied on for climatic information through the course of the field investigations. Details regarding the installation of the various instruments and their characteristics are discussed below.

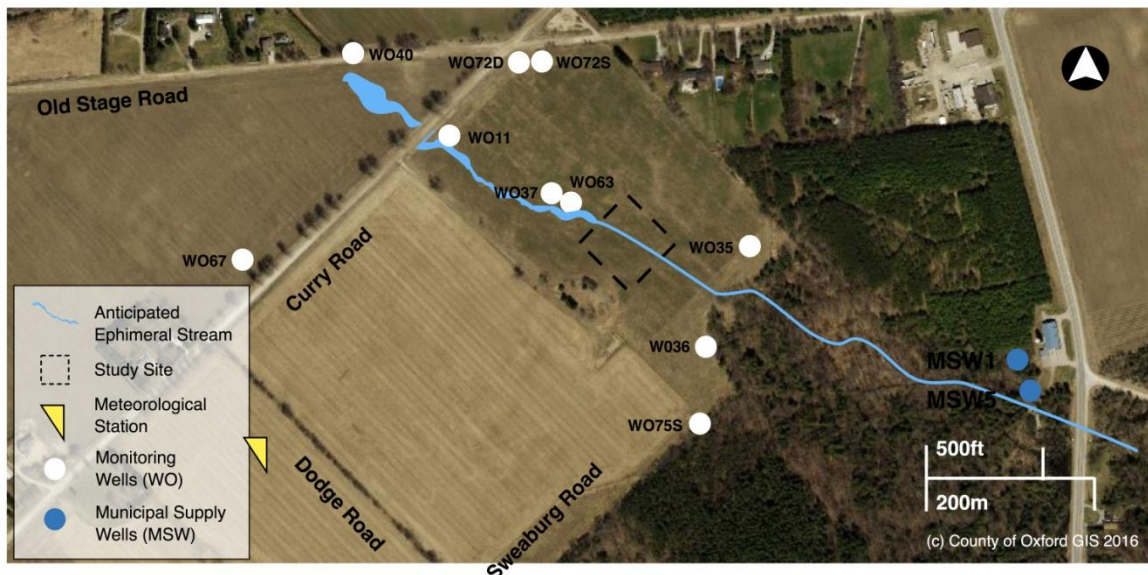
### 3.2.1 Heat monitoring instrumentation

Two different types of instruments were used to monitor thermal conditions in the subsurface. The first system consisted of a vertical string of TidbiT thermistors developed by Onset Computer Corporation, mounted on a PVC pipe at spacings correlating to the various sediment layers observed in the soil cores. The TidbiT v2 Temp logger was used for automatic data collection. The TidbiT thermistor strings logged soil temperature at 10 minute intervals and were installed at Stations 3 and 4. A second set of temperature thermistors developed by Campbell Scientific Incorporation (107B thermistors) was installed at similar depths adjacent to the TidbiT strings to collect backup temperature data. These thermistors required the design of an installation casing which could be inserted in the sediment at specific depths with a small drill rig. The data from the 107B thermistors was used to check the reliability of the readings from the TidbiT thermistors and these data along with details of the 107B thermistor installation is provided in Appendix J. In the present study only the data from the TidbiT thermistors were used for further applications.

### 3.2.2 Groundwater monitoring wells

Multilevel groundwater monitoring wells consisting of bundles of 1.0 cm polyethylene tubes attached to a central 2 cm diameter PVC pipe were installed at three stations (Stations 3, 4 and 5). Each multilevel bundle consisted of 7 monitoring points placed at depth intervals of 25 cm between 1 and 2 meters below ground surface (i.e. at 1, 1.25, 1.5, 1.75 mbgs), and the last 3 at 2.5, 3.5 and 4.5 mbgs respectively. The well depths were selected to permit the monitoring of water table fluctuations during the course of the year and to measure vertical hydraulic gradients during the course of the study. The multilevel wells permitted the sampling of groundwater in the immediate vicinity of the water table thus facilitating the monitoring of changes in groundwater quality during dynamic infiltration events. The multilevel monitoring wells were manually measured because the thin diameter of the wells did not permit the use of conventional pressure transducers.

In addition to the multilevel monitoring wells installed during this study, a network of monitoring wells that had been installed around the study site during previous investigations were also relied upon to monitor water table depth further away from the instrumented stations in order to compare local and regional water table fluctuations. These wells were installed by Haslauer, (2005), Bekeris, (2008) and Brook, (2012) for other investigations at the site. Details regarding the monitoring wells that were used in this study are presented in Appendix H, and their locations with respect to the study site are shown in Figure 7.



**Figure 7: Location of regional monitoring wells used to monitor groundwater levels in the vicinity of the field stations located along the path of the ephemeral stream.**

### 3.2.3 Neutron Probe Access Tubes and TDR Installations

Soil water content measurements were necessary to physically demonstrate infiltration in the field and as input data for the numerical modelling exercise. Soil water content was measured with a model 503 DR Hydroprobe Neutron Moisture Probe (NMP) (CPN International Inc.). To install the neutron probe access tubes at three monitoring stations (Stations 3, 4 and 5), the Geoprobe® Model 7720DT direct push drill rig equipped with an Enviro-Core® sampling system was used to advance a 5-cm (2-in) diameter borehole. A 5-cm (2-in) diameter Schedule 40 PVC riser pipe with a threaded bottom cap was fitted into the borehole. The access tubes were installed to a depth of between 1.2 to 1.6 meters, just above the existing water table levels at each site. The access tubes were installed close to the thermistors and the monitoring well installations to collect moisture content profiles representative of the local conditions in the vicinity of the ephemeral stream. The mechanisms of the site specific calibration used at the field site to convert readings from the neutron probe to moisture content are detailed in Bekeris (2007) and provided in Appendix B. Soil water measurements were collected in 0.10 m intervals along the length of each access tube with the NMP. Measurements using the NMP were taken once a month before and after the spring melt and daily during the week-long spring melt event (March 12th to March 21<sup>st</sup>, 2015).

### 3.2.4 Pressure transducer network in the wells and surface water

Prior to the spring melt, a water pressure, temperature, and electrical conductance recording device (model 3001 LTC Levellogger Junior, Solinst Canada Ltd.) was installed at ground surface at Station 4 beside the neutron access tube. The data collected with this device was used to determine the depth and temperature of the surface water. The data were collected at 15 minutes intervals. Manual

measurements of surface water depth were also taken in order to validate the pressure readings. As with the transducers used in the monitoring wells around the study site, the hydraulic heads recorded by the loggers needed to be barometrically corrected using data from the barologger installed in Well 72-D (See Figure 6 above) which was close to the study site.

### **3.2.5 Relevant Meteorology Data from the MET Station**

A meteorological station equipped with a Campbell Scientific Inc. (CSI) CR23X datalogger was installed on December 9, 2004. It is located approximately 500 meters west of the study site where the topography is flat and there are no nearby trees to obstruct the instrumentation (Figure 6). The station features an array of meteorological sensors measuring: precipitation (including rainfall measurement with a tipping bucket, and snowfall measurement as rainfall equivalent using a snow adapter on the tipping bucket), relative humidity, wind speed and direction, solar radiation, soil heat flux, air temperature and barometric pressure (Bekeris, 2007). The data logger was programmed to collect and record data every 15 or 60 minutes depending on the specific sensor. For the purpose of this study, the meteorological station was used to obtain data on the air temperature, precipitation and barometric pressure which were useful in tracking the parameters controlling melting of the snow pack and consequent factors influencing the development of an ephemeral stream during the spring freshet.

## **3.3 Numerical Modelling tool**

The one-dimensional unsaturated flow package HYDRUS-1D, version 4.17 (Šimůnek et al., 2013) was used to model heat and water flux through the unsaturated zone. It is a finite element model which can simulate the movement of water, heat and solutes under variably saturated conditions. The model accommodates time-variant boundary conditions and transient flow conditions (Šimůnek et al., 2013). For the current application, the water flow and heat transport equations are solved in an integrated fashion for transient simulations. The equations are solved sequentially following the approach of Yeh and Cheng (1999) with the flow equation solved first followed by the heat transport equation. HYDRUS-1D was used to estimate the transient rate and magnitude of groundwater recharge during the course of the spring melt event at different stations.

### **3.3.1 Hydraulic parameters**

As part of the numerical modeling procedure the hydraulic parameter estimates from the following studies were used to constrain the range of parameter estimates used in the model.

#### **3.3.1.1 Unsaturated Hydraulic Parameters**

Values of unsaturated hydraulic parameters for the sediments at the study site were based on 4 previous studies (Wendt, 2005; Bekeris, 2007; Sousa, 2013; Brook, 2012). Wendt (2005) completed laboratory investigations of the grain size distributions and hydraulic properties of various soil types collected from geologic cores obtained in the vicinity of the study stations being considered in the current work. These investigations included sieve and hydrometer analyses for grain size distribution, permeameter tests for saturated hydraulic conductivity, and Tempe cell analyses for soil water retention



data (Bekeris, 2007). The Tempe cell results were used to generate water retention curves and unsaturated hydraulic conductivity parameters were subsequently estimated through the methods of van Genuchten (Van Genuchten, 1991). Bekeris (2007) built on the field investigation completed by Wendt (2005) and used the results of a grain size analysis to determine soil hydraulic characteristics through the use of a subprogram of the Soil-Plant Air-Water (SPAW) model (Saxton, 2002). SPAW estimates hydraulic conductivity and bulk density based on soil texture and also generates soil water potential values at various water contents (Bekeris, 2007). Brook (2012) further expanded on the work done by Bekeris (2007) and used the SPAW generated hydraulic parameters as initial estimates for a numerical model and calibrated these parameters to observed heat and soil water content profiles collected from a location near the study stations.

Sousa (2013) completed a variably saturated, 3-dimensional modeling case study at the Thornton well field to determine travel times in the unsaturated and saturated zones around the public supply wells. For the purpose of the numerical study Sousa (2013) used hydraulic parameters developed using the Rosetta v1.1 model (Schaap et al. 2003) based on the soil stratigraphy of geologic cores from the Thornton well fields study site (Bekeris, 2007; Haslauer, 2005). The Rosetta v1.1 model allows the estimation of van Genuchten parameters using limited textural classes, but also allows for more extensive input data such as bulk density and one or two water retention points (Schaap et. al. 2003).

### ***3.3.1.2 Saturated Hydraulic Parameters***

Missori (2015) completed hydrogeological investigations to characterize the grain size distributions and saturated hydraulic parameters through permeameter tests on core samples taken close to the study stations. The cores were separated into several sub sections based on grain size variations, and a grain size analysis was completed on each of the individual sections using the U.S.A. Standard Test Sieve approach (ASTM E-11 Specification,, W.S. Tyler). The grain size distributions for 26 samples were used to calculate hydraulic conductivity values at approximately 50 cm intervals in each core, through the use of empirical equations adapted in HydrogeoSieveXL (2014). Further to this, Missori (2015) completed falling head permeameter tests on 7 of the samples to compare the hydraulic conductivity values obtained through these analyses to those calculated using grain size distributions. The results of these analyses are provided in detail in Appendix C and D.

### **3.3.2 Heat Transport Parameters**

The heat transport parameters of the subsurface materials used in the study (heat conductance, dispersivity and heat capacity) were taken from literature values for the Chung and Horton (Chung and Horton, 1987) heat transport equation (provided in Appendix I). The equation is utilized by the HYDRUS-1D model for thermal transport and has built-in parameters for 3 different soil textural classes; sand, loam and clay. Heat transport parameters have a much smaller range than hydraulic parameters (Constantz, 2002) and because heat transport analysis was used in the study primarily as a qualitative indicator of infiltration dynamics, these values were considered to be suitable for the purpose of this study.

### 3.3.3 Simulation Approach

The transient soil water, hydraulic head and temperature data sets collected at the monitoring stations were used to provide initial and boundary conditions and calibration targets. As a first step, a model was developed based on the geologic core obtained at one of the study stations (Station 4), with the unsaturated zone being represented as a series of layers with varying properties. The model domain was discretized into 34 equally sized elements of 0.05 m, along a 1.65 meter depth profile. The initial conditions for soil water content and temperature were specified based on those measured in early fall. A zero flux top boundary condition, and a constant soil water content bottom boundary condition for water flow was applied for the initial simulations. The initial time step for the simulation was 1 minute, with a maximum allowable time step of 1 day and the model was run for 100 days to allow for redistribution of the soil moisture profile. This was assumed to represent the initial conditions before the spring melt event. Similarly, specified temperature for the top and bottom heat boundary conditions were used to permit readjustment in the thermal profile based on the specified temperature gradient over the 100 day initial simulation period. The surface temperature specified as the top boundary condition was based on the data obtained from the TidbiT thermistor installed just below the ground surface (0.05 m) for the initial conditions simulation and the bottom temperature boundary condition was based on the data obtained from the TidbiT thermistor at 1.65 mbgs.

The transient simulations were run for a period of 54 days, starting 30 days before the melt event and ending well after the ephemeral stream disappeared. The space and time discretization was similar to the one used in the initial conditions simulation (0.05 m elements and 1 minute time steps). The water flow boundary conditions were specified as variable pressure head/flux top boundary and a variable pressure head bottom boundary condition. Transient surface water depths and groundwater levels were used to inform these boundary conditions. The heat transport boundary conditions were specified based on the transient temperature data collected just below the frost layer at 0.45 mbgs representing the top of the domain, and 1.65 mbgs representing the bottom of the domain. Time variable boundary conditions for both pressure head and heat were derived from the field measured data collected during the recharge event. The boundary conditions were updated every hour over the spring melt period (March 12th-21st) and then every day thereafter till the end of the simulation period. For the time periods where the ephemeral stream was not present, a zero flux top boundary was used for the water flow calculations. The top and bottom temperatures (0.45 cm and 1.65 cm respectively), were specified throughout the simulation period as the heat boundary conditions and the soil temperature profile was allowed to readjust based on these boundary conditions and the thermal transport through the infiltrating surface water pulse.

### 3.3.4 Calibration

The model results of soil water content throughout the profile were compared to field measured data collected during the spring melt event and hydraulic parameters were modified within the specified ranges from the site specific studies to achieve the best possible fit. Due to the insensitivity of thermal parameters, the Chung and Horton (Chung and Horton, 1987) heat parameters provided in the Hydrus

model were considered satisfactory for the purpose of simulating thermal transport and were not varied as calibration parameters.

The total infiltration flux at the upper boundary of the domain was calculated for the entire simulation period to quantify the total groundwater recharge at each of the different stations.

### 3.4 Recharge Estimates

#### 3.4.1 Numerical Modelling

Hydrus 1D uses a mass lumped linear finite elements method for the discretization of the mixed form of the Richards equation, based on the fully implicit discretization of the time derivative and solved with a Picard iterative solution (Šimůnek et al., 2013). Hydrus computes infiltration through water balance computations at defined times for preselected subregions of the flow domain. For the purpose of this study only one subregion was used for mass balance calculations representing infiltration through the entire domain.

The water balance information for each subregion consists of the actual volume of water,  $V$ , in that subregion, and the rate,  $O$  [LT<sup>-1</sup>], of inflow or outflow to or from the subregion (Šimůnek et al., 2013). The equations used for estimating water flow and heat transport in variably saturated porous media (as calculated in Hydrus 1D) are presented in Appendix I and more information regarding the Hydrus 1D variably saturated flow model can be found in Simunek et. al., 2013.

#### 3.4.1 Water Table Fluctuation Method

The water table fluctuation method has been widely used to estimate recharge due to its simplicity and insensitivity to unsaturated zone processes (Healy and Cook, 2002a). The method only requires knowledge of the specific yield and water level fluctuations over time, and recharge is calculated using the following relationship;

$$R = S_y \cdot \frac{dh}{dt} \quad \text{Equation (1)}$$

Where  $S_y$  is the specific yield and  $h$  is the water table height.

The water-table fluctuation method is based on the assumption that the rise in groundwater level in an unconfined aquifer is due to the recharge arriving at the water table (Healy and Cook, 2002a). The method is employed in this study to estimate regional recharge through the water table fluctuation observed in the monitoring wells that are unconfined in the vicinity of the study site. The specific yield estimates for Aquifers 2 and 3, in which the surrounding monitoring wells are screened were obtained from previous studies at the site (Padusenko, 2005; Bekeris, 2007; Haslauer, 2005). The values are calculated based on the difference between the saturated and residual moisture content values measured as part of these previous studies. The method is also used within the study site at Stations 3, 4 and 5, as a comparison to the recharge estimates obtained from the modelling exercise at these stations. This is done in order to evaluate the utility of this more simplistic and common method in estimating infiltration at point locations.

## 4.0 Results and Discussion

The results are presented as a series of interrelated subsections that include the relevant regional scale information collected as part of the current study, the detailed site specific data and results from the local, monitoring stations. The various results are discussed within the individual subsections and where appropriate, correlations are made between the different data sets in support of specific interpretations and observations. Additional numerical analysis of the combined data sets is provided following the presentation of the field results.

### 4.1 Site characterization

Using the data from the topographic survey, a contour plot of the field site was constructed (Figure 9). Based on the data presented in Figure 8 and 9, there is a clear continuous area of lower elevation as noted on Figure 9 where subsequent drilling and instrumentation was focused to track transient recharge phenomena associated with the seasonal formation of an ephemeral stream.

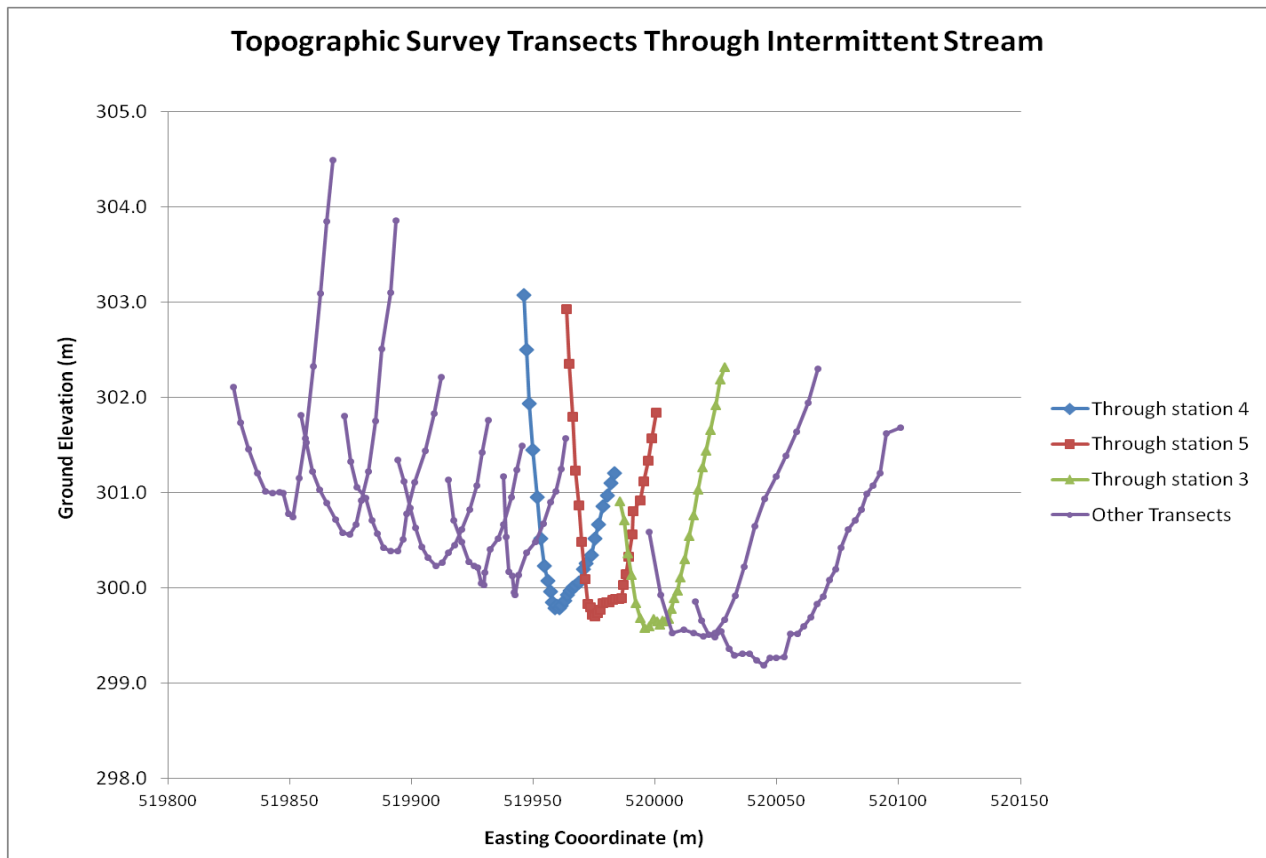
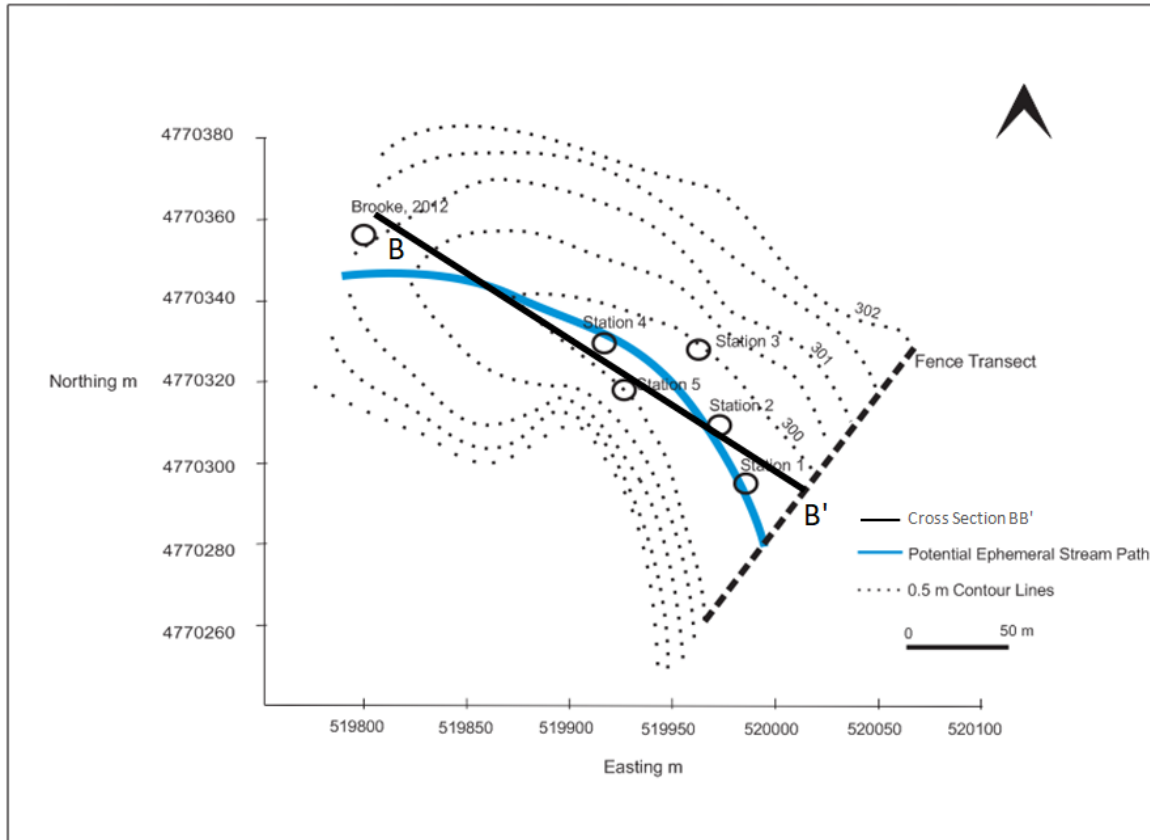
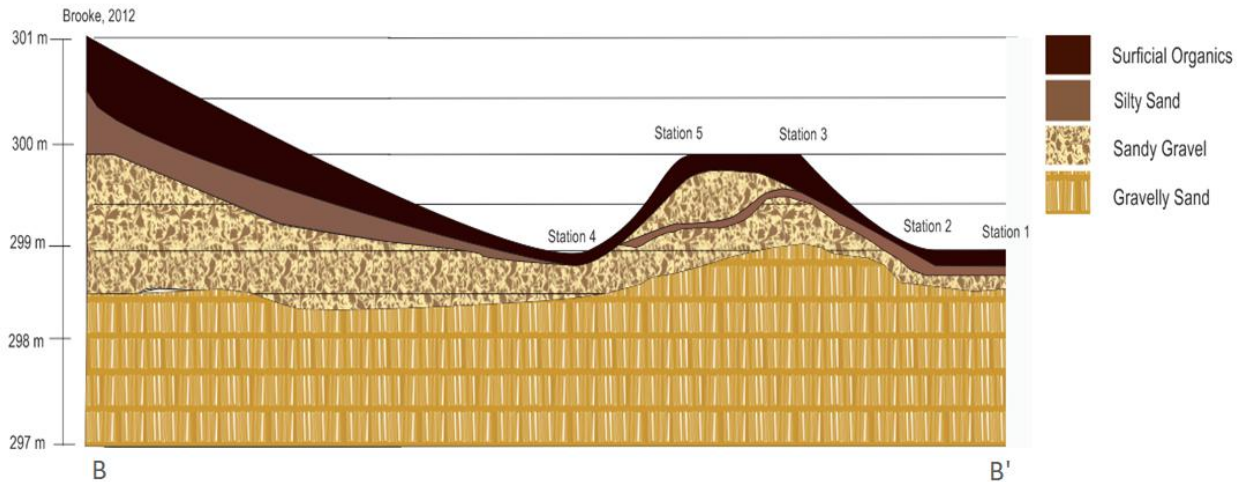


Figure 8: Topographic survey cross sections. Locations are shown on Figure 6



**Figure 9: Topographic contour map within study area based on the survey transect data**

Once the low topographic region was established, a set of 5 subsurface cores (Appendix A) were collected in this area in order to characterize the near-surface sediment type. The locations of the core sites are indicated on Figure 9 and noted as Stations 1 through 5. A cross section of the geologic setting at the study location based on the core information is shown below in Figure 10 with the orientation of the conceptual cross section illustrated on Figure 9. Although the sediments in this area have been documented to be part of a glacial outwash channel (Cowan, 1975) the specific intention of the coring was to locate areas where continuous, relatively permeable material existed throughout the entire profile, suggesting conditions that could lead to significant rates of groundwater recharge. Three of the locations (Stations 3, 4 and 5) were selected for detailed instrumentation and additional descriptions of the material at each site are provided below.



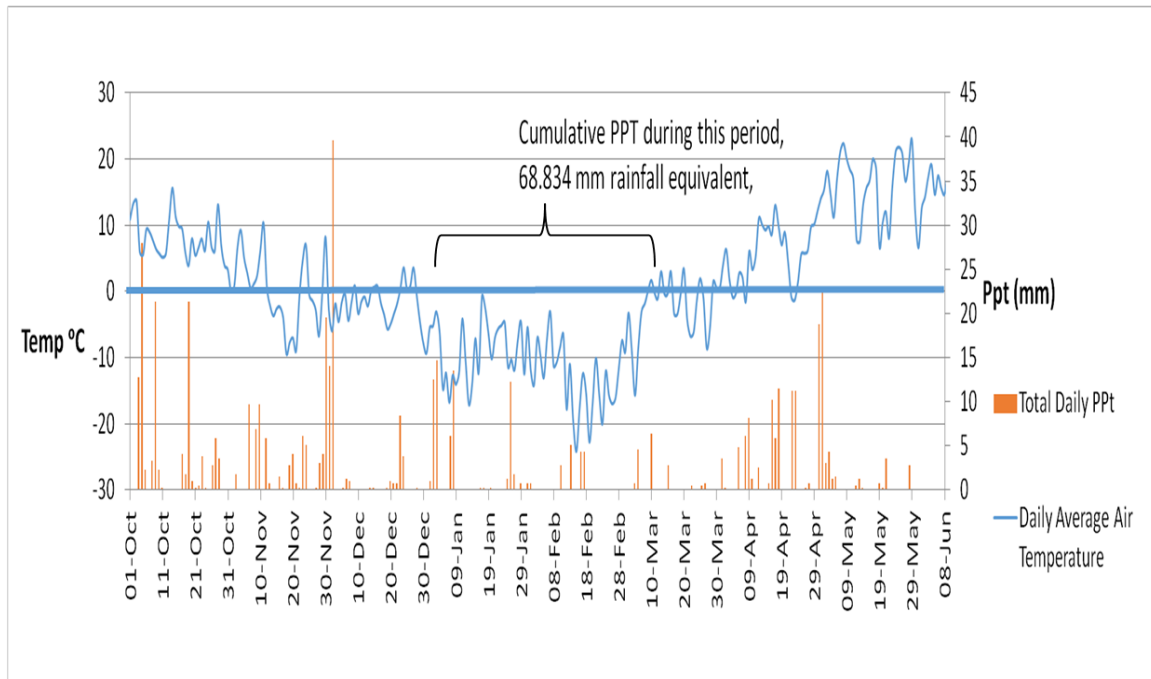
**Figure 10: Geological Cross Section based on sediment core data**

Station 4 location consists of a continuous sequence of fine to medium sand and gravel to a maximum coring depth of 2.5 m underlying a thin (15 cm) layer of silty sand and organic top soil material. Station 3 lies further downstream of Station 4 (Figure 9), and represents a position along the eastern flank of the topographic low. The core collected at Station 3 had a layer of silty sand and minor clay of approximately 20 cm in thickness beneath the organic top soil surface layer which remained close to saturated throughout the study period. These surficial sediments overlay sand and gravel deposits to the maximum coring depth of 3 meters. Station 5 is situated slightly downstream of Station 4 (Figure 9) in what would be anticipated to be the west bank of the topographic low region. The core 5 stratigraphy was similar to that observed at Station 3, with the silty sand layer lying deeper in the geological sequence with a layer of sandy gravel above it. This illustrates the high degree of variability in the surficial sediments within a relatively small area. This may also illustrate the potential for local-scale spatial variability in groundwater recharge. In order to quantify and investigate the spatial variability in groundwater recharge in this local region during an ephemeral flow event, Stations 3, 4 and 5 were instrumented and monitored in detail during the spring melt event in 2015.

## 4.2 Transient Meteorological and Subsurface Data

### 4.2.1 Climate Data and Formation of Ephemeral Stream

The meteorological station located west of the study site (Figure 7) was used to obtain data on the climate conditions over the study period (October 1st, 2014 - June 20<sup>th</sup>, 2015) which included air temperature and precipitation over the study period as shown in Figure 11.



**Figure 11: Daily cumulative precipitation and average daily air temperature**

A heavy precipitation event on November 30th was followed by several weeks of below freezing temperatures. The air temperatures were below zero degrees Celsius consistently after late December and this was considered to be the starting point for the development of the snow pack. After March 10th the air temperatures started to rise and remained above freezing point for approximately a week during which time the snow pack completely melted as seen in Figure 4. After March 20th there was again a few weeks of below 0°C temperature followed by relatively consistent air temperatures above 0°C after April 1<sup>st</sup>, 2015. A total of approximately 7 cm of rainfall equivalent precipitation was recorded at the meteorological station during the period between 30th December and March 10th, where daily average temperatures were below freezing conditions. Manual measurements made of the snow pack on the 2nd, 9th and 12th of March were 44 cm, 52 cm and 49 cm respectively which would represent a precipitation equivalent to snow ratio of 1:7. These manual measurements were taken at the ground surface beside the monitoring well at Station 4 and photographs of the field measurements are shown in Figure 12. Though this is only a point measurement of the snow pack and may not represent the depth over the entire study area it provides an approximation of the surface conditions around the field site prior to the spring melt period.



**Figure 12: Picture of Snow Pack, March 9th, 2015**

Figure 13 shows the air temperature and surface water pressure head measured near Station 4 for March, 2015. Due to the fact that there was snow observed at the site until March 12th, the surface transducer did not provide relevant data with respect to the depth of ephemeral stream before this date. The increase in the average daily air temperature on March 13th, to above zero degrees had an immediate effect on the melting of the snow pack and the formation of the ephemeral stream as manually measurements of the surface water depth data indicate (Figure 13). The ephemeral stream flows for slightly over a week as shown in the pictures from the field site between March 12th and March 20<sup>th</sup> appearing to peak around March 14th, and after March 20th only wet surface conditions exist (Figure 4). The ephemeral stream disappeared completely before the air temperatures dropped below 0°C in late March. The surface water pressure transducer data reflects these field observations and were calibrated to manual measurements of the stream taken at Station 4 during this period as described in the methods section.



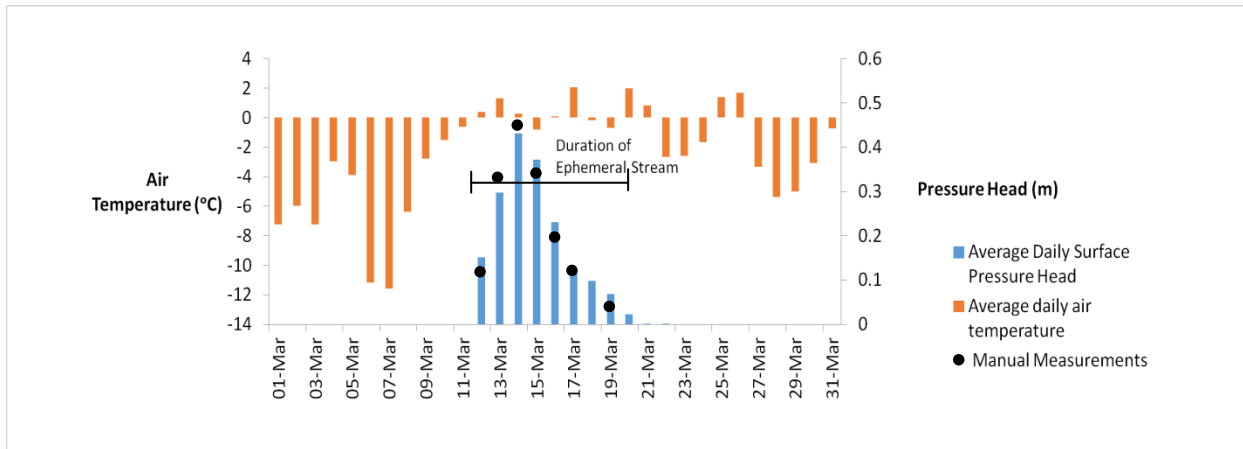


Figure 13: Surface Water Pressure Head and Average daily air temperature (MET Station) during March 2015

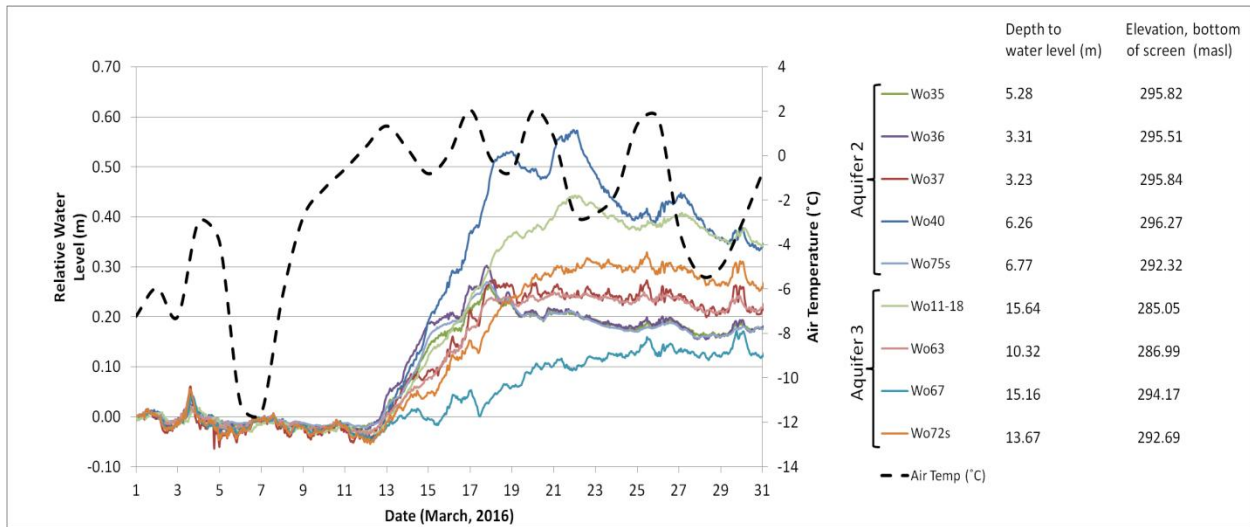


Figure 14: Picture of ephemeral stream (looking south across the field site) on March 17th, 2015

4.2.2 Hydraulic Head Data

Figure 15 shows the water level variations in the regional monitoring well network (Figure 7) relative to the water levels measured on March 1st, along with the depth to the water level in each well on March 1<sup>st</sup> and the elevation of the bottom of the screen (masl). The data illustrate an increase in the

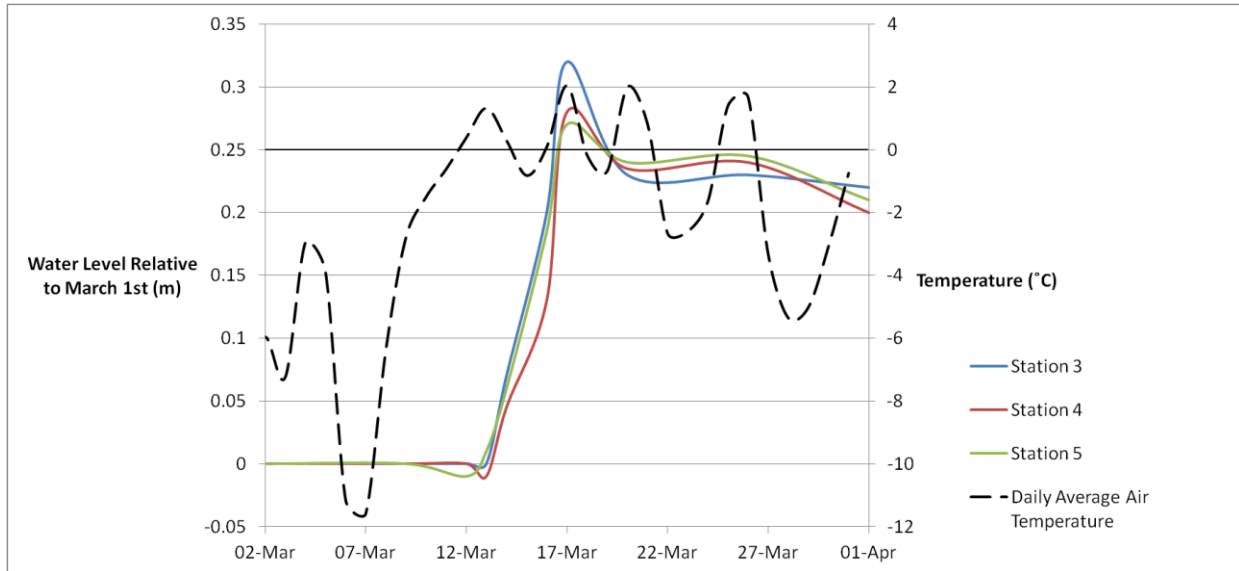
groundwater level during March relative to the water level on the 1st of March at each monitoring location. As observed in Figure 15, there is a relatively rapid response (approximate 5 days) in hydraulic head throughout the study site as the temperature increases to above freezing point, demonstrating the quick response of the groundwater system to changes in climate conditions. It is worth noting, that the wells are installed at various depths within the regional groundwater flow system. For example, wells Wo11-18, Wo63, Wo67 and Wo72s are screened in Aquifer 3 (see Figure 3 for hydrogeological cross section) whereas the rest are screened in the overlying Aquifer 2 unit. It is interesting to note that both Aquifers 2 and 3 responded in a similar fashion during the spring melt period regardless of the difference in the depth to the water level and overlying sediments in each well. The rise in the groundwater level at most wells was between 0.2 and 0.3 meters with the highest increase being observed at Wo40 and Wo11-18 even though they were both screened in different aquifers, 0.55 m and 0.45 m and Aquifer 2 and 3, respectively. Furthermore, Aquifer 2 is unconfined at Wo40, whereas Wo11-18 is in a semiconfined unit and therefore it is unlikely that localized recharge had any significant effect on the groundwater levels at Wo11-18 during this short time period. The response of the water level at all locations was relatively consistent even between the confined and unconfined (Wo37, Wo40, Wo63 and Wo75s) monitoring wells with variable vadose zone thicknesses, suggesting a rapid regional response to spatially variable recharge phenomena as well as evidence of possible hydraulic connections between the aquifer systems. It also indicates that localized recharge may be hard to quantify using this data alone as regional influences would need to be considered.



**Figure 15: Average Daily Air Temperature and groundwater level fluctuations relative to March 1st levels in monitoring wells in the vicinity of the study site**

Groundwater monitoring wells were installed at each of the Stations (3, 4 and 5) to track transient variations in hydraulic head during the course of the field experiments in October, 2015. Manual measurements of hydraulic head at each of the stations were made daily during the spring melt period (March 12th to March 20th), and at regular intervals before and after. Figure 16 shows the hydraulic head data at the three study stations during March, 2015 relative to the hydraulic head on March 1st. The data shown are from the monitoring wells screened at 1.5 mbgs at Stations 3 and 4, and 1.75 mbgs

at Station 5. These represent the shallowest monitoring well at each station that was saturated throughout the study period. As Figure 18 demonstrates, the response of the water table at each of the study stations was very similar regardless of where along the ephemeral stream the stations were located, the depth of the vadose zone and the overlying geology.



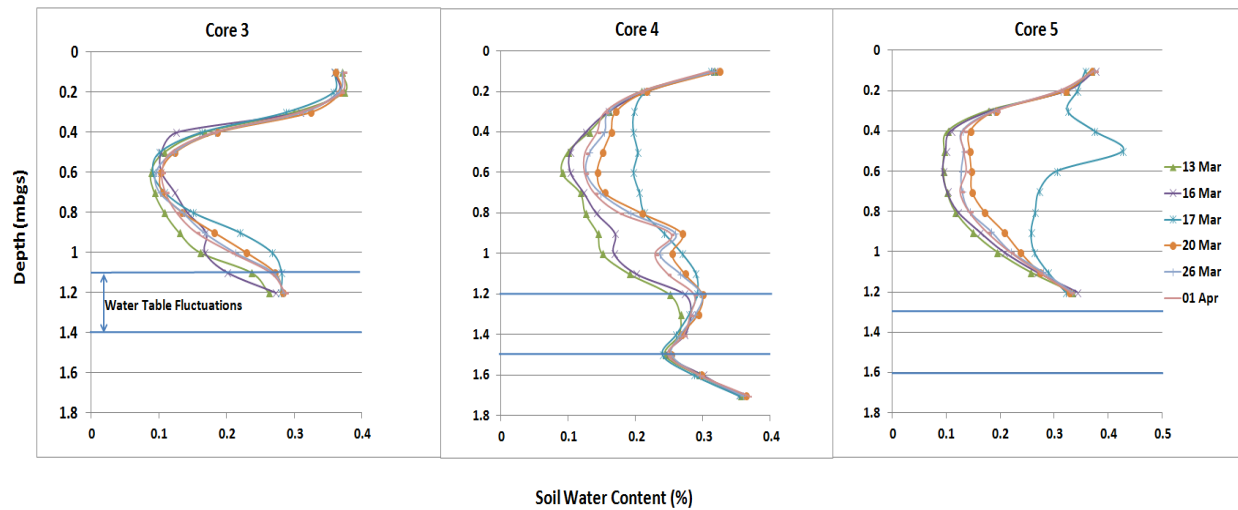
**Figure 16: Water Table fluctuations over the spring melt period at Station 3, 4 and 5**

The hydraulic head at the study Stations 3, 4 and 5, showed a similar response to the regional monitoring wells around the study site (approximately 0.3 m.), despite being screened at considerably shallower depths and with much thinner vadose zones (1.0 to 1.5 m.). The existence of rapid, local-scale and spatially variable infiltration phenomena may be difficult to identify when considering hydraulic head data alone as a similar response in hydraulic head over the entire hydrogeological system is observed, irrespective of the proximity to the ephemeral stream and depth to the water level. Groundwater response to localized recharge tends to be masked and averaged out almost instantaneously (within a couple of days as observed by the duration of the peak in Figure 16), likely because the hydraulic pressure spreads out quickly from the point of infiltration. In this case, the groundwater monitoring wells directly beneath the ephemeral stream where it was hypothesized that significant local infiltration could occur during the spring melt event had a similar response in hydraulic head when compared to the surrounding monitoring wells located quite a distance away from the stream path.

#### 4.2.3 Soil Water Content Data

The soil water content profiles measured using the NMP on concurrent days over the spring melt period (March 9th to March 20<sup>th</sup>, 2015) provided evidence of surface water infiltration at Stations 4 and 5 as the soil water content throughout their profile increased by between 10% and 35% over that short time period (Figure 17). Furthermore, the profiles drained at a rapid rate as well, returning to near initial conditions in several days after the ephemeral water disappeared. As also illustrated on Figure 17, the

water table elevation rose during this time period fluctuating between 1.12 and 1.44 mbgs at Station 3, 1.22 and 1.58 mbgs at Station 4, and 1.32 and 1.58 mbgs at Station 5.



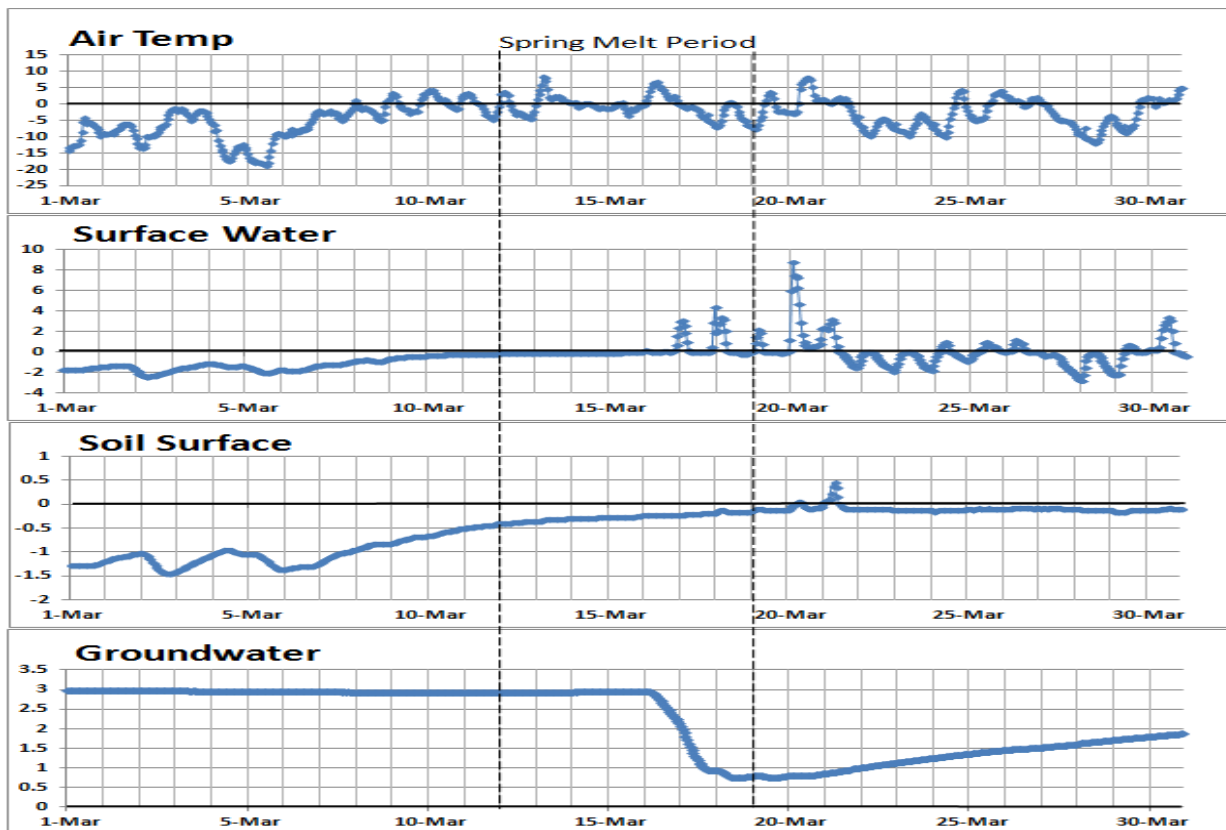
**Figure 17: Moisture content profiles from the Neutron Probe at Stations 3, 4 and 5**

Although there was evidence of an increase in water table elevation at the Station 3 location, the soil water content profile changed very little over the spring melt period and most significantly deeper in the soil profile near the water table. Because Station 3 was located on the eastern side of the ephemeral stream it was only inundated with flowing surface water for a very short time period during March 13 and 16th (following which the ground surface was not inundated with surface water). This, along with the presence of a thin layer of potentially frozen silt underlying the topsoil as shown in Figure 10 may have contributed to the limited increase in soil moisture and overall infiltration observed at this station during the melt period. The increase in the soil moisture at the bottom of the Station 3 profile likely reflects the response of the capillary fringe due to the rising water table on March 16th and 17th. Although there is little evidence of substantial direct infiltration at Stations 3, the immediate rise in the water table at this location suggests the influence of groundwater recharge elsewhere in the immediate vicinity and potentially beneath the adjacent ephemeral stream. The transient moisture content profiles demonstrate the spatial variability in infiltration along the stream bank based on sediment characteristics and the duration of an applied surface water pressure head, as Station 3 was inundated for only part of the melt event.

In examining the transient nature of the soil moisture data at Stations 4 and 5, the highest values were recorded in both profiles on March 17<sup>th</sup> followed by a period of rapid draining with both profiles returning close to the pre-event soil moisture conditions by March 26<sup>th</sup> following the disappearance of the ephemeral surface water on approximately March 19<sup>th</sup> (Figure 4). This again illustrates the event-based nature of the infiltration process.

#### 4.2.4 Temperature Data

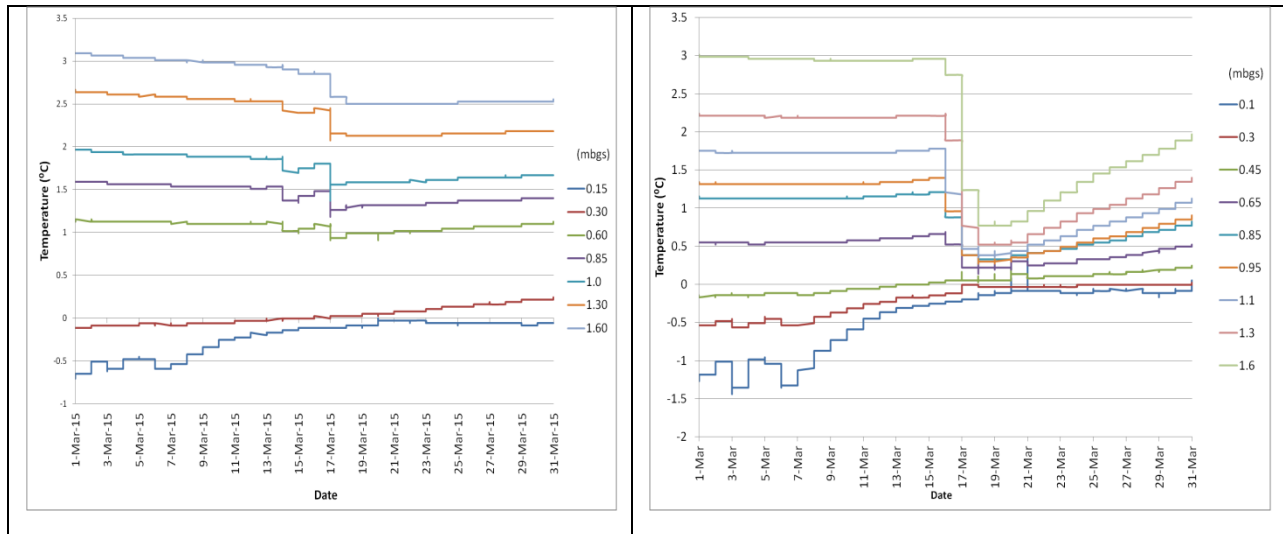
Figure 18 shows the air temperature data from the MET Station located near the study site, along with the surface water, soil surface and groundwater temperatures at Station 4, measured using a temperature probe (surface water) and TidbiT thermistors (soil surface and at 0.05 m and groundwater at 1.65 m). For heat to be of use as a water tracer, there needs to be a contrast in temperature between different water sources that can be monitored and tracked over time (Anderson, 2005; Constantz et al., 2001). Following the winter period, the near-surface environment throughout the frost zone is frozen with temperatures at or below 0°C. Beneath the frozen soil horizon the subsurface temperature increases towards the water table. This condition at Stations 3 and 4 is shown in Figure 19 while Figure 18 shows the response of the subsurface system to changes in the air temperature. These contrasting temperature conditions demonstrated the complexity of the freeze thaw process and its implications to groundwater surface water interactions and also provided valuable conditions for tracing the movement of infiltrating surficial waters.



**Figure 18: Temperature data (Met Station); air, Station 4; surface water, soil surface and groundwater**

The influence of the increasing air temperature during the spring melt period on the surface and subsurface temperatures is evident in Figure 18. The air temperature begins a progressive increase to above freezing conditions on approximately March 6<sup>th</sup> with diurnal air temperatures above 0°C after March 9<sup>th</sup>. The surface temperature progressively increases until surface water flow develops around March 12<sup>th</sup>. The surface water temperature remains around 0°C until March 17<sup>th</sup> when diurnal warming becomes evident. The shallow subsurface (0.1 m. depth) progressively warms from approximately -1.5°C

to 0°C between March 10<sup>th</sup> and March 20<sup>th</sup> remaining close to the freezing point for the rest of March. The groundwater temperature measured using the TidbiT probe at 1.65 mbgs remains constant at nearly 3 °C from March 1<sup>st</sup> to March 16<sup>th</sup> and then drops rapidly to approximately 0.5°C by March 19<sup>th</sup>, which clearly indicates the arrival of colder water from shallower in the soil profile or perhaps recharge from ground surface.



**Figure 19: Comparison of Temperature data at Station 3 and 4 measured with the vertical thermistor arrays**

Figure 19 shows a comparison between the spatial variation of soil temperature profiles during the spring melt, as observed through the shallow subsurface at Stations 3 and 4. The temperature fluctuations at Station 3 were not as pronounced as those observed at Station 4 although the overall trends were very similar. The lower magnitude of temperature change at the Station 3 location relative to Station 4 may indicate a lower rate of infiltration of surface water and a smaller cold water pulse being distributed within the profile. This conclusion would agree with the observations made relative to changes in the soil water profiles at the two sites during the infiltration event. Again the presence of a near-surface silt unit at the Station 3 location may also have reduced the infiltration rate at that site relative to the Station 4 location.

The temperature profile data collected at Station 4 showed a steep decline in subsurface temperatures deeper in the profile starting on March 16<sup>th</sup>, likely as a result of local infiltration of cold surface water. It is interesting to note that flowing surface water appeared several days before the rapid decrease in subsurface temperature was observed, indicating that soil frost may play an important role in the infiltration process under these conditions. The shallowest thermistors (0.1m to 0.5 m) show a progressive warming from frozen conditions to close to 0°C just preceding the major changes in the subsurface temperatures on March 16<sup>th</sup>, representing the melting of the frost layer, which may be a controlling factor in the initiation of the infiltration event.

### 4.3 Numerical model (Hydrus 1D)

#### 4.3.1 Transient Flow Simulations at Station 4

##### 4.3.1.1 Hydraulic Parameters and Initial Conditions Simulation

The initial conditions for the flow simulations at Station 4 were developed by allowing the soil water profile that was measured just prior to the melt period to redistribute and approach steady conditions within the domain for a period of 100 days under constant hydraulic head/flux and temperature boundary conditions. This simulation time period was sufficient to allow full redistribution of the soil water and pressure under the specified initial and boundary conditions. The resulting soil water profile was then compared to the field measured data to ensure consistency. The soil profile used in the numerical model at Station 4 was similar to the one presented in Appendix A and is based on five stratigraphic layers with varying hydraulic parameters. Five layers were chosen to represent the domain to allow for flexibility in capturing the variability in the hydraulic properties throughout the profile, particularly the residual and saturated moisture content and Ks values for each layer. This was done in order to simulate, as closely as possible, the moisture content distribution during both the initial (near steady state) and transient condition simulations. A comparison between the modelled and observed soil profile at Station 4 is shown in Figure 20. The range of values for hydraulic parameters were constrained based on data collected at the site during the current study and through previous work completed on site as well as literature values. These parameter ranges are presented in Table 1.

Core 4					
Depth (m)	Hydrus 1D Profile	Hydrus 1D Initial Estimates Ks (m/min) $\theta_r = \theta$ Residual [-] $\theta_s = \theta$ Saturated [-]	Lithology	USCS	Lithological Description
0.1	Blue	$\theta_r = 0.10$ $\theta_s = 0.35$ $K_s = 7.0E-05$	Blue pattern	PT	Topsoil; Organics, dark brown, wet
0.3	Orange	$\theta_r = 0.05$ $\theta_s = 0.25$ $K_s = 5.0E-03$	Orange pattern	GP	Sandy Gravel: medium gravel size <2cm, moist
0.5	Brown	$\theta_r = 0.06$ $\theta_s = 0.30$ $K_s = 1.0E-03$	Yellow pattern	GP	Sandy Gravel: more sand, medium to fine gravel size, moist to dry
0.7			Yellow pattern	GP	Sandy Gravel: coarse gravel
0.9			Yellow pattern	GP	Sandy Gravel: coarse gravel, reddish brown, dry
1.1	Pink	$\theta_r = 0.12$ $\theta_s = 0.30$ $K_s = 3.0E-03$	Yellow pattern	GP	Sandy Gravel: coarse gravel, reddish brown, dry
1.3			Orange	Miss	MISSING: Poor Recovery
1.5	Pink	$\theta_r = 0.12$ $\theta_s = 0.42$ $K_s = 4.0E-03$	Yellow pattern	GP	Sandy Gravel: coarse gravel

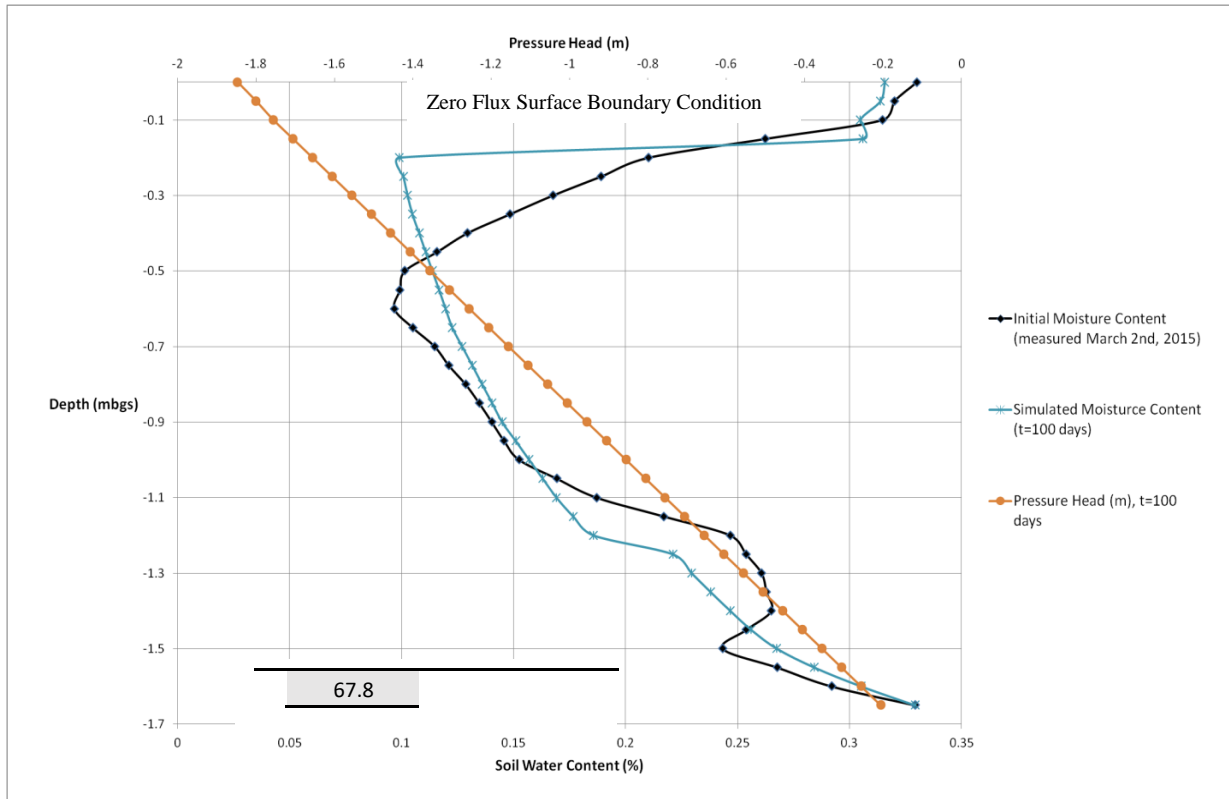
Figure 20: Soil profile used for initial Hydrus1D model domain simulation

**Table 1: Combined values for range of hydraulic parameters used for initial conditions simulations**

Material	Data Source	Ks (m/min)	$\alpha$ [1/m] , $\eta$ [-]	Adopted Ks value for initial simulation	Adopted $\alpha, \eta$ value for initial simulation
Medium Sand	Missori - Lab Sample 4-9 Grain Size Bekeris, 2007 (Trace silt and clay) Literature [1], [2]	1.00E-01 1.80E-03 3.00E-02 - 5.40E-05 <sup>[1],[2]</sup>	$\alpha = 1.34, \eta = 1.17$ <sup>[1]</sup>	1.00E-03	$\alpha = 1.5, \eta = 2.5$
Sandy Silt	Brook, 2014 (minor gravel) Bekeris, 2007 Literature [1]	3.07E-02 6.00E-07 - 1.20E-04 3.00E-02	$\alpha = 1.34, \eta = 1.17$	7.00E-05	$\alpha = 0.5, \eta = 1.5$
Sandy Gravel	Brook, 2014 (minor silt) Missori - Lab Sample 4-8 Grain Size Missori - Lab Sample 4-8 Falling head Literature [3]	1.22E-01 1.00E-01 4.70E-02 6.94E-03 - 3.47E-02	$\alpha = 10.9, \eta = 2.09$	4.00E-03	$\alpha = 2, \eta = 2.5$

Average Ks values based on the combined information in Table 1 formed the initial estimates for Ks used to develop the initial water content distributions. The  $\alpha$  and  $n$  parameters of the soil water retention curves used in the initial conditions simulation were chosen between the range of those found in literature and those from the sediment types that were encountered at the field sites (Brook, 2012).





**Figure 21: Soil water content initial conditions and hydrostatic pressure head distribution in soil profile for Station 4**

Figure 21 shows the initial soil water content profile that was specified based on field observations on March 2nd, 2015 and assumed to be the initial fully drained conditions before the spring melt period. The resulting pressure head distribution based on the specified van Genuchten retention parameters was calculated in Hydrus 1D and forms a linear distribution from the ground surface to the water table representing hydrostatic conditions were reached during the simulated period.

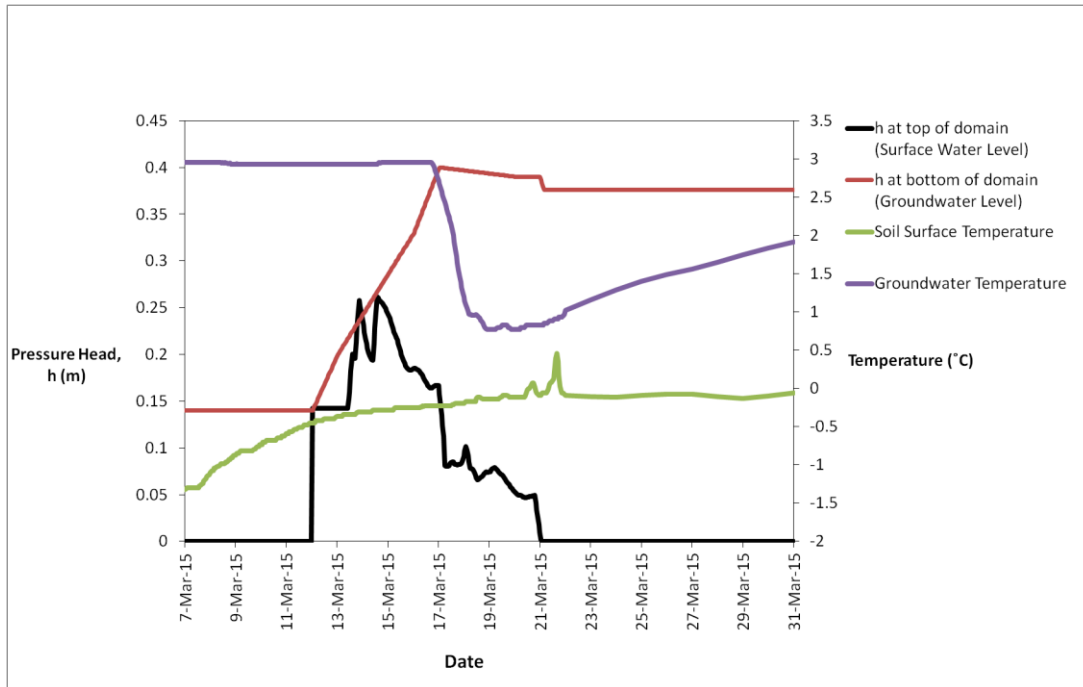
The initial conditions show a reasonable similarity to the observed soil water content data with the only notable deviation between the depths of 0.2 and 0.4 mbgs. This is likely due to the gentler distribution of soil water content between changes in materials observed in the field, and also due to the averaging of soil water content within a certain radius by the neutron probe. These changes in soil water content between layers are more abrupt in Hydrus 1D based on material properties.

#### **4.3.1.2 Results of Flow Simulations**

Once steady pressure heads and soil water conditions were established throughout the simulation domain as described above, transient boundary conditions based on field measurements collected during the melt period were applied and the behaviour of the soil water content profile simulated by the model was compared to the transient data measured in the field. The transient simulation period began on March 7th, just prior to the initiation of the melt event and was continued until April 1<sup>st</sup>. This end date was well after the disappearance of the ephemeral waters to allow for redistribution of the

infiltrated water within the vadose zone after the recharge event. Following the initial appearance of the ephemeral stream (March 13<sup>th</sup>), the surface water depth and the disappearance of the surface water (March 21<sup>st</sup>) were carefully monitored throughout the melt period. These observations were used to inform the transient hydraulic head boundary conditions at the top of the domain during the melt event. However, as the near surface environment was initially frozen (frost zone) there may have been a reduction in hydraulic conductivity in the near-surface environment due to the cold climate conditions that resulted in an initial delay of direct infiltration of the surface water. A combination of observations derived from the changes in the soil water content and subsurface temperatures were used to further inform the specification of the surface flux boundary condition. More specifically, a zero flux surface boundary condition was used to represent the presence of a frost layer and was changed to a specified pressure head boundary condition when changes in near surface soil water content and temperature were first observed in the field. The transient pressure head and temperature data used to define the domain boundary conditions are shown in Figure 22.

Although flowing surface water first appeared on March 13<sup>th</sup>, there were no noticeable changes in the soil water content or subsurface temperature profiles which would provide evidence of infiltrating surface water until March 16<sup>th</sup> (Figure 17 and Figure 19). As such, a zero flux boundary condition was prescribed to the upper boundary of the domain until March 16<sup>th</sup>, following which the boundary condition was changed to a specified pressure head that was updated on an hourly basis based on the data collected from the pressure transducer within the ephemeral stream until the ephemeral water disappeared on March 20<sup>th</sup> after which the upper boundary condition was again assigned as zero flux. The surface water pressure head readings shown in Figure 22 are with respect to the ground surface at Station 4 where the transducer was installed just above the ground surface. The boundary condition at the bottom of the domain profile was assigned as a specified pressure head value based on a linear distribution of the manual field measurements taken daily from the multi level monitoring wells (Figure 22). The bottom pressure head boundary condition was also updated on an hourly basis from March 13<sup>th</sup> to March 21<sup>th</sup> and then daily until the end of the simulation (April 1<sup>st</sup>). The soil water temperatures observed using the TidbiT thermistor arrays show a sudden decrease throughout the soil profile after March 16<sup>th</sup> (Figure 19) likely as a result of cold surface water infiltrating rapidly and causing the groundwater temperatures to fall.



**Figure 22: Time variable boundary conditions used in the transient simulations for Station 4**

The set of hydraulic properties developed to define the initial conditions for the transient model runs, were modified slightly within the range provided in Table 1 during the calibration process to reflect the transient soil water data collected during the infiltration period. The simulated soil water content profiles are compared to the field measured data for a series of days during the melt period in Figure 25. The final set of hydraulic parameters derived through the calibration process is presented in Table 2. Figure 23 demonstrates that the model was able to capture the transient evolution of the soil water content profile during the dynamic melt period. The Figure shows that the soil water profile responded quickly to the infiltration event and the bulk of the profile was able to transmit a large pulse of water without being completely saturated.

**Table 2: Hydraulic Parameters selected for the transient simulations following the calibration process**

Hydraulic Parameters (L=m, t=min)					
$\theta_r$	$\theta_s$	$\alpha$	$\eta$	Ks	I [-]
0.1	0.35	0.5	1.3	8.00E-05	0.5
0.05	0.3	2.5	2	0.0033	0.5
0.04	0.3	1.5	4	0.0016	0.5
0.12	0.3	1.9	4.2	0.0035	0.5

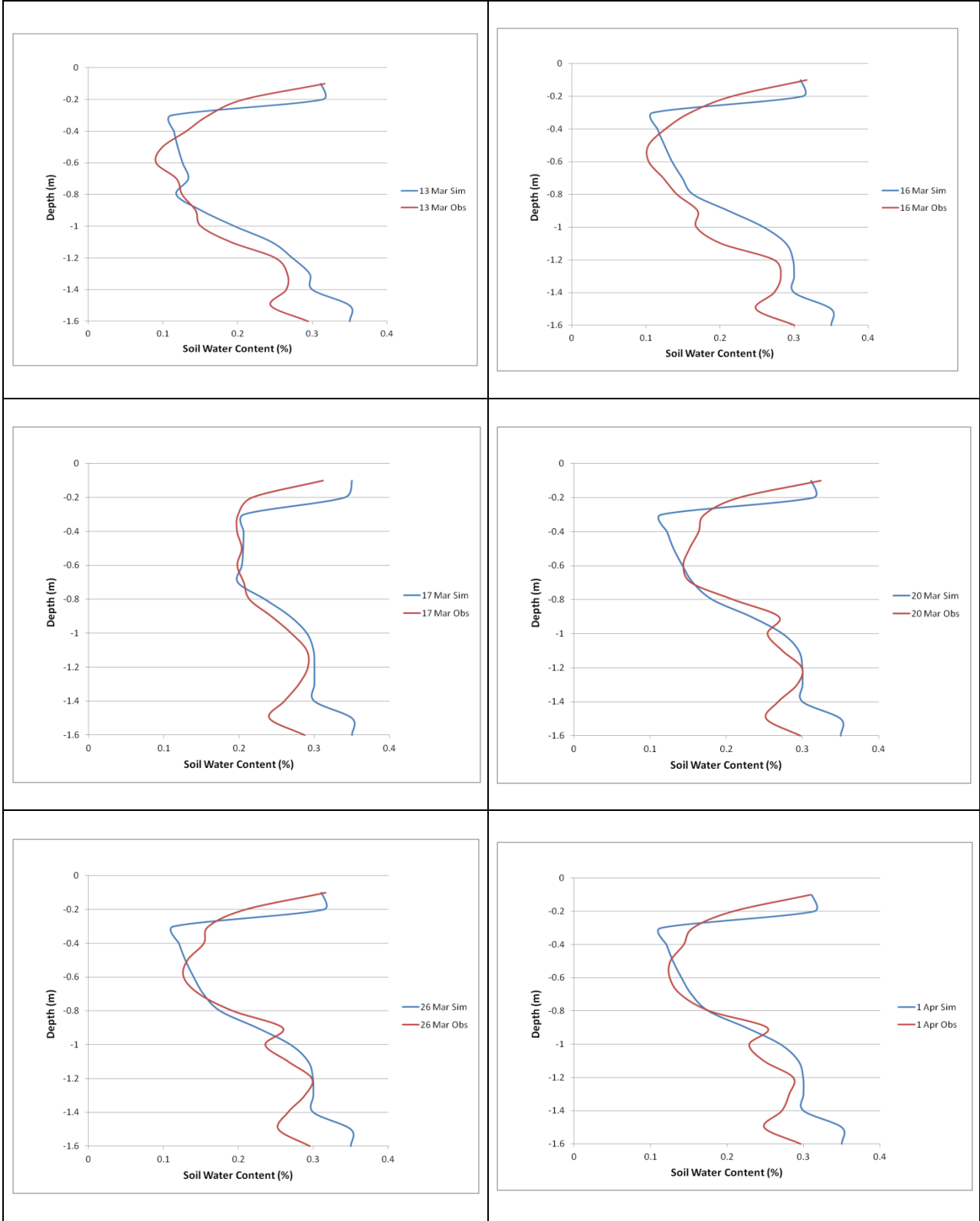
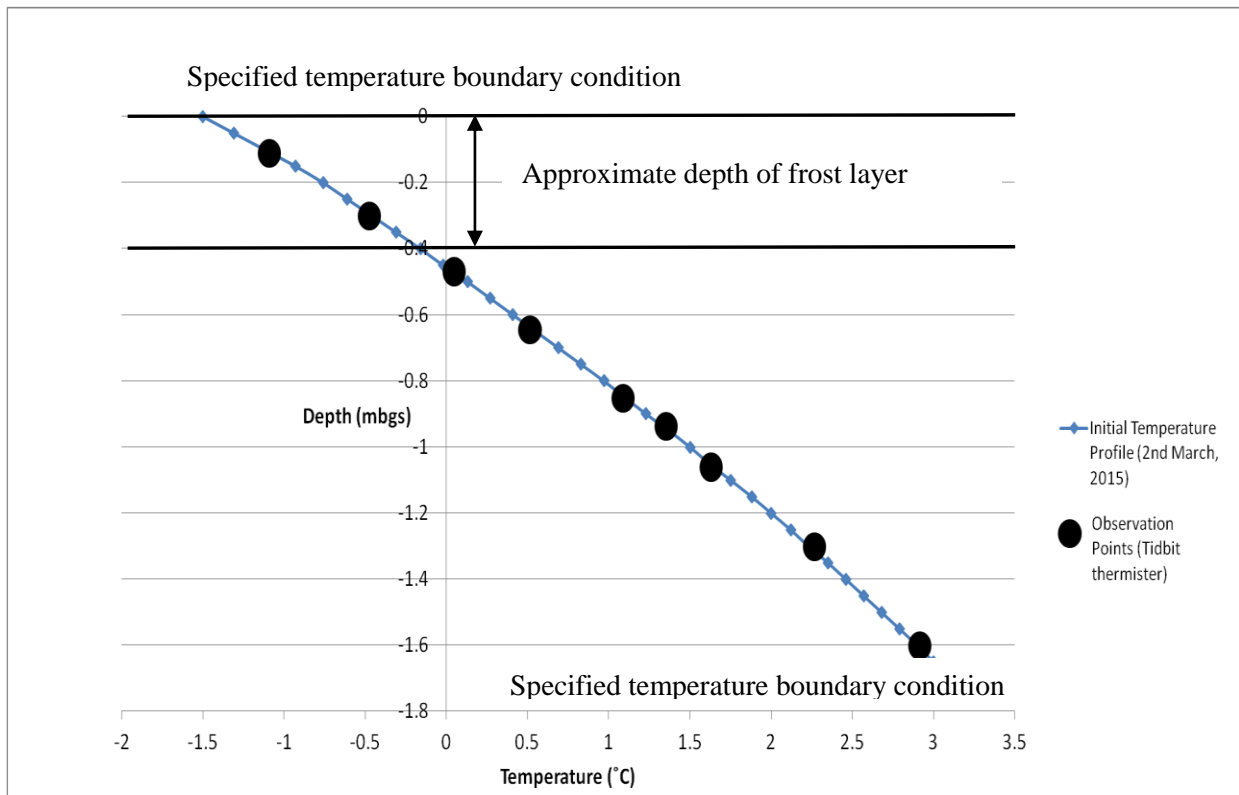


Figure 23: Comparison of the simulated soil water content profiles (Sim) at Station 4 with the field data measured with the neutron probe (Obs)

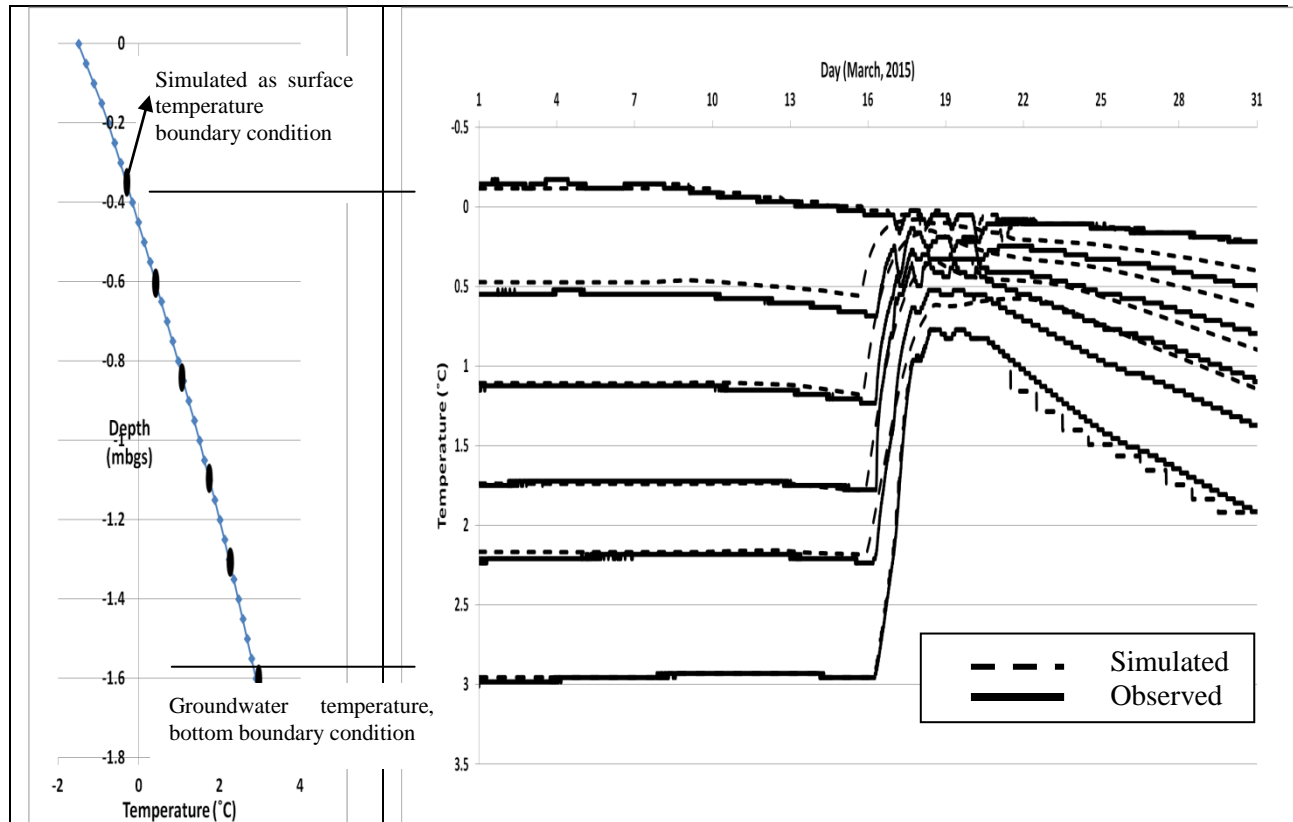
### 4.3.1.3 Heat transport at Station 4

The initial temperature profile measured using the vertical thermistor arrays on March 2nd, 2015 was used to represent the soil temperature conditions prior to the initiation of the infiltration event as shown in Figure 24. The soil surface temperature is below -1 C and the top surficial soil layer of approximately 50 cm remains below the freezing point. The soil temperature profile steadily increases towards the groundwater table where the temperature is approximately 3 C.



**Figure 24: Initial conditions for soil temperature profile at Station 4**

The heat transport simulations are based on the calibrated transient flow results described above and the physical parameters governing heat transport derived through the Hydrus 1-D model and literature values. These parameters are provided along with the governing heat equations in Appendix I. The transient top and bottom temperature boundary conditions were specified based on the data from the tidbit thermisters at 0.45 mbgs (top boundary) and 1.65 mbgs (bottom boundary), and were updated hourly during the spring melt period (March 12th to March 21st) and then daily until the end of the simulation period (April 1st) similar to the water flow time variable boundary conditions. Figure 25 shows the surface and groundwater boundary conditions specified in the transient heat transport simulation, as well as the simulated heat time series at various depths along the profile.



**Figure 25: Comparison between simulated and observed soil temperature profiles at Station 4**

The left side of Figure 25 shows the initial temperature profile observed in the field from the ground surface till the depth of the simulation domain (1.65 mbgs). The right side of Figure 25 shows the simulated transient heat profile during the period of the spring melt at different depths in the soil profile. The coldest time series represents the top boundary condition that was specified using field observations from the thermistor placed at 0.45 mbgs. Due to the fact that Hydrus 1D cannot handle frozen conditions, and in order to avoid the complex dynamics of the freeze thaw cycle, the temperature simulation domain was specific to begin at the 0.45 mbgs at the base of the frost zone.

The results of the heat transport simulation suggest that the model was able to simulate the transient heat profiles at all depths along the profile monitored using the thermistor arrays. This includes the sudden decrease in temperatures throughout the profile as the cold surface water pulse infiltrates shortly after the 16th of March, and then the gradual return of soil temperatures towards regionally consistent soil temperatures after the end of the infiltration event (March 19th). The results also indicate that the model was able to capture the transient nature (fluxes and boundary conditions) of cold surface water infiltrating through the profile as this cold pulse of infiltrating surface water would have significant effects on the transient temperature time series at various depths in the soil profile.

#### 4.3.2 Modeling Results for Station 3 and 5

The modelling exercise for Stations 3 and 5 was similar to that used in Station 4 and was done to demonstrate the spatial variability in infiltration flux and groundwater recharge. The stratigraphic

profiles were modified to match those encountered at the different sites and the hydraulic parameters determined through the calibration of the flow simulations at Station 4 were adopted, with minor modifications based on calibration for these subsequent simulations. The duration of the infiltrating event at Stations 3 (approximately 1 day) was much shorter than that observed at Station 4 due to the fact that this station was not consistently in the path of the stream (no surface water observed above Station 3 on March 17th, see Figure 4) and therefore was not inundated for the entire duration of the spring melt event. The hydraulic parameters and time variable boundary conditions for Stations 3 and 5 model simulations are provided in Appendix L.

The simulation results were again compared to the transient soil water data collected at Stations 3 and 5 and are presented in Figure 26 and Figure 27. At both locations, the transient soil water profiles were well represented by the model, demonstrating that these models were able to capture the transient flow conditions. As there was no noticeable infiltration at Station 3 as observed qualitatively through the soil water content and temperature profiles, fitting the simulations to the observed data was simpler. At Station 5, due to the presence of a low permeability layer at approximately 0.5 mbgs, the soil water content in the profile above this depth showed a significant increase on March 17th, and the model was able to capture this shift in soil water content along with the rapid draining of the profile by March 20th.

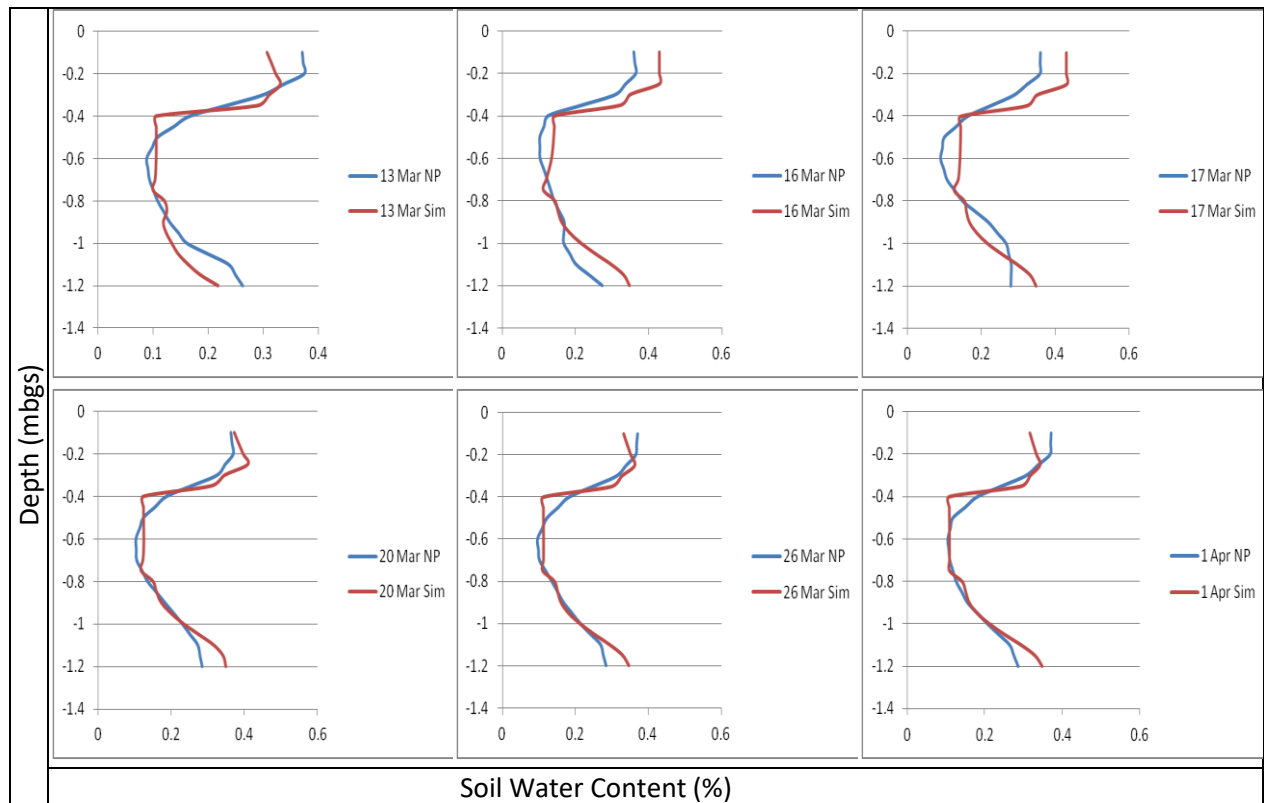


Figure 26: Comparison of the simulated soil water content profiles (Sim) at Station 3 with the field data measured with the neutron probe (NMP)

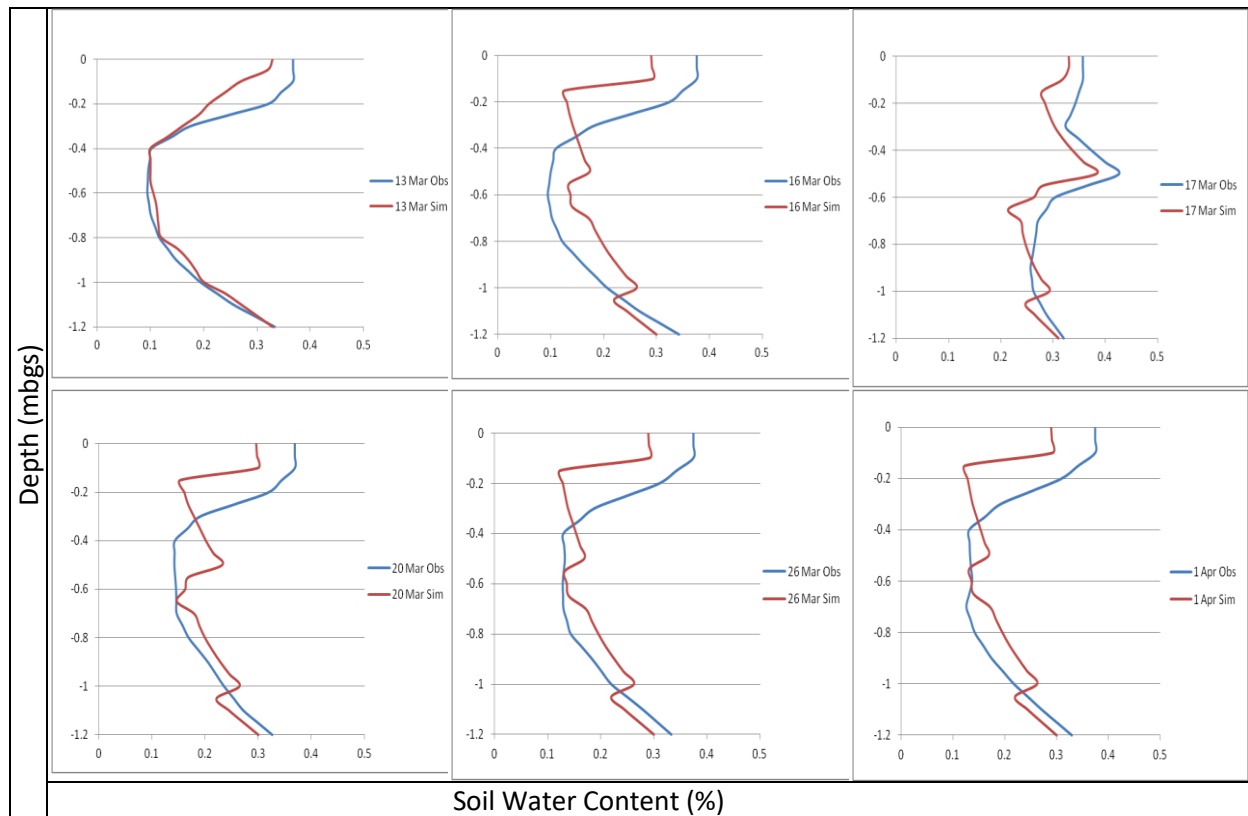


Figure 27: Comparison of the simulated soil water content profiles (Sim) at Station 5 with the field data measured with the neutron probe (NMP)

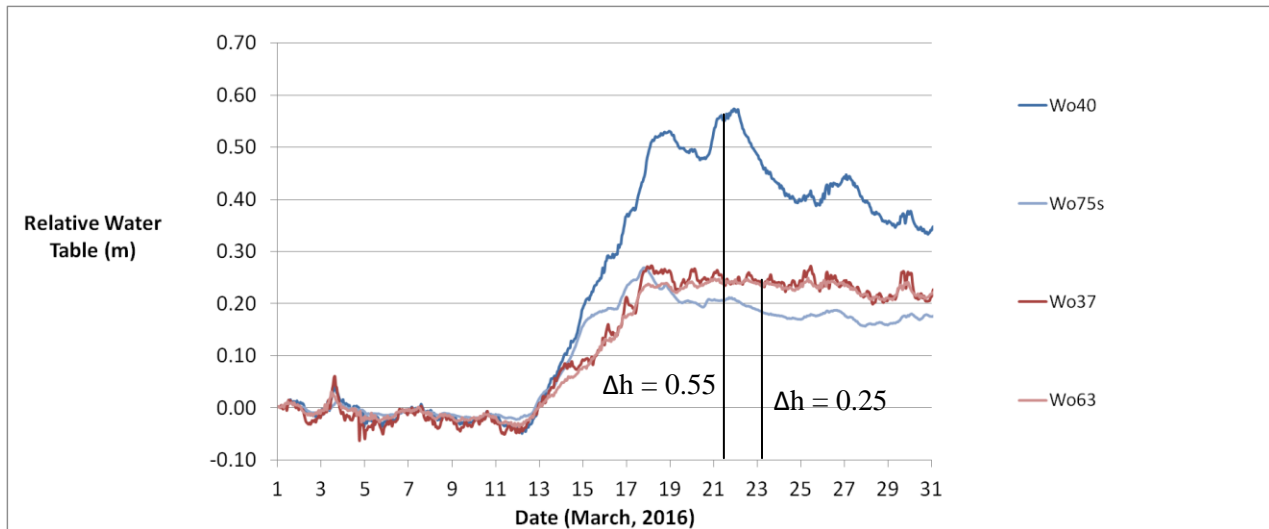
## 4.4 Recharge Estimates

### 4.4.1 Water Table Fluctuation Method

An initial estimate of spatially variable recharge across the field site during the spring melt event was based on the water table fluctuation (WTF) method described in the Methods section and based on Equation 1. Four of the monitoring wells were completed in unconfined strata and were used to estimate recharge based on the WTF method. These were wells Wo-Wo37, Wo40 and Wo75-s which were screened in aquifer 2, and Wo63 which was screened in Aquifer 3 (Brook, 2012; Haslauer, 2005).

The sustainable yield ( $S_y$ ) of Aquifers 2 and 3 at the study site was estimated from the difference between the saturated and residual soil water content that were determined in previous studies at the site. Padusenko, 2005 estimated average  $\theta_s$  and  $\theta_r$  to be 0.3 and 0.08 respectively for Aquifer 2 and 0.35 and 0.1 for Aquifer 3, using volumetric water content estimates from soil cores at the study site and further calibrating those values within numerical model experiments. Koch (2009) and Bekeris (2007), also estimated values for  $S_y$  in the range of 0.2 for Aquifer 2 and 0.25 for Aquifer 3 based on modeling exercises. This range of values is used in the recharge estimates in Aquifer 2 and 3 using the water table fluctuation method (equation 1).





**Figure 28: Magnitude of groundwater level fluctuations in surrounding unconfined monitoring wells relative to initial levels measured on March**

The relative water level increase in Aquifer 2 is highly variable, as observed through a difference of almost 0.30 m between the water level increase in Wo40 and the other wells, over a very short period (March 13th to March 21st). While Wo37 and Wo63 were in the vicinity of the ephemeral stream, Wo75s was not, however the increase in water levels in all these wells was consistent. The recharge estimates using equation 1 was in the range of 0.06 m and 0.12 m for aquifer 2 ( $S_y = 0.22$ ) and 0.06 m for aquifer 3 since only Wo63 was screened in this aquifer ( $S_y = 0.25$ ).

#### 4.4.2 Cumulative Infiltration Estimates from Numerical Modelling

The cumulative infiltration was calculated using the calibrated results of the flow simulations with the Hydrus 1-D model at each of the three stations. This was done through water balance calculations for the model domain at every time step and summing the total volume of water entering and leaving the domain. During the simulated period the cumulative infiltration values were 0.72 meters at Station 4, 0.42 meters at Station 5 and 0.06 meters at Station 3, at an average infiltration rate between  $3.6E-05$  m/min to  $1.3E-4$  m/min (Figure 29). The calculated infiltration at Station 4 and 5 is considerably larger than the estimates obtained through the WTF method and while considering the field evidence of infiltration at these stations (soil water content and temperature fluctuations), it is clear that the WTF was not able to correctly represent the recharge magnitude associated with this transient event. In the case of Station 3, where the influence of the surface water infiltration appeared to be negligible, the model and the WTF fluctuation method provided similar estimates of recharge. The significantly large model estimates of infiltration rates at Stations 4 and 5 in comparison to previous studies at the site (Koch, 2006; Bekeris, 2009; Brook, 2012) demonstrate that infiltration directly beneath the ephemeral stream may contribute a large, event-based pulse of surface water to the aquifer system in close proximity to municipal drinking wells. Where this ephemeral water is carrying pathogens such as E-Coli, as demonstrated at this study site (Christie, 2009), these results are significant with respect to the associated risk to municipal wells of contamination from these transient events.

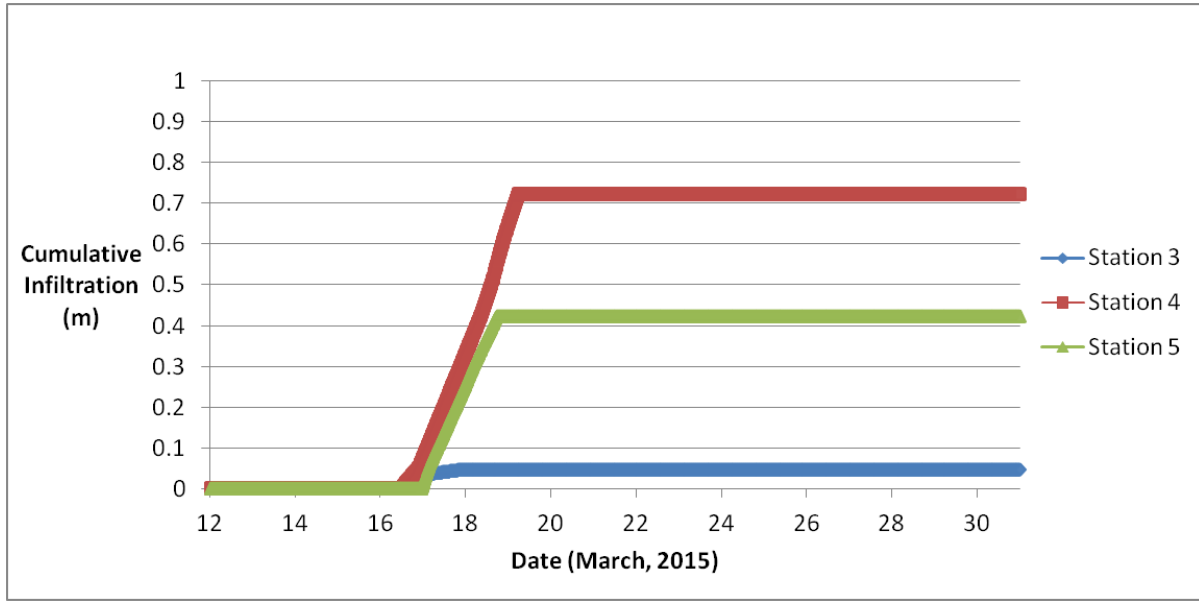
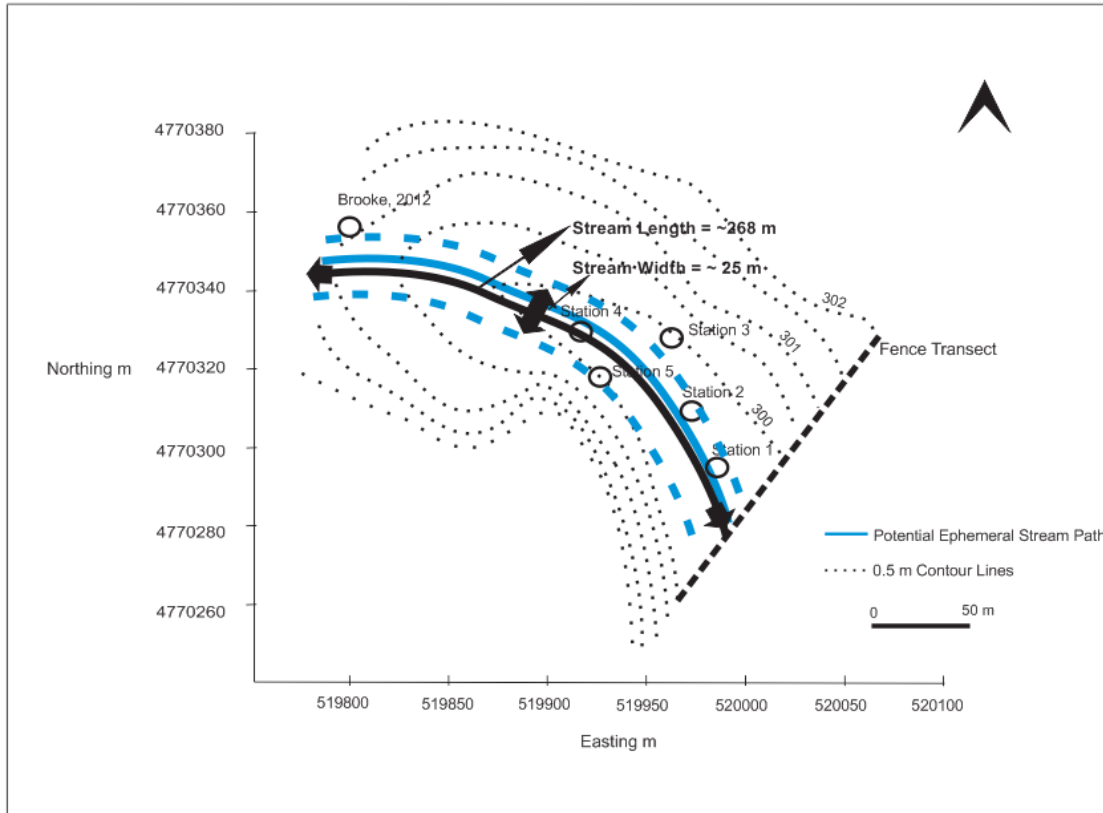


Figure 29: Cumulative infiltration estimates from numerical methods for Stations 3,4 and 5

#### 4.4.3 Total Volume of Recharge at Study Site

An estimate of the total recharge volume over a portion of the field site during the spring melt period was calculated based on the approximate size of the inundated ground surface, infiltration estimates from the monitoring stations, and the estimated duration of the infiltration event (3 days March 16 to 19th). The picture below illustrates the approximate dimensions of the stream during this period and this was further delineated using a combination of the surface water pressure head data at Station 4 and the topographical survey of the site provided in Figure 8.



**Figure 30: Ephemeral stream dimensions for total recharge estimate**

The stream had a width of approximately 25 metres on the 16th and 17th of March in the vicinity of Stations 3, 4 and 5. If the segment of the ephemeral stream where the surficial sediments are highly permeable (southeast of the Brook (2012) site on Figure 30) to the fence line is considered for this estimation a total approximate area of infiltration would be 7100 m<sup>2</sup>. If infiltration rates equal to those estimated at Station 4 (0.72 m.) and Station 5 (0.42 m.) are used for the calculation over the three day period, a total volume of recharge beneath this short segment of the ephemeral stream at the study site can be approximated to be between 0.5 and 1 million imperial gallons considering the limitations of the approach described below. It is still very probable that this is an underestimation of the total event-based recharge in this area as the ephemeral water flows over a larger distance than the one used in the above approximation (268 meters) both upstream from the study site (where ponded water north of Curry Road is observed) as well as further downstream closer to the wells. The range in recharge estimates at the site demonstrates the spatial variability of infiltration flux but more importantly demonstrates that even with a conservative estimate of groundwater recharge from the spring melt event in the vicinity of the ephemeral stream there may be significant concern for well vulnerability when these waters are carrying contaminants, as recharge can occur in event based time periods as demonstrated in this study.



**Figure 31: Picture of field site showing approximate width of ephemeral stream on March 17th, 2015**

The recharge estimates at Station 3, 4 and 5 using the water table fluctuation approach were 0.12 m ( $\pm$  0.06 m) which were consistent with the estimates at monitoring wells screened in deeper aquifers and not directly in the path of the ephemeral stream. The total recharge in the vicinity of the stream using this method would therefore be in the range of 90,000 to 270,000 imperial gallons.

The field investigations showed surface water infiltrating at Stations 4 and 5 through changes in groundwater temperature and soil water profiles, whereas this was not observed at Station 3 that was on the left bank of the ephemeral stream and only temporarily inundated. This demonstrates that the water level data itself was not able to capture the transient nature of the event as the water levels in various monitoring wells around the study site rose to similar levels regardless of their proximity to the ephemeral stream or the depth to the water table. The WTF method therefore, gave a similar estimate for recharge at all stations whereas the field and modeling exercise provided evidence that much higher infiltration rates were occurring directly beneath the ephemeral stream.

The approach to quantifying groundwater recharge through the integration of field and numerical modelling methods has its challenges and limitations, most notably with regard to the density and frequency of field data collection, which was used as input data and calibration targets for the numerical model. The difficulty and costs associated with installing and maintaining field monitoring equipment in cold climates dictates that only a limited number of monitoring locations could be relied upon to get

representative infiltration rates along the stream channel. These few monitoring stations therefore cannot fully represent the infiltration dynamics along the entire length of the ephemeral stream, and therefore where possible, multiple locations along the stream channel should be monitored to capture the spatial variability in infiltration fluxes. In addition, the difficulties in installing and maintaining real time sensor networks connected to data loggers that could be used to monitor, for example, transient changes in heat and soil water content profiles, meant that small changes in these parameters would have been missed. This is particularly evident in the use of the neutron probe to obtain soil water content readings, where only manual point measurements could be made and therefore the transient shift of the moisture content curves may not have been fully captured. Finally, even with the low density field soil water content data set, the model was only able to simulate the transient changes in the soil water content profiles up to a certainty of 80 percent as estimated through a regression analysis of the combined soil water content data set (simulated versus observed) which is presented in Appendix P. This further demonstrates the difficulty in calibrating numerical models to transient data sets, particularly in heterogeneous unsaturated porous media where the hydraulic properties of multiple soil layers needs to be considered.

The study was able to demonstrate clear evidence of surface water from the ephemeral stream infiltrating and reaching the groundwater table, through changes in pressure, temperature and soil water content. The modelling exercise, despite its limitations showed that a large pulse of water would be able to infiltrate under the conditions observed and even a conservative estimate of total volume of recharge beneath the ephemeral stream indicated that such events may indeed introduce a large pulse of potentially contaminated surface water to the municipal aquifer system resulting in an increased threat to water quality within the public supply wells.

## 5.0 Conclusions

This study focussed on quantifying infiltration and groundwater recharge within the vicinity of an ephemeral stream that develops due to large overland flow over partially frozen soils during the spring freshet within glacial drift in southern Ontario. The main hypothesis of the work was that significant amounts of recharge flux can occur beneath ephemeral surface water features during the spring freshet, even under partially frozen conditions during these dynamic events. Natural infiltration experiments of dynamic recharge events in cold regions have not been commonly carried out due to the transient nature of the events and the difficulty of conducting field investigations in harsh climates.

Hydraulic head data from monitoring wells across the study site showed an increase in pressure head throughout the regional aquifer system during the spring melt, including in the deeper aquifer units. This demonstrated recharge phenomenon at a much larger, regional scale during these dynamic events but also indicated that hydraulic head data alone was not able to capture the transient nature of the infiltration event. The study showed evidence of infiltration such as through soil water content and temperature changes beneath the ephemeral stream which was not observed away from the stream (such as at Station 3), while water level fluctuations were similar at all stations and did not capture these differences. The numerical modelling exercise showed that under the transient conditions of flowing ephemeral waters, infiltration continues (as observed at the study stations) after the soil water content has risen to a level where water flow can be conducted without any noticeable changes in soil water content.

The water table fluctuation calculations provided an insight in to regional recharge dynamics in both the shallow and deeper aquifer units and estimated recharge to be within the range of 0.06 and 0.12 meters using equation 1 (at Wo37, and Wo40 respectively). In the present study, the infiltrating pulse from a transient surface water body that existed for a very short duration was, through the use of numerical methods estimated to be several times larger (up to 0.73 m) than that predicted by the water table fluctuation method. It is likely that the water table rises to a maximum value after which water moves away from the infiltrating point whereby further infiltration does not contribute to a rise in the water level.

The large range in recharge estimates from the numerical modelling exercise for three sites in the vicinity of the ephemeral stream and in relatively close proximity to each other not only shows the high degree of spatial variability in recharge but also highlights the significance of the location of these transient surface water bodies to recharge dynamics. The present study demonstrates the importance of measuring several locations along the stream path to more accurately assess the vulnerability of nearby drinking water wells as large pulses of surficial contaminants infiltrating in event based time periods can be overlooked by water table fluctuation methods or larger scale water balance computations.

Further, the duration of the infiltration event is essential in accurate estimates of recharge due to the high infiltration flux at certain locations. In cold climate conditions the frost layer plays an important role in the timing of the infiltrating pulse and therefore under such conditions measurements of the transient frost conditions are extremely valuable in making more accurate estimates of localized recharge. Numerical models however, should be calibrated to as many field observations as possible and soil water content, temperature and pressure data as used in the present study can help constrain the model results. The closeness of fit of the numerical models to transient field data within the context of this study show that when used in unison these data can be effective in estimating recharge at various point locations.

The study indicates that localized recharge from transient surface water can be significantly large and may present a contamination risk to groundwater resources particularly when these transient surface water features are in the vicinity of drinking water wells. We propose that this type of event-based recharge phenomena can provide a significant pulse of contaminant loading and presents a threat to the drinking water quality of near-by public supply wells. Finally, the results from this study show the importance of monitoring ephemeral events in sufficient detail to better understand the transient infiltration dynamics in the vicinity of the stream. This will allow a better assessment of the vulnerability of drinking water wells through considering the heterogeneity in various data sets.

## References

- Aeby PG (1998) Quantitative fluorescence imaging of tracer distributions in soil profiles. Diss Thesis, Swiss Federal Institute of Technology, Zurich, 72 pp
- Allen RG, Howell TA, Pruitt WO, Walter IA, Jensen ME (eds) (1991) Lysimeters for evapotranspiration and environmental measurements. In: Proc Int Symp on Lysimetry, American Society of Civil Engineers, New York, 444 pp
- Andersen, M.S., Acworth, R.I., 2009. Stream-aquifer interactions in the Maules Creek catchment, Namoi Valley, New South Wales, Australia. *Hydrogeol. J.* 17, 2005–2021. doi:10.1007/s10040-009-0500-9
- Anderson, M.P., 2005. Heat as a Groundwater Tracer
- Athavale RN, Rangarajan R (1988) Natural recharge measurements in the hard-rock regions of semi-arid India using tritium injection – a review. In: Simmers I (ed) Estimation of natural groundwater recharge. Reidel, Dordrecht, pp 175–195
- Baskaran, S., Ransley, T., Brodie, R.S., Baker, P., 2009. Investigating groundwater-river interactions using environmental tracers. *Aust. J. Earth Sci.* 56, 13–19. doi:10.1080/08120090802541887
- Batlle-Aguilar, J., Cook, P.G., 2012. Transient infiltration from ephemeral streams: A field experiment at the reach scale. *Water Resour. Res.* 48. doi:10.1029/2012WR012009
- Bayard, D., M. Stähli, A. Parriaux, and H. Flüeler (2005), The influence of seasonally frozen soil on the snowmelt runoff at two Alpine sites in southern Switzerland, *J. Hydrol.*, 309,66–84, doi:10.1016/j.jhydrol.2004.11.012.
- Bekeris, L., 2007. Field Scale Evaluation of Enhanced Agricultural Management Practices Using a Novel Unsaturated Zone Nitrate Mass Load Approach 0.
- Belan, R. A., & Matlock, W. G. (1973, May). Groundwater recharge from a portion of the Santa Catalina Mountains. In *Hydrology and Water Resources in Arizona and the Southwest*. Arizona-Nevada Academy of Science.
- Berthold, S., 2004. Integrated hydrogeological and geophysical study of depression-focused groundwater recharge in the Canadian prairies. *Water Resour. Res.* doi:10.1029/2003WR002982
- Brook, J., 2012. Evaluating Innovative Nutrient Management Options and Seasonal Groundwater Recharge Dynamics in an Agricultural Source Water Protection Area.
- Brutsaert W (1982) Evaporation into the atmosphere, theory, his- tory and applications. Reidel, London
- Callegary, J.B., Leenhouts, J.M., Paretti, N. V., Jones, C. a., 2007. Rapid estimation of recharge potential in ephemeral-stream channels using electromagnetic methods, and measurements of channel and vegetation characteristics. *J. Hydrol.* 344, 17–31. doi:10.1016/j.jhydrol.2007.06.028



- Cey, E.E., Rudolph, D.L., Parkin, G.W., Aravena, R., 1998. Quantifying groundwater discharge to a small perennial stream in southern Ontario, Canada. *J. Hydrol.* 210, 21–37. doi:10.1016/S0022-1694(98)00172-3
- Christie, M., Rudolph, D.L., Payment, P., and Locas, A., 2009. Monitoring the Occurrence of Microbial Contaminants within the Wellhead Protection Area of a Municipal Well Field in an Agricultural Setting. *Microbial Transport and Survival in the Subsurface: 1st International Conference, May 10-13, Niagara-on-the-Lake, Ontario, Canada.*
- Chung, I.M., Kim, N.W., Lee, J., Sophocleous, M., 2010. Assessing distributed groundwater recharge rate using integrated surface water-groundwater modelling: Application to Mihocheon watershed, South Korea. *Hydrogeol. J.* 18, 1253–1264. doi:10.1007/s10040-010-0593-1
- Chung, S. O, Horton, R., 1987. Soil heat and water flow with a partial surface mulch. *Water Resour. Res.* 23, 2175–2186. doi:10.1029/WR023i012p02175
- Constantz, J., 2010. Heat as a tracer to determine streambed water exchanges. *Water Resour. Res.* 46, 1–20. doi:10.1029/2008WR006996
- Constantz, J., 2002. Analysis of temperature profiles for investigating stream losses beneath ephemeral channels. *Water Resour. Res.* doi:10.1029/2001WR001221
- Constantz, J., Stonestrom, D., Stewart, A.E., Niswonger, R., Smith, T.R., 2001. Analysis of streambed temperatures in ephemeral channels to determine streamflow frequency and duration. *Water Resour. Res.* 37, 317–328. doi:10.1029/2000WR900271
- Corporation of the County of Oxford. 2015. *Topography - Contours: The Corporation of the County of Oxford, Woodstock, Ontario, Canada.*
- Cowan, W.R. Quaternary Geology of the Woodstock Area – Southern Ontario; Geological Report 119. Tech. Rep., Ontario Ministry of Natural Resources, Division of Mines, 1975.
- Davidson, E. S. (1973), *Geohydrology and water resources of the Tucson basin, Arizona, U.S. Geol. Surv. Water Supply Pap.* 1939– E, 81 pp. Doherty, J. (1994), *PEST Model-Independent Parameter Estimation Man*
- Derby, N.E., Knighton, R.E., 2001. Field-scale preferential transport of water and chloride tracer by depression-focused recharge. *J. Environ. Qual.* 30, 194–199.
- Dripps, W.R., Bradbury, K.R., 2010. The spatial and temporal variability of groundwater recharge in a forested basin in northern Wisconsin. *Hydrol. Process.* 24, 383–392. doi:10.1002/hyp.7497
- Doherty, J., Johnston, J.M., 2003. Methodologies for calibration and predictive analysis of a watershed model. *J. Am. Water Resour. Assoc.* 39 (2), 251–265.

- Doviak, R. J.; Zrnic, D. S. (1993). *Doppler Radar and Weather Observations* (2nd ed.). San Diego CA: Academic Press. ISBN 0-12-221420-X.
- Environment Canada. 2015. National Climate data and Information Archive. Canadian Climate Normals 1971-2016. Exeter, Ontario. Retrieved from
- Finch, J.W., 1998. Estimating direct groundwater recharge using a simple water balance model - sensitivity to land surface parameters. *J. Hydrol.* 211, 112–125. doi:10.1016/S0022-1694(98)00225-X
- Fleckenstein, J.H., Niswonger, R.G., Fogg, G.E., 2006. River-aquifer interactions, geologic heterogeneity, and low-flow management, in: *Ground Water*. pp. 837–852. doi:10.1111/j.1745-6584.2006.00190.x
- Flury, M., Flühler, H., Jury, W. a., Leuenberger, J., 1994. Susceptibility of soils to preferential flow of water: A field study. *Water Resour. Res.* 30, 1945. doi:10.1029/94WR00871
- Frind, E.O., Molson, J.W., Rudolph, D.L., 2006. Well vulnerability: A quantitative approach for source water protection. *Ground Water*. doi:10.1111/j.1745-6584.2006.00230.x
- Gerhart JM (1986) Ground-water recharge and its effect on nitrate concentrations beneath a manured field site in Pennsylvania. *Ground Water* 24:483–389
- Hanson, R. T., and J. F. Benedict (1994), Simulation of ground-water flow and potential land subsidence, upper Santa Cruz basin, Arizona, U.S. Geol. Surv. Water Resour. Invest. Rep. 93–4196, 47 pp.
- Haslauer, C., 2005. Hydrogeologic Analysis of a Complex Aquifer System and Impacts of Changes in Agricultural Practices on Nitrate Concentrations in a Municipal Well Field: Woodstock, Ontario 185.
- Haws, N.W., Liu, B., Boast, C.W., Rao, P.S.C., Kladvko, E.J., Franzmeier, D.P., 2004. Spatial variability and measurement scale of infiltration rate on an agricultural landscape. *Soil Sci. Soc. Am. J.* 68, 1818–1826.
- Healy, R.W., Cook, P.G., 2002a. Using groundwater levels to estimate recharge. *Hydrogeol. J.* 10, 91–109. doi:10.1007/s10040-001-0178-0
- Healy, R.W., Cook, P.G., 2002b. Using groundwater levels to estimate recharge. *Hydrogeol. J.* 10, 91–109. doi:10.1007/s10040-001-0178-0
- Hendrickx, J.M.H., Flury, M., 2001. Uniform and preferential flow mechanisms in the vadose zone. *Concept. Model. flow Transp. Fract. vadose Zo.* Washington, DC 149–187.
- Hogan, J.F., Phillips, F.M., Scanlon, B.R., 2004. *Groundwater Recharge in a Desert Environment: the Southwestern United States*, American Geophysical Union.
- Hopmans, J.W., Smu°nek, J., 1997. Review of inverse estimation of soil hydraulic properties. In: van Genuchten, Th, M., Leij, F.J., Wu, L. (Eds.), *Characterization and Measurement of Hydraulic Properties of Unsaturated Porous Media*. University of California, Riverside, CA, pp. 643–660.

- Hornero, J., Manzano, M., Ortega, L., Custodio, E., 2016. Integrating soil water and tracer balances, numerical modelling and GIS tools to estimate regional groundwater recharge: Application to the Alcadozo Aquifer System (SE Spain). *Sci. Total Environ.* 568, 415–432. doi:10.1016/j.scitotenv.2016.06.011
- Iwata, Y., Hayashi, M., Suzuki, S., Hirota, T., Hasegawa, S., 2010. Effects of snow cover on soil freezing, water movement, and snowmelt infiltration: A paired plot experiment. *Water Resour. Res.* 46, 1–11. doi:10.1029/2009WR008070
- Iwata, Y., and T. Hirota (2005a), Development of tensiometer for monitoring soil-water dynamics in a freezing and snow covered environment, *J. Agric. Meteorol.*, 60, 1065–1068.
- Iwata, Y., and T. Hirota (2005b), Monitoring over-winter soil water dynamics in a freezing and snow covered environment using thermally insulated tensiometer, *Hydrol. Processes*, 19,3013–3019, doi:10.1002/hyp.5813.
- Iwata, Y., M. Hayashi, and T. Hirota (2008a), Comparison of snowmelt infiltration under different soil-freezing conditions influenced by snow cover, *Vadose Zone J.*, 7,79–86, doi:10.2136/vzj2007.0089.
- Iwata, Y., M. Hayashi, and T. Hirota (2008b), Effects of snow cover on soil heat flux and freeze-thaw processes, *J. Agric. Meteorol.*, 64,301–309, doi:10.2480/agrmet.64.4.12.
- Jackson, T. J. (2002), Remote sensing of soil moisture: Implications for groundwater recharge, *Hydrogeol. J.*, 10, 40–51, doi:10.1007/s10040-001-0168-2.
- Jyrkama, M.I., Sykes, J.F., 2007. The impact of climate change on spatially varying groundwater recharge in the grand river watershed (Ontario). *J. Hydrol.* 338, 237–250. doi:10.1016/j.jhydrol.2007.02.036
- Kite GW (1995) The SLURP model. In: Singh VP (ed) Computer models of watershed hydrology. Water Resources Publications, Highlands Ranch, Colorado, pp 521–562
- Koch, J.T., 2009. Evaluating Regional Aquifer Vulnerability and BMP Performance in an Agricultural Environment Using A Multi-Scale Data Integration Approach 278.
- Liu, Y., Yamanaka, T., Zhou, X., Tian, F., Ma, W., 2014. Combined use of tracer approach and numerical simulation to estimate groundwater recharge in an alluvial aquifer system: A case study of Nasunogahara area, central Japan. *J. Hydrol.* 519, 833–847. doi:10.1016/j.jhydrol.2014.08.017
- Lu, X., Jin, M., Van Genuchten, M.T., Wang, B., 2011. Groundwater Recharge at Five Representative Sites in the Hebei Plain, China. *Ground Water* 49, 286–294. doi:10.1111/j.1745-6584.2009.00667.x
- Meinzer OE, Stearns ND (1929) A study of ground water in the Pomperaug Basin, Connecticut, with special reference to intake and discharge. US Geol Surv Water-Supply Pap 597B:73–146
- Metcalf, J. R., Ishida, S., & Goodison, B. E. (1994). A corrected precipitation archive for the Northwest Territories of Canada. In Stewart Cohen (Ed.), Mackenzie Basin Impact Study, Interim Report #2 –

Proceedings of the sixth biennial AES-DIAND meeting of Northern Climate & Mid Study Workshop of the Mackenzie Basin Impact Study, Yellowknife, Northwest Territories (Canada)

Missori, 2015. Study of hydrogeologic characterization of a glaciofluvial aquifer of Ontario (Canada): A comparison of field and laboratory methods to estimate hydraulic conductivity in heterogeneous porous media

Niswonger, R.G., Prudic, D.E., Pohl, G., Constantz, J., 2005. Incorporating seepage losses into the unsteady streamflow equations for simulating intermittent flow along mountain front streams. *Water Resour. Res.* 41 (6), W06006

Nakhaei, M., Šimůnek, J., 2014. Parameter estimation of soil hydraulic and thermal property functions for unsaturated porous media using the HYDRUS-2D code. *J. Hydrol. Hydromech* 62, 7–15.  
doi:10.2478/johh-2014-0008

Okkonen, J., Kløve, B., 2011. A sequential modelling approach to assess groundwater-surface water resources in a snow dominated region of Finland. *J. Hydrol.* 411, 91–107.  
doi:10.1016/j.jhydrol.2011.09.038

Padusenko, G.R., 2001 Regional hydrogeologic evaluation of a complex glacial aquifer system in an agricultural landscape : implications for nitrate distribution

Rasmussen WC, Andreasen GE (1959) Hydrologic budget of the Beaverdam Creek Basin, Maryland. *US Geol Surv Water-Supply Pap* 1472:106

Rudolph, D.L., Devlin, J. F. and Bekeris, L., 2015. Challenges and a strategy for agricultural BMP monitoring and remediation of nitrate contamination in unconsolidated aquifers. *Ground Water Mon. and Remediation*, 35, no.1, Winter 2015, 97-109.

Ronan, A.D., Prudic, D.E., Thodal, C.E., Constantz, J., 1998. Field study and simulation of diurnal temperature effects on infiltration and variably saturated flow beneath an ephemeral stream. *Water Resour. Res.* 34 (9), 2137–2153

Saxton, Keith E. 2002. *Soil-Plant-Atmosphere-Water Field and Pond Hydrology, User's Manual* version 6.1. USDA-ARS, Washington State University.

Scanlon, B.R., Healy, R.W., Cook, P.G., 2002. Choosing appropriate techniques for quantifying groundwater recharge. *Hydrogeol. J.* 10, 18–39. doi:10.1007/s10040-001-0176-2

Scanlon, B.R., Healy, R.W., Cook, P.G., 2002. Choosing appropriate techniques for quantifying groundwater recharge (vol 10, pg 18, 2002). *Hydrogeol. J.* 10, 347. doi:Doi 10.1007/S10040-002-0200-1

Schaap, M. 2003. Rosetta help file: Predicting soil hydraulic parameter from basic soil data. Rosetta Lite Version 1.1. George E. Brown Jr. Salinity Laboratory and UC Riverside, Department of Environmental Sciences

Scott, R. L., W. J. Shuttleworth, T. O. Keefer, and A. W. Warrick (2000), Modeling multiyear observations of soil moisture recharge in the semi- arid American Southwest, *Water Resour. Res.*, 36, 2233 – 2247, doi:10.1029/2000WR900116

Shanafield, M., Niswonger, R. G., Prudic, D. E., Pohll, G., Susfalk, R., & Panday, S. (2014). A method for estimating spatially variable seepage and hydraulic conductivity in channels with very mild slopes. *Hydrological Processes*, 28(1), 51–61. <https://doi.org/10.1002/hyp.9545>

Shanafield, M., Cook, P.G., 2014. Transmission losses, infiltration and groundwater recharge through ephemeral and intermittent streambeds: A review of applied methods. *J. Hydrol.* 511, 518–529. doi:10.1016/j.jhydrol.2014.01.068

Sharma ML, Cresswell ID, Watson JD (1985) Estimates of natural groundwater recharge from the depth distribution of an applied tracer, subsurface flow, pollutant transport, and salinity. In: Proc Natl Conf Institute of Engineers, Melbourne, Victoria, Australia, Publ 85/13, pp 64–70

Sharma ML (1989) Groundwater recharge. AA Balkema, Rotterdam

Shentsis, I., Rosenthal, E., 2003. Recharge of aquifers by flood events in an arid region. *Hydrol. Process.* 17 (4), 695–712

Shentsis, I., Meirovich, L., Ben-Zvi, A., Rosenthal, E., 1999. Assessment of transmission losses and groundwater recharge from runoff events in a wadi under shortage of data on lateral inflow, Negev, Israel. *Hydrol. Process.* 13 (11), 1649–1663

Šimůnek, J., M. Šejna, a, Saito, H., Sakai, M., Genuchten, M.T. Van, 2013. The HYDRUS-1D Software Package for Simulating the Movement of Water, Heat, and Multiple Solutes in Variably Saturated Media, Version 4.17, HYDRUS Software Series 3, 343.

Singh VP (1995) Computer models of watershed hydrology Resources Publications, Highlands Ranch, Colorado

Smith, G. E. P. (1910), Groundwater supply and irrigation in the Rillito Valley: Tucson, AZ, Bull. 64, pp. 81– 243, Univ. of Arizona Agric. Exp. Stn., Tucson.

Sophocleous, M., 2002. Interactions between groundwater and surface water: The state of the science. *Hydrogeol. J.* 10, 52–67. doi:10.1007/s10040-001-0170-8

Sorman, A.U., Abdulrazzak, M.J., 1993. Infiltration-recharge through wadi beds in arid regions. *Hydrol. Sci. J.* 38 (3), 173–186

Sorman, A.U., Abdulrazzak, M.J., Morel-Seytoux, H., 1997. Groundwater recharge estimation from ephemeral streams. Case study: Wadi Tabalah, Saudi Arabia. *Hydrol. Process.* 11 (12), 1607–1619

- Sousa, M. R., Jones, J. P., Frind, E. O., & Rudolph, D. L. (2013). A simple method to assess unsaturated zone time lag in the travel time from ground surface to receptor. *Journal of contaminant hydrology*, 144(1), 138-151
- Stewart-deaker, B.A.E., Stonestrom, D. a, Moore, S.J., 2000. Streamflow , Infiltration , and Ground-Water Recharge at Abo Arroyo , New Mexico. USGS Prof. Pap. 1703.
- Stonestrom, D.A., Constantz, J., Ferré, T., Leake, S.A., 2007. "Ground-Water Recharge in the Arid and Semiarid Southwestern United States". US Geological Survey professional paper(1703).
- Subyani, A.M., 2004. Use of chloride-mass balance and environmental isotopes for evaluation of groundwater recharge in the alluvial aquifer, Wadi Tharad, western Saudi Arabia. *Environ. Geol.* 46 (6), 741–749
- Turnadge, C., Smerdon, B.D., 2014. A review of methods for modelling environmental tracers in groundwater: Advantages of tracer concentration simulation. *J. Hydrol.* doi:10.1016/j.jhydrol.2014.10.056
- Twarakavi, N.K.C., Šimůnek, J., Seo, S., 2008. Evaluating Interactions between Groundwater and Vadose Zone Using the HYDRUS-Based Flow Package for MODFLOW. *Vadose Zo. J.* doi:10.2136/vzj2007.0082
- van Genuchten, M. Th., F. J. Leij, and S. R. Yates. 1991. The RETC code for quantifying the hydraulic functions of unsaturated soils. Robert S. Kerr Environmental Research Laboratory, Office of Research and Development, U. S. Environmental Protection Agency, Ada, OK.
- Van Der Kamp, G., Hayashi, M., 1998. 1998 GPR vanderkamp&Hayashi-wetland recharge.pdf. *Gt. Plains Res.*
- Vereecken, H., Huisman, J.A., Bogena, H., Vanderborght, J., Vrugt, J.A., Hopmans, J.W., 2010. On the value of soil moisture measurements in vadose zone hydrology: A review. *Water Resour. Res.* 46. doi:10.1029/2008WR006829
- Wendt, S. 2005. Hydraulic parameter investigation and ID-modelling of water flow and solute transport in the vadose zone of the Thornton well field in Woodstock, Ontario, Canada. Student Project in Hydrogeology, Waterloo, Ontario: Department of Earth Sciences , University of Waterloo.
- Wicklund, R. E., and N. R. Richards, 1961. The Soil Survey of Oxford County: Report No. 28. Ontario: Ontario Soil Survey, Research Branch, Canada Department of Agriculture and the Ontario Agricultural College.
- Wilson, L. G., K. J. DeCook, and S. P. Neuman (1980), Regional recharge research for southwest alluvial basins, *Water Resour. Res. Cent.*, Univ. of Ariz., Ariz., Tucson.
- Winter, T.C., Harvey, J.W., Franke, O.L., Alley, W.M., 1998. Ground water and surface water: A single resource. USGS Publ. 79.

Woo, M. K., and T. C. Winter (1993), The role of permafrost and seasonal frost in the hydrology of northern wetlands in North America, *J. Hydrol.*, 141, 5 – 31.

Xu, Y., Beekman, H.E., 2003. Groundwater Recharge Estimation in Southern Africa, Challenges. doi:10.3109/00016486709127791

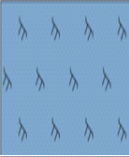


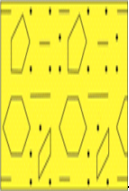



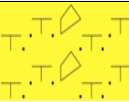
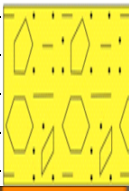

Yeh, T.-C.J., Šimůnek, J., 2002. Stochastic Fusion of Information for Characterizing and Monitoring the Vadose Zone. *Vadose Zo. J.* doi:10.2136/vzj2002.0207

Young MH, Wierenga PJ, Mancino CF (1996) Large weighing lysimeters for water use and deep percolation studies. *Soil Sci Soc Am J* 161:491–501





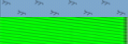












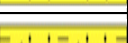





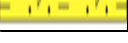


## **Appendices**



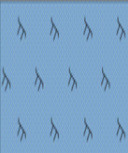

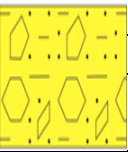





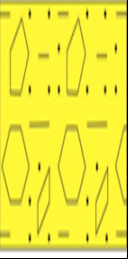

## **Appendix A: Soil Cores**














Core 1			
Depth (m)	Lithology	USCS	Lithological Description
0		PT	Topsoil; Organics, dark brown, moist
0.1			
0.2			
0.3		PT	Topsoil; very dark brown, silty-sand
0.4			
0.5		SC	Silty-Clay: Light brownish, contains medium sand, moist
0.6			
0.7		GP	Sandy Gravel: Medium to coarse gravel size 2-5cm, dry
0.8			
0.9			
1			
1.1		Miss	MISSING: Poor Recovery
1.2			
1.3			
1.4		GP	Sandy Gravel: Medium brown, well graded, increasing particle size
1.5			
1.6		SC	Silty-Clay: Light brownish, contains medium sand, moist
1.7			
1.8			Silty Sand: Some gravel similar grain size as above, wet
1.9			
2		GP	Sandy Gravel: fine to medium gravel size <2cm, wet
2.1			
2.2			
2.3			
2.4			
2.5			
2.6			
2.7			
2.8			

Core 2			
Depth (m)	Core No. and Lithology	USCS	Lithological Description

0			
0.1		PT	Topsoil; Organics, dark brown, moist
0.2			
0.3			
0.4		PT	Topsoil; very dark brown, silty-sand
0.5		CL	Clayey Silt, meadium to dark brown
0.6		SC	Silty-Clay: some fine gravel
0.7			
0.8		GP	Sandy Gravel: Medium gravel size <2cm, wet
0.9			
1		GP	Sandy Gravel: Medium to coarse gravel size >2cm, moist
1.1			
1.2			
1.3		Miss	MISSING: Poor Recovery
1.4			
1.5		GP	Sandy Gravel: fine to medium gravel
1.6			
1.7		GP	Sandy Gravel: large gravel >5 cm
1.8			
1.9			
2			
2.1			
2.2			
2.3		GP	Sandy Gravel: well mixed, wet, aquifer
2.4			
2.5			

Core 3			
Depth (m)	Core No. and Lithology	USCS	Lithological Description

0			
0.1		PT	Topsoil; Organics, dark brown, wet
0.2			
0.3			
0.4		CL	Clayey Silt, meadium to dark brown
0.5			
0.6			
0.7		GP	Sandy Gravel: Large gravel size <2cm, moist
0.8			
0.9		GP	Sandy Gravel: Shale/sandstone, layered deposit, moist
1		GP	Sandy Gravel: medium gravel, wet
1.1			
1.2			MISSING: Poor Recovery
1.3		Miss	
1.4			
1.5		GP	Sandy Gravel: coarse gravel
1.6			
1.7		GP	Sandy Gravel:medium to fine gravel
1.8			
1.9			
2			
2.1			
2.2			
2.3		GP	Sandy Gravel: Medium to Coarse Gravel, wet
2.4			
2.5			
2.6			MISSING: Poor Recovery
2.7		Miss	
2.8			

Core 4			
Depth (m)	Lithology	USCS	Lithological Description
0.1		PT	Topsoil; Organics, dark brown, wet
0.3		GP	Sandy Gravel: medium gravel size <2cm, moist
0.5		GP	Sandy Gravel: more sand, medium to fine gravel size, moist to dry
0.7		GP	Sandy Gravel: coarse gravel
0.9			
1.1		GP	Sandy Gravel: coarse gravel, reddish brown, dry
1.3		Miss	MISSING: Poor Recovery
1.5			Sandy Gravel: coarse gravel
1.7			
1.9			
2.1		GP	Sandy Gravel: well mixed, aquifer
2.3			
2.5			

Core 5			
Depth (m)	Lithology	USCS	Lithological Description

0		PT	Topsoil; Organics, dark brown, wet
0.1			
0.2		GP	Sandy Gravel: more sand, medium to fine gravel size, moist to dry
0.3			
0.4			
0.5			
0.6		GM	Gravelly Silt: medium sand
0.7			
0.8			
0.9			
1		GP	Sandy Gravel: coarse gravel, reddish brown, dry
1.1			
1.2		Miss	MISSING: Poor Recovery
1.3			
1.4			
1.5		GP	Sandy Gravel: coarse gravel
1.6			
1.7			
1.8			
1.9			
2			
2.1		GP	Sandy Gravel: well mixed, aquifer
2.2			
2.3			
2.4		Miss	MISSING: Poor Recovery
2.5			
2.6			
2.7			

## **Appendix B: Neutron Probe Calibration (Bekeris, 2007)**

**Description:** Soil water content was estimated with the Model 503 DR Hydroprobe Neutron Moisture Probe (CPN International Inc.). The probe uses 50mCi Americium-241/Beryllium as a source of fast neutrons, and measures the proportion of emitted fast neutrons that are redirected to the probe as slow neutrons after colliding with the hydrogen atoms in the water molecule. Moisture content is usually determined from the neutron probe count ratio (CR; raw neutron count/neutron count in a standard medium) using a linear calibration equation. In order to collect CRs, the neutron moisture probe is lowered down an access tube at user-specified intervals. At each measurement point along the profile, the probe emits fast neutrons and measures reflected slow neutrons.

**Calibration:** The 503 DR Hydroprobe was supplied with a factory calibration equation for measurements taken in a 5-cm (2-in) PVC access tube. Literature suggests, however, that site- and soil-specific calibrations are necessary for reliable measurements (Yao et al., 2004; Greacen et al., 1981). Therefore a field calibration program was conducted in the study area on November 17 and 18, 2005, and was based on the comparison of probe measurements in several newly-installed access tubes with the volumetric water content of the core collected during tube installation. These access tubes are not included in the set installed for regular water content measurements as described in Section 3.1.4.

The locations of the calibration access tubes were Recharge Stations 2, 4 and 5. At each station, a Vibra-Push® direct push rig equipped with the Enviro-Core® sampling system was used to advance a 5-cm (2-in) diameter borehole and collect continuous geologic core. The 0.9- m (3-ft) long core samples were sealed in the field to preserve moisture content and refrigerated at the University of Waterloo until analysis as described below. A 5-cm (2-in) diameter Schedule 40 PVC riser pipe with a bottom cap was fitted snugly into the borehole. Air space and surface water leakage between the access tube and the geologic material were minimized to ensure representative measurements. The riser pipe was cut at 0.2 m above ground surface and raw neutron counts were measured at 0.1-m intervals along the access tube within 30 minutes of installation. The standard count of the neutron probe was determined in the field using the probe shield as an adsorber before the field measurements began.

The geologic cores from the access tube boreholes were subsequently sampled at 0.1 m intervals and analyzed in the laboratory for volumetric water content (VWC) and bulk density as described in Section 3.3.

**Analysis.** To determine the site-specific calibration equation for the neutron probe, the CR at each measurement point was compared to the corresponding VWC determined from the core samples. The radius of influence of the probe is approximately 0.15 m (Greacen et al., 1981); therefore for the CR measured at a given depth, the corresponding VWC was calculated as the average of the VWC measurements at that depth, 0.1 m above and 0.1 m below that depth. In the case where core material was missing from the core tube, one or two VWC measurements were used instead of three, with the measurement at the depth of the CR weighted twice as much as the adjacent VWC value. If the VWC could not be accurately estimated due to loss of a non-cohesive material from the core tube, the CR/VWC data pair was excluded from the analysis.

VWC was then regressed on CR to determine the calibration equation. This is contrary to Greacen et al.'s (1981) recommendation to regress CR on VWC based on greater confidence in



and reliability of VWC measurements. In this study, as in Grismer et al.'s (1995), greater reliability was assigned to CR values, due to their reproducibility and the potential error associated with having only one VWC measurement at each depth.

Two additional corrections to the calibration data recommended in the literature were also applied and evaluated for their effect on the calibration equation. A correction for soil bulk density was recommended by Greacen and Hignett (1976) to account for the potential "trapping" of fast neutrons in higher density material. Based on an empirical relationship between count rate at constant VWC and the square root of density, the correction factor to CR was  $(p_b/p_{bi})^{1/2}$  where  $p_b$  is the average bulk density at the site and  $p_{bi}$  is the soil bulk density at a given depth. The regression of VWC on CR was repeated after this adjustment.

The presence of constitutionally bound hydrogen in clay minerals and organic matter also affects the response of the neutron moisture probe. The equivalent water content of hydrogen may be estimated as  $0.124(\pm 0.012)C + 0.015$ , where C is the fractional clay content of the soil (Greacen et al., 1981). The maximum clay content of any of the site materials is 10-15%, which corresponds to  $\rho_e$  of approximately 2.7 to 3.4%. The regression was repeated after increasing the overall VWC for materials assumed to have clay content of >10% by 3%, to reflect the  $\rho_e$  contribution.

*Results.* The uncorrected VWC and CR data are shown in Figure B.1. The calibration equation ( $r^2 = 0.83$ ) for the conversion of CR to VWC is

$$VWC = 35.8(\pm 3.4) \cdot CR - 10.1(\pm 2.7) \quad (B.1)$$

where

VWC is the volumetric water content (percentage)  
 CR is the count ratio (raw neutron count/standard count)

For the density correction, an average  $P_b$  of  $1.8 \text{ g/cm}^3$  was calculated from the laboratory analysis of all the samples. The ranges for  $P_{bi}$  and  $(p_b/p_{bi})^{1/2}$  were 1.2 to  $2.6 \text{ g/cm}^3$  and 0.8 to 1.2, respectively. Applying the density correction reduced the  $r^2$  value from 0.83 to 0.74 and yielded the following calibration equation:

$$VWC = 33.7(\pm 4.1) \cdot CR - 8.4(\pm 3.3) \quad (B.2)$$

The coefficients in the density-corrected equation are within the 95% confidence interval of the uncorrected equation. Applying the density correction to the calibration would require that subsequent neutron probe measurements at the site be corrected for density, and density values along the entire profile of every access tube are unknown. Given this limitation and the reduction in the correlation coefficient, the density correction was omitted from the final calibration. Grismer et al. (1995) also found that the density correction were of limited value for field calibrations.

When the correction for clay content was applied to the original uncorrected data, the correlation coefficient was unchanged (0.83) and again the coefficients of the calibration equation fell within the 95% confidence interval of the uncorrected data:

$$VWC = 39.0(\pm 3.6) \cdot CR - 11.4(\pm 3.0) \quad (B.3)$$

Given the limited benefit of applying this correction and the increased labour required to correct all future readings for clay content, this correction was also omitted for the final calibration. Consequently the final site-specific calibration equation for the neutron moisture probe is Equation B.1.

A soil-specific calibration was also attempted for each of the clay, silt, fine sand and well-graded sand units common to the site. This analysis required subsets of the uncorrected data set, grouped by soil type and limited to CRs at points more than 0.15 m from soil type interfaces and their associated VWC data. This criterion was applied to encompass the 0.15 m radius of influence of the probe and to avoid bias related to averaging across different units. The distribution of soil-specific data is shown in Figure B.2. Linear regression was attempted on the individual data sets for each soil type, but the data sets were found to be too limited in range to be used for soil-specific calibration. The data set for silty clay, for example, consisted of 22 data pairs, 18 of which were clustered between 20 and 24% VWC. The soil-specific calibration was not possible for the available data set. Although the use of one equation for all soil types may result in decreased accuracy (Yao et al., 2004), it is convenient for sites where the detailed stratigraphy and soil characteristics along each access tube are unknown.

Additional sources of error in the derivation of the calibration equation include:

- Spatial variability in the soil water content, which limits the accuracy of comparing volumetric water content of material collected from the access tube hole to the neutron counts of the material surrounding the access tube;
- Compaction of the soil around the tube during installation.

Although there are numerous neutron probe calibration efforts described in the literature, few of these employed PVC access tubes. Yao et al. (2004) conducted soil-specific calibrations for a vertically-stratified vadose zone using two-inch Sch. 40 PVC access tubes. For a general calibration line fitted through all soil types, they reported a similar slope (38.6) as in this calibration but a significantly different intercept (-30). Their soil-specific calibration lines had significantly shallower slopes than the general calibration. The fact that Yao et al. reported a

similar range of measured water content values as in this calibration, but count ratios that ranged from 1 to 1.6, as compared to 0.4 to 1.3 here, suggests that other elements of the installation, sampling, or measurement processes differed between the two studies, or there are variations in site characteristics that preclude comparison of the results. For example, Yao et al. obtained standard count measurements with the probe at 2 m depth in an access tube, which may have yielded different standard count values compared to this study and consequently may have affected the slope of the calibration line.

**Large diameter tube calibration:** A separate analysis of the calibration data was conducted to derive a calibration equation for the larger 7.5 cm (3 in) diameter access tubes present at the site. The use of 7.5 cm access tubes is not ideal, as the larger diameter increases neutron loss and the potential for eccentric positioning of the probe (Greacen et al., 1981). The 7.5 cm tubes, however, are deeper on average than the 5 cm tubes and offer additional information about the general water content profile at each station.

The 7.5 cm tube calibration followed the method described for the 5 cm tubes described above. The raw neutron counts were measured in the existing 7.5 cm tubes at Stations 2, 4 and 5 at the time of installation of the 5 cm calibration tubes and collection of geologic core. The maximum distance between the 7.5 cm access tube and the 5 cm hole at each station was approximately one metre. The data is plotted in Figure B.3. The calibration equation ( $t' = 0.75$ ) for the 7.5 cm tubes is

$$VWC = 54.7(\pm 7.2) \cdot CR - 17.1(\pm 4.3) \tag{B.4}$$

In addition to the potential errors associated with the use of a 7.5 cm tube described above, this calibration is also limited by the fact that the gravimetric moisture content values were measured on core material from a borehole approximately one metre from the 7.5 cm tube.

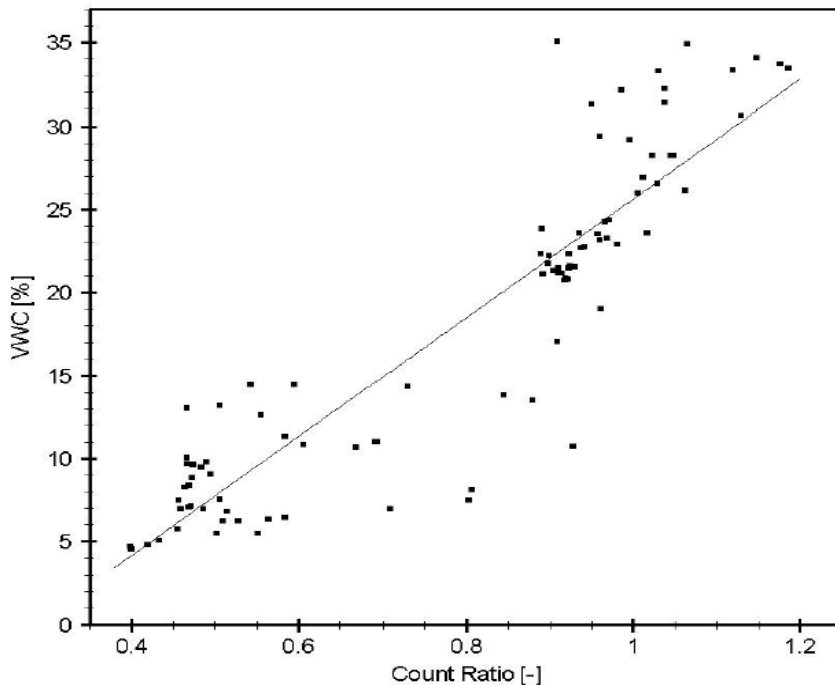


Figure B.1. Calibration data for 5-cm access tube

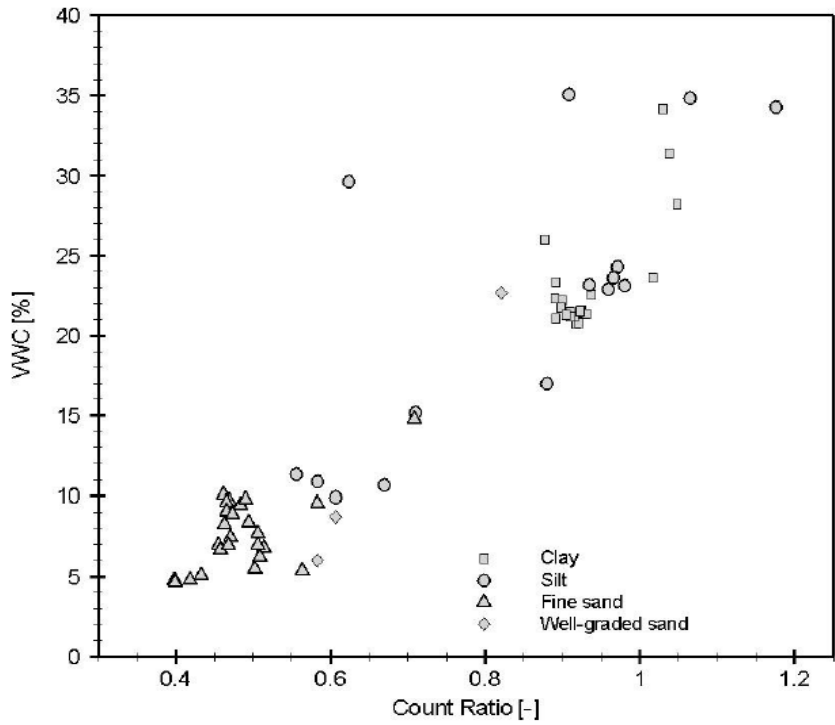


Figure B.2. Soil-specific calibration data (5-cm access tube)

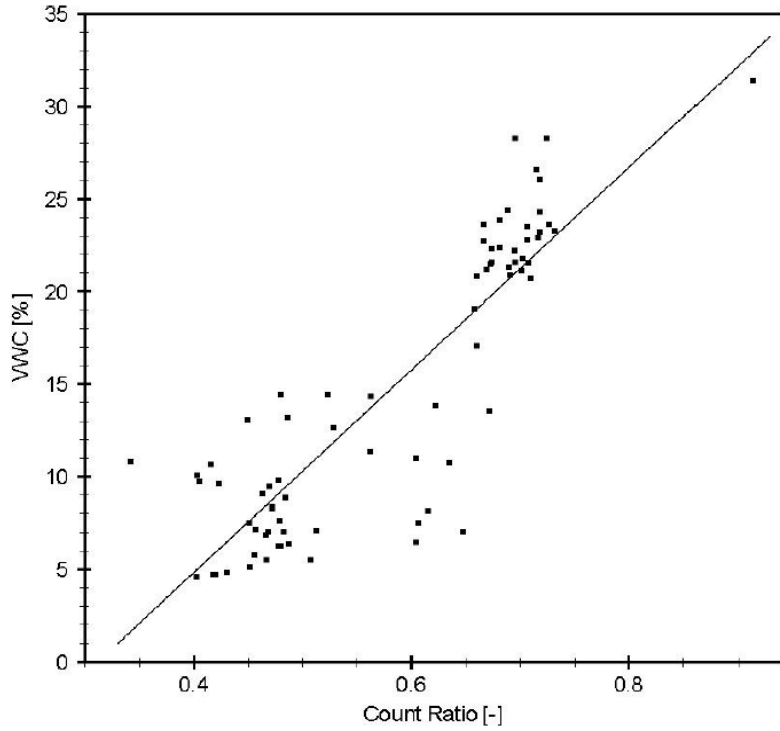


Figure B.3. Calibration data for 7.5-cm access tube

## **Appendix C: Grain Size Distribution (Missori, 2015)**



Grain Size Analysis Report

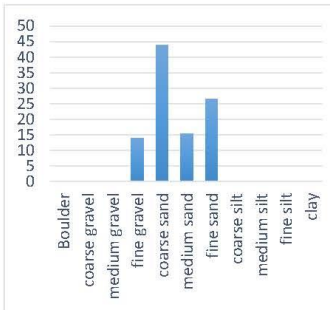
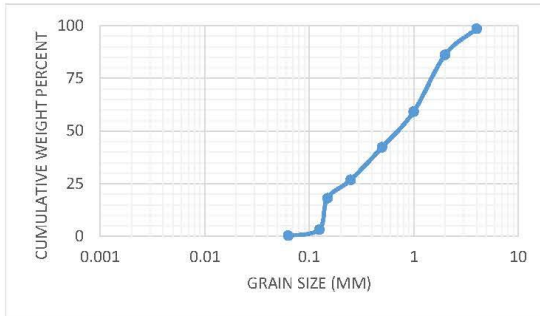
Date: 23 June 2015

Sample Name: Core 3 -1

Mass Sample (g): 67.8

T (oC) 20

Poorly sorted gravelly sand low in fines



Sieve opening (ps) d <sub>i</sub> (mm)	Mass of retained (mr) (g)	mass fraction (mf)	Percent Passing (pp)
4	1	0.014749	98.52507
2	8.4	0.123894	86.13569
1	18.3	0.269912	59.14454
0.5	11.4	0.168142	42.33038
0.25	10.5	0.154867	26.84366
0.15	5.9	0.087021	18.14159
0.125	10.1	0.148968	3.244838
0.063	2	0.029499	0.294985
	0.2	0.002	0

Effective Grain Diameters (mm)		Other Useful Parameters	
d <sub>10</sub>	0.136	Uniformity Coef.	7.57
d <sub>17</sub>	0.148	n computed	0.32
d <sub>20</sub>	0.171	g (cm/s <sup>2</sup> )	980.00
d <sub>50</sub>	0.728	ρ (g/cm <sup>3</sup> )	0.9981
d <sub>60</sub>	1.032	μ (g/cm s)	0.0098
de (Kruger)	0.257	ρg/μ (1/cm s)	9.9327E+04
de (Kozeny)	0.235	tau (Sauerbrei)	1.053
de (Zunker)	0.242	d <sub>geometric mean</sub>	0.589
de (Zamarin)	0.250	σ <sub>φ</sub>	1.647
lo (Alyameni)	-0.073		
mm	0	% in sample	
>64	Boulder		
16 - 64	coarse gravel		
8 - 16	medium gravel		
2 - 8	fine gravel		13.86430678
0.5 - 2	coarse sand		43.80530973
0.25 - 0.5	medium sand		15.48672566
0.063 - 0.25	fine sand		26.54867257
0.016 - 0.063	coarse silt		
0.008 - 0.016	medium silt		
0.002 - 0.008	fine silt		
<0.002	clay		



Grain Size Analysis Report

Date:

25 June 2015

Sample Name:

Core 3-2

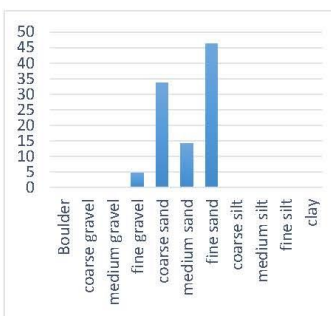
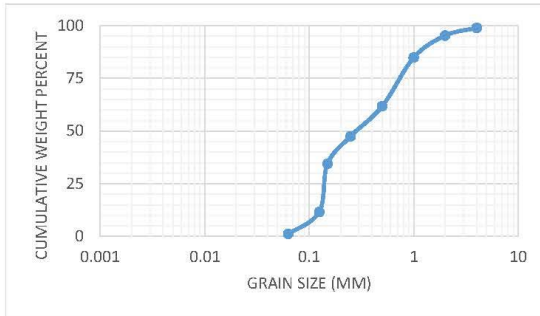
Mass Sample (g):

57.2

T (oC)

20

Moderately well sorted sand low in fines



Sieve opening (ps) d <sub>i</sub> (mm)	Mass of retained (mr) (g)	mass fraction (mf)	Percent Passing (pp)
4	0.6	0.01049	98.95105
2	2.1	0.036713	95.27972
1	6	0.104895	84.79021
0.5	13.2	0.230769	61.71329
0.25	8.1	0.141608	47.55245
0.15	7.5	0.131119	34.44056
0.125	13.1	0.229021	11.53846
0.063	5.9	0.103147	1.223776
	0.7	0.012238	0

Effective Grain Diameters (mm)		Other Useful Parameters	
d <sub>10</sub>	0.116	Uniformity Coef.	4.06
d <sub>17</sub>	0.131	n computed	0.37
d <sub>20</sub>	0.134	g (cm/s <sup>2</sup> )	980.00
d <sub>50</sub>	0.293	ρ (g/cm <sup>3</sup> )	0.9981
d <sub>60</sub>	0.470	μ (g/cm s)	0.0098
d <sub>e</sub> (Kruzer)	0.205	ρg/μ (1/cm s)	9.9327E+04
d <sub>e</sub> (Kozeny)	0.188	tau (Sauerbrei)	1.053
d <sub>e</sub> (Zunker)	0.193	d <sub>geometric mean</sub>	0.335
d <sub>e</sub> (Zamarin)	0.199	σ <sub>φ</sub>	1.416
lo (Alyameni)	0.046		
mm		0	% in sample
>64		Boulder	
16 - 64		coarse gravel	
8 - 16		medium gravel	
2 - 8		fine gravel	4.72027972
0.5 - 2		coarse sand	33.56643357
0.25 - 0.5		medium sand	14.16083916
0.063 - 0.25		fine sand	46.32867133
0.016 - 0.063		coarse silt	
0.008 - 0.016		medium silt	
0.002 - 0.008		fine silt	
<0.002		clay	



Grain Size Analysis Report

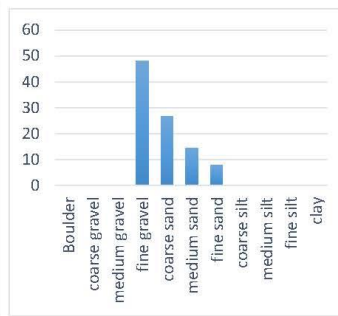
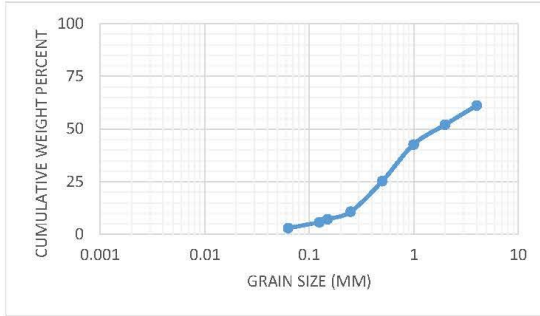
Date: 23 June 2015

Sample Name: Core 3 -3

Mass Sample (g): 107.6

T (oC) 20

Poorly sorted gravelly sand low in fines



Sieve opening (ps) d <sub>i</sub> (mm)	Mass of retained (mr) (g)	mass fraction (mf)	Percent Passing (pp)
4	41.8	0.388476	61.15242
2	9.8	0.091078	52.04461
1	10.1	0.093866	42.65799
0.5	18.8	0.174721	25.18587
0.25	15.5	0.144052	10.78067
0.15	3.8	0.035316	7.249071
0.125	1.6	0.01487	5.762082
0.063	3	0.027881	2.973978
	3.2		0

Effective Grain Diameters (mm)		Other Useful Parameters	
d <sub>10</sub>	0.228	Uniformity Coef.	16.44
d <sub>17</sub>	0.358	n computed	0.27
d <sub>20</sub>	0.410	g (cm/s <sup>2</sup> )	980.00
d <sub>50</sub>	1.782	ρ (g/cm <sup>3</sup> )	0.9981
d <sub>60</sub>	3.747	μ (g/cm s)	0.0098
d <sub>e</sub> (Kruzer)	0.522	ρg/μ (1/cm s)	9.9327E+04
d <sub>e</sub> (Kozeny)	0.480	tau (Sauerbrei)	1.053
d <sub>e</sub> (Zunker)	0.492	d <sub>g</sub> geometric mean	1.494
d <sub>e</sub> (Zamarin)	0.505	σ <sub>φ</sub>	1.889
l <sub>o</sub> (Alyameni)	-0.489		
mm		0	% in sample
>64		Boulder	
16 - 64		coarse gravel	
8 - 16		medium gravel	
2 - 8		fine gravel	47.95539033
0.5 - 2		coarse sand	26.85873606
0.25 - 0.5		medium sand	14.40520446
0.063 - 0.25		fine sand	7.80669145
0.016 - 0.063		coarse silt	
0.008 - 0.016		medium silt	
0.002 - 0.008		fine silt	
<0.002		clay	





Grain Size Analysis Report

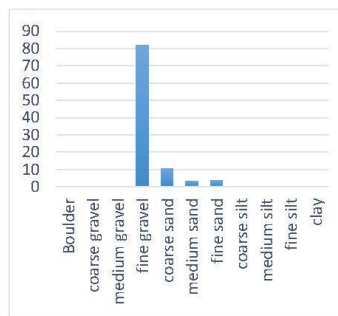
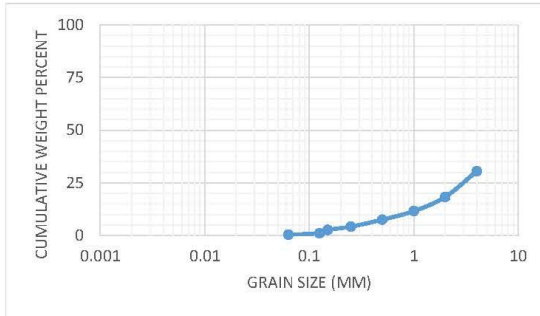
Date: 23 June 2015

Sample Name: Core 3 -1

Mass Sample (g): 132.7

T (oC) 20

Poorly sorted sandy gravel low in fines



Sieve opening (ps) di (mm)	Mass of retained (mr) (g)	mass fraction (mf)	Percent Passing (pp)
4	92.2	0.6948	30.51997
2	16.2	0.12208	18.31198
1	8.9	0.067069	11.60512
0.5	5.4	0.040693	7.535795
0.25	4.4	0.033157	4.220045
0.15	2.1	0.015825	2.637528
0.125	2.1	0.015825	1.055011
0.063	0.8	0.006029	0.452148
	0.6		0

Effective Grain Diameters (mm)		Other Useful Parameters	
d10	0.803	Uniformity Coef.	9.80
d17	1.804	n computed	0.30
d20	2.277	g (cm/s <sup>2</sup> )	980.00
d50	6.553	ρ (g/cm <sup>3</sup> )	0.9981
d60	7.864	μ (g/cm s)	0.0098
de (Kruger)	1.041	ρg/μ (1/cm s)	9.9327E+04
de (Kozeny)	0.946	tau (Sauerbrei)	1.053
de (Zunker)	0.968	d <sub>geometric mean</sub>	4.922
de (Zamarin)	0.989	σ <sub>φ</sub>	1.491
lo (Alyameni)	0.290		
mm		0	% in sample
>64		Boulder	
16 - 64		coarse gravel	
8 - 16		medium gravel	
2 - 8		fine gravel	81.68801809
0.5 - 2		coarse sand	10.77618689
0.25 - 0.5		medium sand	3.315749812
0.063 - 0.25		fine sand	3.767897513
0.016 - 0.063		coarse silt	
0.008 - 0.016		medium silt	
0.002 - 0.008		fine silt	
<0.002		clay	



Grain Size Analysis Report

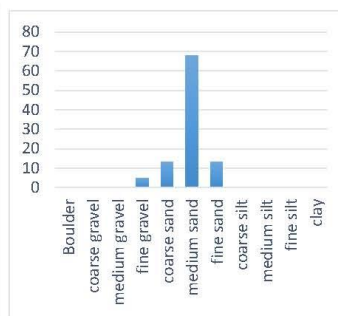
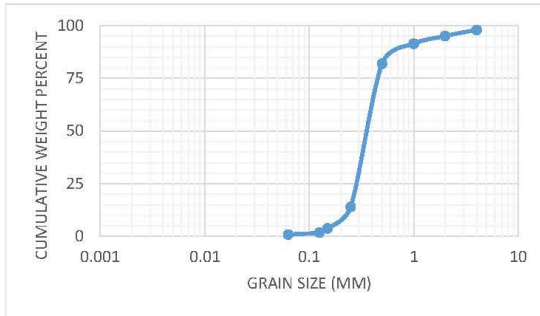
Date: 23 June 2015

Sample Name: Core 3 -5

Mass Sample (g): 81.5

T (oC) 20

Uniform sand low in fines



Sieve opening (ps) d <sub>i</sub> (mm)	Mass of retained (mr) (g)	mass fraction (mf)	Percent Passing (pp)
4	1.63363	0.020045	97.99555
2	2.359688	0.028953	95.10022
1	2.994989	0.036748	91.42539
0.5	7.714365	0.094655	81.95991
0.25	55.36192	0.679287	14.03118
0.15	8.349666	0.10245	3.786192
0.125	1.63363	0.020045	1.781737
0.063	0.726058	0.008909	0.890869
	0.8		0

Effective Grain Diameters (mm)		Other Useful Parameters	
d <sub>10</sub>	0.211	Uniformity Coef.	1.99
d <sub>17</sub>	0.261	n computed	0.43
d <sub>20</sub>	0.272	g (cm/s <sup>2</sup> )	980.00
d <sub>50</sub>	0.382	ρ (g/cm <sup>3</sup> )	0.9981
d <sub>60</sub>	0.419	μ (g/cm s)	0.0098
de (Kruzer)	0.214	ρg/μ (1/cm s)	9.9327E+04
de (Kozeny)	0.201	tau (Sauerbrei)	1.053
de (Zunker)	0.205	d <sub>geometric mean</sub>	0.391
de (Zamarin)	0.209	σ <sub>φ</sub>	0.857
lo (Alyameni)	0.221		
mm		0	% in sample
>64		Boulder	
16 - 64		coarse gravel	
8 - 16		medium gravel	
2 - 8		fine gravel	4.89977283
0.5 - 2		coarse sand	13.1403118
0.25 - 0.5		medium sand	67.92873051
0.063 - 0.25		fine sand	13.1403118
0.016 - 0.063		coarse silt	
0.008 - 0.016		medium silt	
0.002 - 0.008		fine silt	
<0.002		clay	



Grain Size Analysis Report

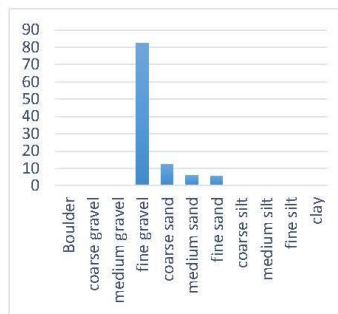
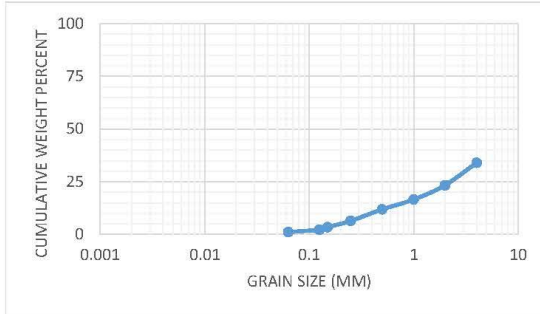
Date: 23 June 2015

Sample Name: Core 3 -6

Mass Sample (g): 96.3

T (oC) 20

Poorly sorted sandy gravel low in fines



Sieve opening (ps) d <sub>i</sub> (mm)	Mass of retained (mr) (g)	mass fraction (mf)	Percent Passing (pp)
4	68.4	0.71028	33.97683
2	11	0.114226	23.35907
1	7.1	0.073728	16.50579
0.5	4.8	0.049844	11.87259
0.25	5.7	0.05919	6.370656
0.15	3.1	0.032191	3.378378
0.125	1.2	0.012461	2.220077
0.063	1.2	0.012461	1.061776
	1.1		0

Effective Grain Diameters (mm)		Other Useful Parameters	
d <sub>10</sub>	0.415	Uniformity Coef.	17.02
d <sub>17</sub>	1.072	n computed	0.27
d <sub>20</sub>	1.510	g (cm/s <sup>2</sup> )	980.00
d <sub>50</sub>	5.886	ρ (g/cm <sup>3</sup> )	0.9981
d <sub>60</sub>	7.064	μ (g/cm s)	0.0098
de (Kruger)	0.829	ρg/μ (1/cm s)	9.9327E+04
de (Kozeny)	0.762	tau (Sauerbrei)	1.053
de (Zunker)	0.777	d <sub>geometric mean</sub>	3.802
de (Zamarin)	0.793	σ <sub>φ</sub>	1.722
lo (Alyameni)	-0.426		
mm		0	% in sample
>64		Boulder	
16 - 64		coarse gravel	
8 - 16		medium gravel	
2 - 8		fine gravel	82.45067497
0.5 - 2		coarse sand	12.35721703
0.25 - 0.5		medium sand	5.919003115
0.063 - 0.25		fine sand	5.711318795
0.016 - 0.063		coarse silt	
0.008 - 0.016		medium silt	
0.002 - 0.008		fine silt	
<0.002		clay	



Grain Size Analysis Report

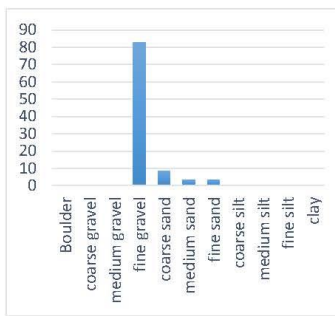
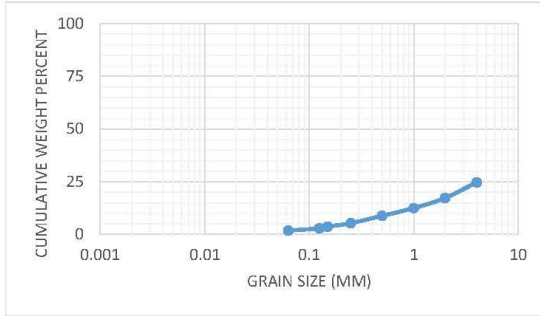
Date: 23 June 2015

Sample Name: Core 3 -7

Mass Sample (g): 145.4

T (oC) 20

Poorly sorted sandy gravel low in fines



Sieve opening (ps) d <sub>i</sub> (mm)	Mass of retained (mr) (g)	mass fraction (mf)	Percent Passing (pp)
4	109.5506	0.753443	24.65574
2	10.7739	0.074098	17.2459
1	6.960131	0.047869	12.45902
0.5	5.339279	0.036721	8.786885
0.25	5.053246	0.034754	5.311475
0.15	2.383607	0.016393	3.672131
0.125	1.239475	0.008525	2.819672
0.063	1.525508	0.010492	1.770492
	2.7		0

Effective Grain Diameters (mm)		Other Useful Parameters	
d <sub>10</sub>	0.665	Uniformity Coef.	14.63
d <sub>17</sub>	1.949	n computed	0.27
d <sub>20</sub>	2.743	g (cm/s <sup>2</sup> )	980.00
d <sub>50</sub>	8.112	ρ (g/cm <sup>3</sup> )	0.9981
d <sub>60</sub>	9.734	μ (g/cm s)	0.0098
de (Kruzer)	1.182	ρg/μ (1/cm s)	9.9327E+04
de (Kozeny)	1.078	tau (Sauerbrei)	1.053
de (Zunker)	1.099	d <sub>geometric mean</sub>	5.769
de (Zamarin)	1.119	σ <sub>φ</sub>	1.661
lo (Alyameni)	0.002		
mm		0	% in sample
>64		Boulder	
16 - 64		coarse gravel	
8 - 16		medium gravel	
2 - 8		fine gravel	82.75409836
0.5 - 2		coarse sand	8.459016393
0.25 - 0.5		medium sand	3.475409836
0.063 - 0.25		fine sand	3.540983607
0.016 - 0.063		coarse silt	
0.008 - 0.016		medium silt	
0.002 - 0.008		fine silt	
<0.002		clay	



Grain Size Analysis Report

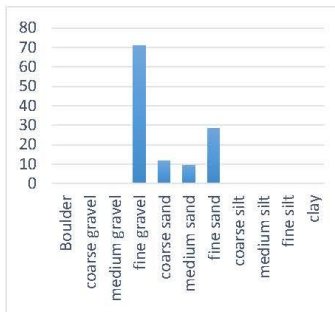
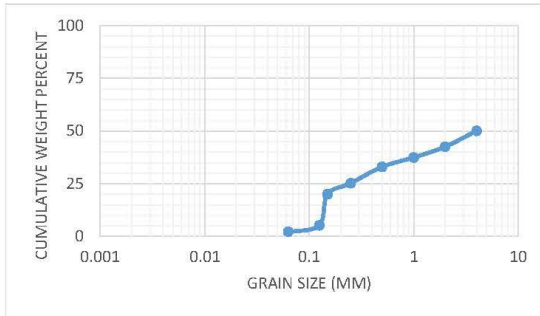
Date: 23 June 2015

Sample Name: Core 3 -8

Mass Sample (g): 108.3

T (oC) 20

Poorly sorted sandy gravel low in fines



Sieve opening (ps) d <sub>i</sub> (mm)	Mass of retained (mr) (g)	mass fraction (mf)	Percent Passing (pp)
4	66.7	0.615882	50.07485
2	10.1	0.093259	42.51497
1	6.8	0.062789	37.42515
0.5	5.9	0.054478	33.00898
0.25	10.4	0.09603	25.22455
0.15	7	0.064635	19.98503
0.125	19.8	0.182825	5.164671
0.063	4	0.036934	2.170659
	2.9		0

Effective Grain Diameters (mm)		Other Useful Parameters	
d <sub>10</sub>	0.133	Uniformity Coef.	35.99
d <sub>17</sub>	0.145	n computed	0.26
d <sub>20</sub>	0.150	g (cm/s <sup>2</sup> )	980.00
d <sub>50</sub>	3.980	ρ (g/cm <sup>3</sup> )	0.9981
d <sub>60</sub>	4.793	μ (g/cm s)	0.0098
de (Kruzer)	0.295	ρg/μ (1/cm s)	9.9327E+04
de (Kozeny)	0.268	tau (Sauerbrei)	1.053
de (Zunker)	0.276	d <sub>geometric mean</sub>	1.564
de (Zamarin)	0.284	σ <sub>φ</sub>	2.291
lo (Alyameni)	-1.017		
mm		0	% in sample
>64		Boulder	
16 - 64		coarse gravel	
8 - 16		medium gravel	
2 - 8		fine gravel	70.91412742
0.5 - 2		coarse sand	11.72668513
0.25 - 0.5		medium sand	9.602954755
0.063 - 0.25		fine sand	28.43951985
0.016 - 0.063		coarse silt	
0.008 - 0.016		medium silt	
0.002 - 0.008		fine silt	
<0.002		clay	



Grain Size Analysis Report

Date:

25 June 2015

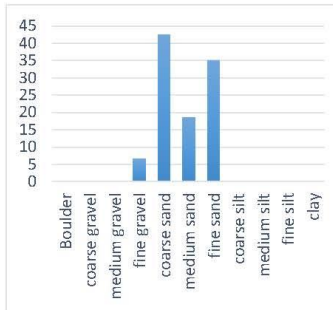
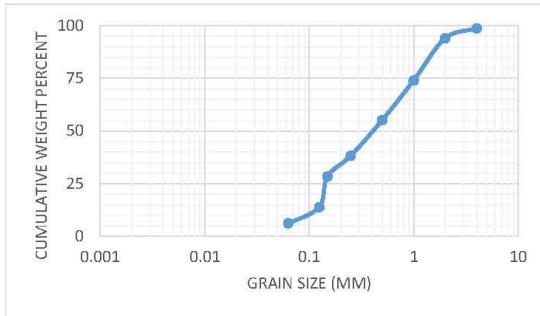
Sample Name:

Core4-1

Mass Sample (g): 71.5

T (oC) 20

Poorly sorted sand low in fines



Sieve opening (ps) d <sub>i</sub> (mm)	Mass of retained (mr) (g)	mass fraction (mf)	Percent Passing (pp)
4	1	0.013986	98.71795
2	3.7	0.051748	93.97436
1	15.6	0.218182	73.97436
0.5	14.7	0.205594	55.12821
0.25	13.2	0.184615	38.20513
0.15	7.6	0.106294	28.46154
0.125	11.4	0.159441	13.84615
0.063	6	0.083916	6.153846
	4.8		0

Effective Grain Diameters (mm)		Other Useful Parameters	
d <sub>10</sub>	0.094	Uniformity Coef.	6.69
d <sub>17</sub>	0.130	n computed	0.33
d <sub>20</sub>	0.136	g (cm/s <sup>2</sup> )	980.00
d <sub>50</sub>	0.424	ρ (g/cm <sup>3</sup> )	0.9981
d <sub>60</sub>	0.629	μ (g/cm s)	0.0098
de (Kruger)	0.234	ρg/μ (1/cm s)	9.9327E+04
de (Kozeny)	0.215	tau (Sauerbrei)	1.053
de (Zunker)	0.221	d <sub>geometric mean</sub>	0.434
de (Zamarin)	0.228	σ <sub>φ</sub>	1.730
lo (Alyameni)	0.006		
mm		0	% in sample
>64		Boulder	
16 - 64		coarse gravel	
8 - 16		medium gravel	
2 - 8		fine gravel	6.573426573
0.5 - 2		coarse sand	42.37762238
0.25 - 0.5		medium sand	18.46153846
0.063 - 0.25		fine sand	34.96503497
0.016 - 0.063		coarse silt	
0.008 - 0.016		medium silt	
0.002 - 0.008		fine silt	
<0.002		clay	



Grain Size Analysis Report

Date:

25 June 2015

Sample Name:

Core4-2

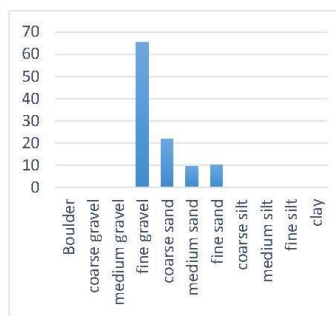
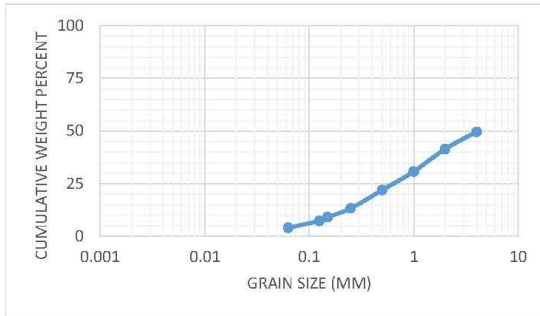
Mass Sample (g):

62

T (oC)

20

Poorly sorted sandy gravel low in fines



Sieve opening (ps) di (mm)	Mass of retained (mr) (g)	mass fraction (mf)	Percent Passing (pp)
4	34.9	0.562903	49.63925
2	5.7	0.091935	41.41414
1	7.4	0.119355	30.73593
0.5	6.1	0.098387	21.93362
0.25	6	0.096774	13.27561
0.15	2.9	0.046774	9.090909
0.125	1.2	0.019355	7.359307
0.063	2.3	0.037097	4.040404
	2.8		0

Effective Grain Diameters (mm)		Other Useful Parameters	
d10	0.172	Uniformity Coef.	28.15
d17	0.358	n computed	0.26
d20	0.444	g (cm/s <sup>2</sup> )	980.00
d50	4.029	ρ (g/cm <sup>3</sup> )	0.9981
d60	4.835	μ (g/cm s)	0.0098
de (Kruzer)	0.588	ρg/μ (1/cm s)	9.9327E+04
de (Kozeny)	0.542	tau (Sauerbrei)	1.053
de (Zunker)	0.555	d <sub>geometric mean</sub>	2.077
de (Zamarin)	0.567	σ <sub>φ</sub>	2.086
lo (Alyameni)	-0.762		
mm		0	% in sample
>64		Boulder	
16 - 64		coarse gravel	
8 - 16		medium gravel	
2 - 8		fine gravel	65.48387097
0.5 - 2		coarse sand	21.77419355
0.25 - 0.5		medium sand	9.677419355
0.063 - 0.25		fine sand	10.32258065
0.016 - 0.063		coarse silt	
0.008 - 0.016		medium silt	
0.002 - 0.008		fine silt	
<0.002		clay	



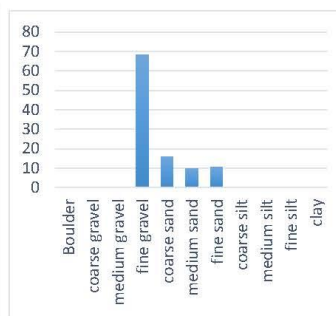
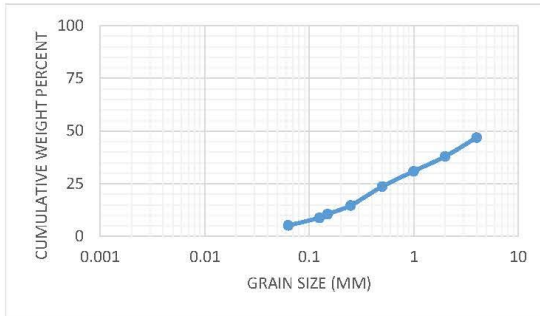
Sample Name:

Core4-3

Mass Sample (g): 72.5

T (oC) 20

Poorly sorted sandy gravel low in fines



Sieve opening (ps) d <sub>i</sub> (mm)	Mass of retained (mr) (g)	mass fraction (mf)	Percent Passing (pp)
4	42.3	0.583448	46.8593
2	7.1	0.097931	37.9397
1	5.6	0.077241	30.90452
0.5	5.8	0.08	23.61809
0.25	7.1	0.097931	14.69849
0.15	3.3	0.045517	10.55276
0.125	1.4	0.01931	8.79397
0.063	2.9	0.04	5.150754
	4.1		0

Effective Grain Diameters (mm)		Other Useful Parameters	
d <sub>10</sub>	0.142	Uniformity Coef.	36.03
d <sub>17</sub>	0.315	n computed	0.26
d <sub>20</sub>	0.399	g (cm/s <sup>2</sup> )	980.00
d <sub>50</sub>	4.268	ρ (g/cm <sup>3</sup> )	0.9981
d <sub>60</sub>	5.122	μ (g/cm s)	0.0098
de (Kruzer)	0.624	ρg/μ (1/cm s)	9.9327E+04
de (Kozeny)	0.576	tau (Sauerbrei)	1.053
de (Zunker)	0.589	d <sub>geometric mean</sub>	2.061
de (Zamarin)	0.602	σ <sub>φ</sub>	2.230
lo (Alyameni)	-0.887		
mm		0	% in sample
>64		Boulder	
16 - 64		coarse gravel	
8 - 16		medium gravel	
2 - 8		fine gravel	68.13793103
0.5 - 2		coarse sand	15.72413793
0.25 - 0.5		medium sand	9.793103448
0.063 - 0.25		fine sand	10.48275862
0.016 - 0.063		coarse silt	
0.008 - 0.016		medium silt	
0.002 - 0.008		fine silt	
<0.002		clay	





Grain Size Analysis Report

Date:

25 June 2015

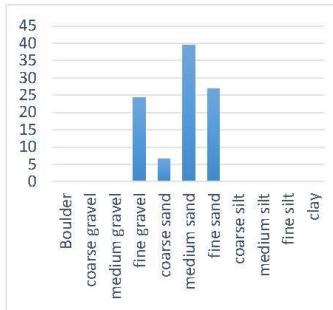
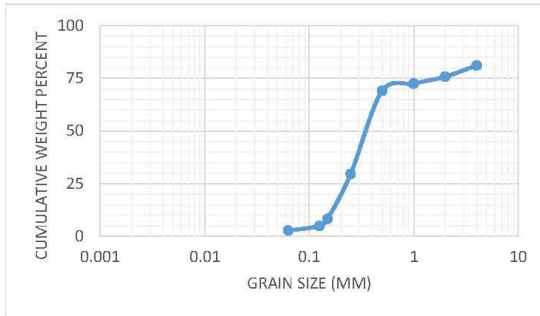
Sample Name:

Core4-4

Mass Sample (g): 87.9

T (oC) 20

Moderately well sorted gravelly sand low in fines



Sieve opening (ps) d <sub>i</sub> (mm)	Mass of retained (mr) (g)	mass fraction (mf)	Percent Passing (pp)
4	16.60741	0.188935	81.10647
2	4.679436	0.053236	75.78288
1	2.844363	0.032359	72.54697
0.5	3.027871	0.034447	69.1023
0.25	34.68288	0.394572	29.64509
0.15	18.71775	0.212944	8.350731
0.125	3.027871	0.034447	4.906054
0.063	1.926827	0.021921	2.713987
	2.6		0

Effective Grain Diameters (mm)		Other Useful Parameters	
d <sub>10</sub>	0.158	Uniformity Coef.	2.80
d <sub>17</sub>	0.191	n computed	0.41
d <sub>20</sub>	0.205	g (cm/s <sup>2</sup> )	980.00
d <sub>50</sub>	0.379	ρ (g/cm <sup>3</sup> )	0.9981
d <sub>60</sub>	0.442	μ (g/cm s)	0.0098
de (Kruger)	0.243	ρg/μ (1/cm s)	9.9327E+04
de (Kozeny)	0.230	tau (Sauerbrei)	1.053
de (Zunker)	0.234	d <sub>geometric mean</sub>	0.664
de (Zamarin)	0.238	σ <sub>φ</sub>	1.910
lo (Alyameni)	0.128		
mm		0	% in sample
>64		Boulder	
16 - 64		coarse gravel	
8 - 16		medium gravel	
2 - 8		fine gravel	24.217119
0.5 - 2		coarse sand	6.680584551
0.25 - 0.5		medium sand	39.45720251
0.063 - 0.25		fine sand	26.93110647
0.016 - 0.063		coarse silt	
0.008 - 0.016		medium silt	
0.002 - 0.008		fine silt	
<0.002		clay	



Grain Size Analysis Report

Date:

25 June 2015

Sample Name:

Core4-5

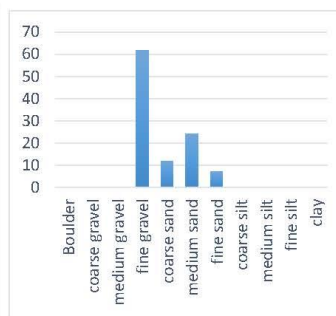
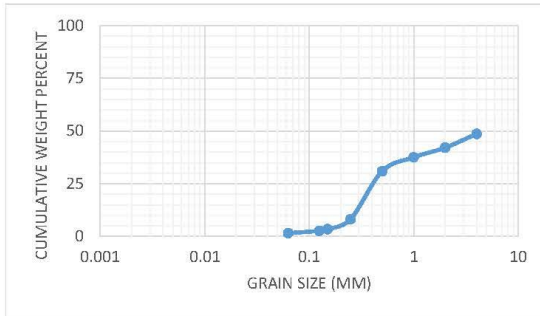
Mass Sample (g):

115.2

T (oC)

20

Poorly sorted sandy gravel low in fines



Sieve opening (ps) d <sub>i</sub> (mm)	Mass of retained (mr) (g)	mass fraction (mf)	Percent Passing (pp)
4	63	0.546875	48.61338
2	8	0.069444	42.08809
1	5.6	0.048611	37.52039
0.5	8.1	0.070313	30.91354
0.25	27.8	0.241319	8.238173
0.15	5.9	0.051215	3.425775
0.125	1	0.008681	2.610114
0.063	1.3	0.011285	1.549755
	1.9		0

Effective Grain Diameters (mm)		Other Useful Parameters	
d <sub>10</sub>	0.269	Uniformity Coef.	18.32
d <sub>17</sub>	0.347	n computed	0.26
d <sub>20</sub>	0.380	g (cm/s <sup>2</sup> )	980.00
d <sub>50</sub>	4.114	ρ (g/cm <sup>3</sup> )	0.9981
d <sub>60</sub>	4.937	μ (g/cm s)	0.0098
de (Kruzer)	0.465	ρg/μ (1/cm s)	9.9327E+04
de (Kozeny)	0.433	tau (Sauerbrei)	1.053
de (Zunker)	0.442	d <sub>geometric mean</sub>	2.120
de (Zamarin)	0.451	σ <sub>φ</sub>	1.912
lo (Alyameni)	-0.801		
mm		0	% in sample
>64		Boulder	
16 - 64		coarse gravel	
8 - 16		medium gravel	
2 - 8		fine gravel	61.63194444
0.5 - 2		coarse sand	11.89236111
0.25 - 0.5		medium sand	24.13194444
0.063 - 0.25		fine sand	7.118055556
0.016 - 0.063		coarse silt	
0.008 - 0.016		medium silt	
0.002 - 0.008		fine silt	
<0.002		clay	



Grain Size Analysis Report

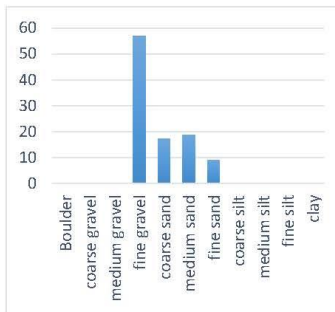
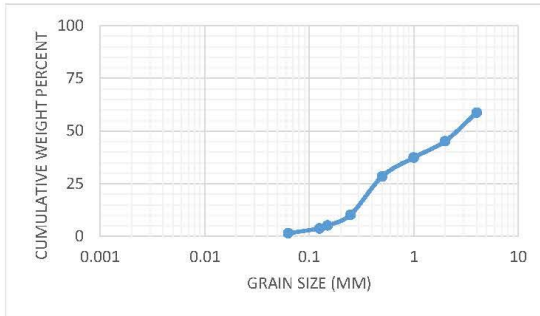
Date: 25 June 2015

Sample Name: Core 4 -6

Mass Sample (g): 162.3

T (oC) 20

Poorly sorted sandy gravel low in fines



Sieve opening (ps) di (mm)	Mass of retained (mr) (g)	mass fraction (mf)	Percent Passing (pp)	Effective Grain Diameters (mm)	Other Useful Parameters		
4	69.5	0.428219	58.75371	d10	0.244	Uniformity Coef.	16.76
2	22.9	0.141097	45.1632	d17	0.342	n computed	0.27
1	13.1	0.080715	37.38872	d20	0.384	g (cm/s <sup>2</sup> )	980.00
0.5	15.1	0.093038	28.4273	d50	2.712	ρ (g/cm <sup>3</sup> )	0.9981
0.25	30.5	0.187924	10.32641	d60	4.085	μ (g/cm s)	0.0098
0.15	8.7	0.053604	5.163205	de (Kruger)	0.481	ρg/μ (1/cm s)	9.9327E+04
0.125	2.4	0.014787	3.738872	de (Kozeny)	0.447	tau (Sauerbrei)	1.053
0.063	3.8	0.023413	1.48368	de (Zunker)	0.457	d <sub>geometric mean</sub>	1.720
	2.5		0	de (Zamarin)	0.467	σ <sub>φ</sub>	1.858
				lo (Alyameni)	-0.593		
				mm	0	% in sample	
				>64	Boulder		
				16 - 64	coarse gravel		
				8 - 16	medium gravel		
				2 - 8	fine gravel	56.93160813	
				0.5 - 2	coarse sand	17.37523105	
				0.25 - 0.5	medium sand	18.79235983	
				0.063 - 0.25	fine sand	9.180529883	
				0.016 - 0.063	coarse silt		
				0.008 - 0.016	medium silt		
				0.002 - 0.008	fine silt		
				<0.002	clay		



Grain Size Analysis Report

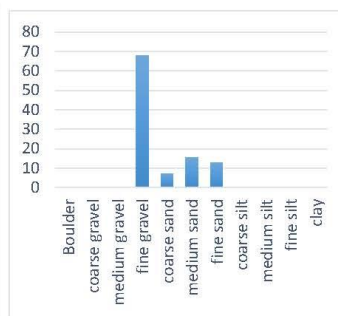
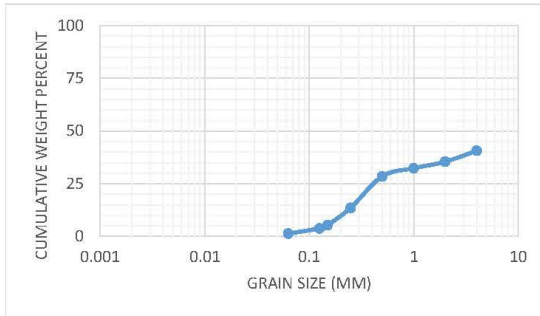
Date: 25 June 2015

Sample Name: Core 4 -7

Mass Sample (g): 151.1

T (oC) 20

Poorly sorted sandy gravel low in fines



Sieve opening (ps) d <sub>i</sub> (mm)	Mass of retained (mr) (g)	mass fraction (mf)	Percent Passing (pp)
4	94.1	0.622766	40.59343
2	8.2	0.054269	35.41667
1	4.9	0.032429	32.32323
0.5	6.1	0.040371	28.47222
0.25	23.6	0.156188	13.57323
0.15	13	0.086036	5.366162
0.125	2.5	0.016545	3.787879
0.063	4	0.026473	1.262626
	2		0

Effective Grain Diameters (mm)		Other Useful Parameters	
d <sub>10</sub>	0.206	Uniformity Coef.	28.64
d <sub>17</sub>	0.308	n computed	0.26
d <sub>20</sub>	0.358	g (cm/s <sup>2</sup> )	980.00
d <sub>50</sub>	4.927	ρ (g/cm <sup>3</sup> )	0.9981
d <sub>60</sub>	5.912	μ (g/cm s)	0.0098
de (Krugler)	0.506	ρg/μ (1/cm s)	9.9327E+04
de (Kozeny)	0.475	tau (Sauerbrei)	1.053
de (Zunker)	0.483	d <sub>geometric mean</sub>	2.279
de (Zamarin)	0.491	σ <sub>φ</sub>	2.120
lo (Alyameni)	-1.094		
mm		0	% in sample
>64		Boulder	
16 - 64		coarse gravel	
8 - 16		medium gravel	
2 - 8		fine gravel	67.70350761
0.5 - 2		coarse sand	7.279947055
0.25 - 0.5		medium sand	15.6187955
0.063 - 0.25		fine sand	12.90536069
0.016 - 0.063		coarse silt	
0.008 - 0.016		medium silt	
0.002 - 0.008		fine silt	
<0.002		clay	



Grain Size Analysis Report

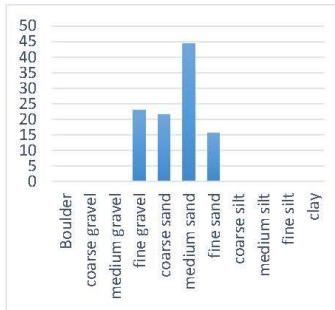
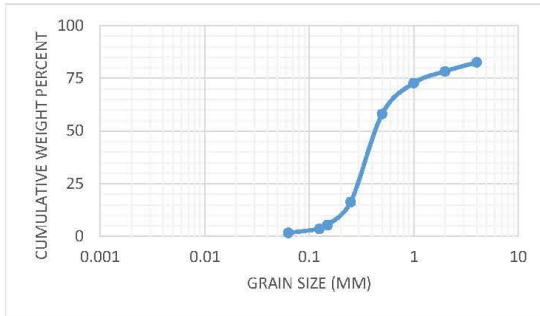
Date: 25 June 2015

Sample Name: Core 4 -8

Mass Sample (g): 122.2

T (oC) 20

Moderately well sorted gravelly sand low in fines



Sieve opening (ps) di (mm)	Mass of retained (mr) (g)	mass fraction (mf)	Percent Passing (pp)
4	22.6	0.184943	82.57517
2	5.5	0.045008	78.33462
1	7.3	0.059738	72.70625
0.5	19	0.155483	58.05705
0.25	54.2	0.443535	16.26831
0.15	14.1	0.115385	5.39707
0.125	2.4	0.01964	3.546646
0.063	2.5	0.020458	1.619121
	2.1		0

Effective Grain Diameters (mm)		Other Useful Parameters	
d10	0.192	Uniformity Coef.	2.94
d17	0.254	n computed	0.40
d20	0.272	g (cm/s <sup>2</sup> )	980.00
d50	0.452	ρ (g/cm <sup>3</sup> )	0.9981
d60	0.566	μ (g/cm s)	0.0098
de (Kruzer)	0.260	ρg/μ (1/cm s)	9.9327E+04
de (Kozeny)	0.244	tau (Sauerbrei)	1.053
de (Zunker)	0.249	d <sub>geometric mean</sub>	0.769
de (Zamarin)	0.254	σ <sub>φ</sub>	1.766
lo (Alyameni)	0.176		
mm		0	% in sample
>64		Boulder	
16 - 64		coarse gravel	
8 - 16		medium gravel	
2 - 8		fine gravel	22.99509002
0.5 - 2		coarse sand	21.52209493
0.25 - 0.5		medium sand	44.35351882
0.063 - 0.25		fine sand	15.54828151
0.016 - 0.063		coarse silt	
0.008 - 0.016		medium silt	
0.002 - 0.008		fine silt	
<0.002		clay	



Grain Size Analysis Report

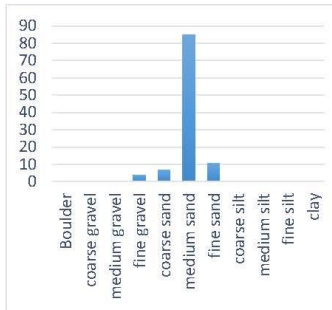
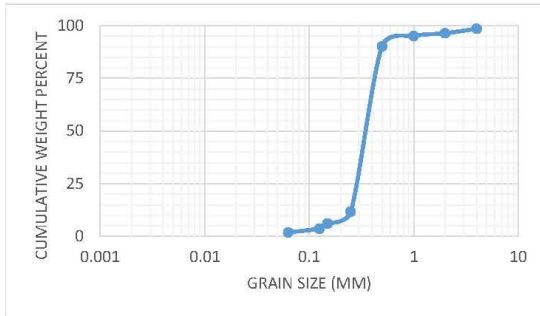
Date: 25 June 2015

Sample Name: Core 4 -9

Mass Sample (g): 92.6

T (oC) 20

Uniform sand low in fines



Sieve opening (ps) di (mm)	Mass of retained (mr) (g)	mass fraction (mf)	Percent Passing (pp)
4	1.5	0.016199	98.5015
2	2.1	0.022678	96.4036
1	1.3	0.014039	95.1049
0.5	4.9	0.052916	90.20979
0.25	78.5	0.847732	11.78821
0.15	5.7	0.061555	6.093906
0.125	2.4	0.025918	3.696304
0.063	1.8	0.019438	1.898102
	1.9		0

Effective Grain Diameters (mm)		Other Useful Parameters	
d10	0.219	Uniformity Coef.	1.85
d17	0.267	n computed	0.44
d20	0.276	g (cm/s <sup>2</sup> )	980.00
d50	0.372	ρ (g/cm <sup>3</sup> )	0.9981
d60	0.404	μ (g/cm s)	0.0098
de (Kruger)	0.194	ρg/μ (1/cm s)	9.9327E+04
de (Kozeny)	0.182	tau (Sauerbrei)	1.053
de (Zunker)	0.186	d <sub>geometric mean</sub>	0.361
de (Zamarin)	0.190	σ <sub>φ</sub>	0.646
lo (Alyameni)	0.232		
mm	0	% in sample	
>64	Boulder		
16 - 64	coarse gravel		
8 - 16	medium gravel		
2 - 8	fine gravel		3.887688985
0.5 - 2	coarse sand		6.695464363
0.25 - 0.5	medium sand		84.77321814
0.063 - 0.25	fine sand		10.69114471
0.016 - 0.063	coarse silt		
0.008 - 0.016	medium silt		
0.002 - 0.008	fine silt		
<0.002	clay		



Grain Size Analysis Report

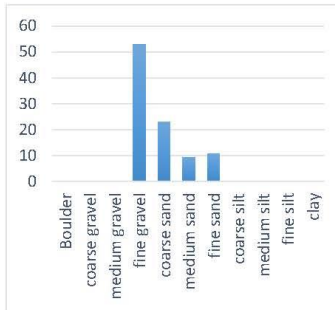
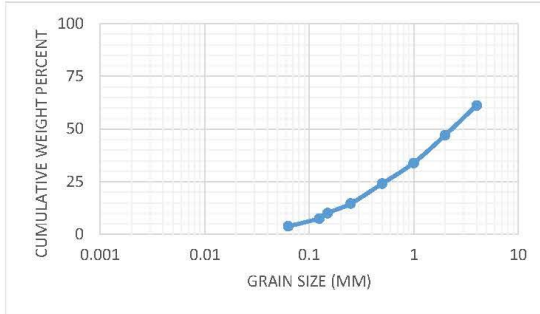
Date: 23 June 2015

Sample Name: Core 5 -1

Mass Sample (g): 78

T (oC) 20

Poorly sorted sandy gravel low in fines



Sieve opening (ps) d <sub>i</sub> (mm)	Mass of retained (mr) (g)	mass fraction (mf)	Percent Passing (pp)
4	30.25784	0.387921	61.2079
2	11.05226	0.141696	47.03833
1	10.23693	0.131243	33.91405
0.5	7.700348	0.098722	24.04181
0.25	7.337979	0.094077	14.63415
0.15	3.533101	0.045296	10.10453
0.125	1.993031	0.025552	7.549361
0.063	2.898955	0.037166	3.832753
	0.2		0

Effective Grain Diameters (mm)		Other Useful Parameters	
d <sub>10</sub>	0.149	Uniformity Coef.	25.71
d <sub>17</sub>	0.313	n computed	0.26
d <sub>20</sub>	0.393	g (cm/s <sup>2</sup> )	980.00
d <sub>50</sub>	2.418	ρ (g/cm <sup>3</sup> )	0.9981
d <sub>60</sub>	3.830	μ (g/cm s)	0.0098
de (Kruzer)	0.577	ρg/μ (1/cm s)	9.9327E+04
de (Kozeny)	0.531	tau (Sauerbrei)	1.053
de (Zunker)	0.544	d <sub>geometric mean</sub>	1.560
de (Zamarin)	0.558	σ <sub>φ</sub>	2.010
lo (Alyameni)	-0.566		
mm		0	% in sample
>64		Boulder	
16 - 64		coarse gravel	
8 - 16		medium gravel	
2 - 8		fine gravel	52.96167247
0.5 - 2		coarse sand	22.99651568
0.25 - 0.5		medium sand	9.407665505
0.063 - 0.25		fine sand	10.80139373
0.016 - 0.063		coarse silt	
0.008 - 0.016		medium silt	
0.002 - 0.008		fine silt	
<0.002		clay	



Grain Size Analysis Report

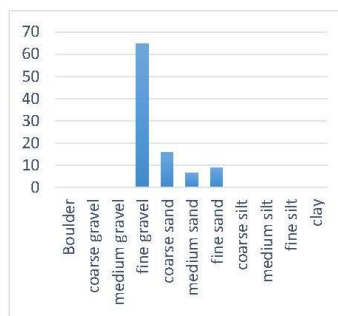
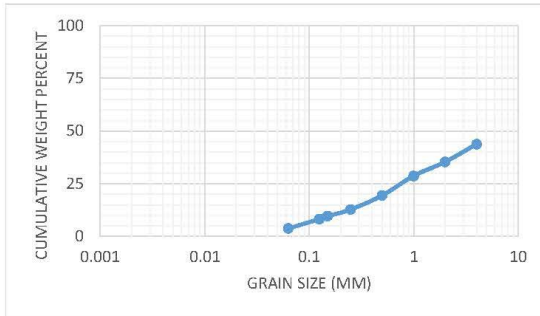
Date: 23 June 2015

Sample Name: Core 5 -2

Mass Sample (g): 104.4

T (oC) 20

Poorly sorted sandy gravel low in fines



Sieve opening (ps) di (mm)	Mass of retained (mr) (g)	mass fraction (mf)	Percent Passing (pp)	Effective Grain Diameters (mm)	Other Useful Parameters		
4	58.74635	0.562704	43.72955	d10	0.163	Uniformity Coef.	33.72
2	8.766412	0.083969	35.33261	d17	0.409	n computed	0.26
1	6.94482	0.066521	28.68048	d20	0.532	g (cm/s <sup>2</sup> )	980.00
0.5	9.677208	0.092694	19.41112	d50	4.574	ρ (g/cm <sup>3</sup> )	0.9981
0.25	6.94482	0.066521	12.759	d60	5.488	μ (g/cm s)	0.0098
0.15	3.301636	0.031625	9.59651	de (Krugler)	0.773	ρg/μ (1/cm s)	9.9327E+04
0.125	1.480044	0.014177	8.178844	de (Kozeny)	0.710	tau (Sauerbrei)	1.053
0.063	4.66783	0.044711	3.707743	de (Zunker)	0.727	d <sub>geometric mean</sub>	2.354
	3.4		0	de (Zamarin)	0.743	σ <sub>φ</sub>	2.115
				lo (Alyameni)	-0.860		
				mm	0	% in sample	
				>64	Boulder		
				16 - 64	coarse gravel		
				8 - 16	medium gravel		
				2 - 8	fine gravel	64.66739368	
				0.5 - 2	coarse sand	15.9214831	
				0.25 - 0.5	medium sand	6.652126499	
				0.063 - 0.25	fine sand	9.051254089	
				0.016 - 0.063	coarse silt		
				0.008 - 0.016	medium silt		
				0.002 - 0.008	fine silt		
				<0.002	clay		





Grain Size Analysis Report

Date:

25 June 2015

Sample Name:

Core 5- 3

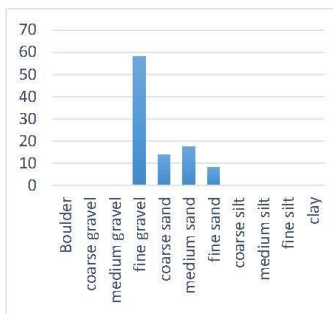
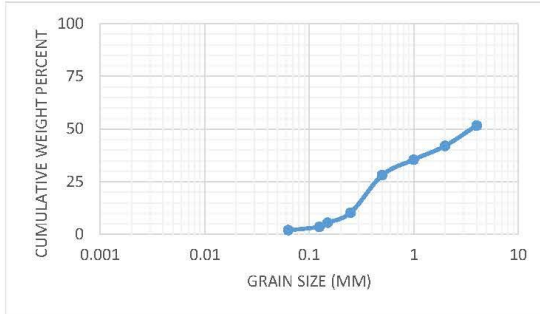
Mass Sample (g):

86.3

T (oC)

20

Poorly sorted sandy gravel low in fines



Sieve opening (ps) d <sub>i</sub> (mm)	Mass of retained (mr) (g)	mass fraction (mf)	Percent Passing (pp)
4	41.71321	0.483351	51.66488
2	8.342642	0.09667	41.99785
1	5.654458	0.065521	35.44576
0.5	6.396026	0.074114	28.03437
0.25	15.29484	0.177229	10.31149
0.15	4.078625	0.047261	5.585392
0.125	1.761224	0.020408	3.544576
0.063	1.39044	0.016112	1.933405
	1.8		0

Effective Grain Diameters (mm)		Other Useful Parameters	
d <sub>10</sub>	0.243	Uniformity Coef.	19.08
d <sub>17</sub>	0.344	n computed	0.26
d <sub>20</sub>	0.387	g (cm/s <sup>2</sup> )	980.00
d <sub>50</sub>	3.656	ρ (g/cm <sup>3</sup> )	0.9981
d <sub>60</sub>	4.645	μ (g/cm s)	0.0098
de (Kruzer)	0.511	ρg/μ (1/cm s)	9.9327E+04
de (Kozeny)	0.474	tau (Sauerbrei)	1.053
de (Zunker)	0.484	d <sub>geometric mean</sub>	1.987
de (Zamarin)	0.495	σ <sub>φ</sub>	1.936
lo (Alyameni)	-0.731		
mm		0	% in sample
>64		Boulder	
16 - 64		coarse gravel	
8 - 16		medium gravel	
2 - 8		fine gravel	58.00214823
0.5 - 2		coarse sand	13.96348013
0.25 - 0.5		medium sand	17.72287863
0.063 - 0.25		fine sand	8.378088077
0.016 - 0.063		coarse silt	
0.008 - 0.016		medium silt	
0.002 - 0.008		fine silt	
<0.002		clay	



Grain Size Analysis Report

Date:

25 June 2015

Sample Name:

Core 5- 4

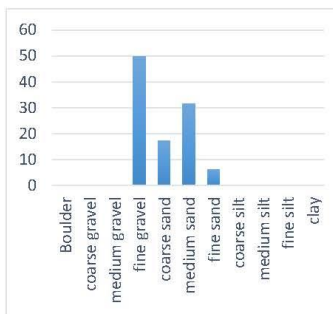
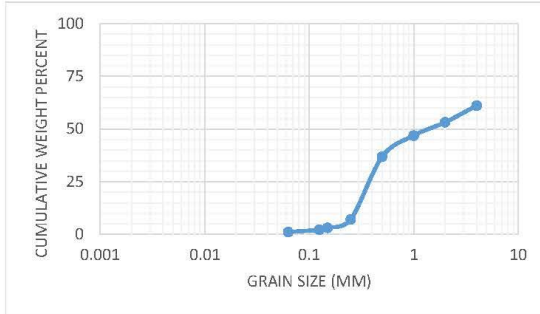
Mass Sample (g):

118

T (oC)

20

Poorly sorted gravelly sand low in fines



Sieve opening (ps) d <sub>i</sub> (mm)	Mass of retained (mr) (g)	mass fraction (mf)	Percent Passing (pp)
4	48.7	0.412712	61.10224
2	9.9	0.083898	53.19489
1	7.9	0.066949	46.88498
0.5	12.6	0.10678	36.82109
0.25	37.2	0.315254	7.108626
0.15	5	0.042373	3.115016
0.125	1.2	0.010169	2.15655
0.063	1.3	0.011017	1.118211
	1.4		0

Effective Grain Diameters (mm)		Other Useful Parameters	
d <sub>10</sub>	0.274	Uniformity Coef.	13.56
d <sub>17</sub>	0.333	n computed	0.28
d <sub>20</sub>	0.358	g (cm/s <sup>2</sup> )	980.00
d <sub>50</sub>	1.494	ρ (g/cm <sup>3</sup> )	0.9981
d <sub>60</sub>	3.721	μ (g/cm s)	0.0098
d <sub>e</sub> (Kruzer)	0.391	ρg/μ (1/cm s)	9.9327E+04
d <sub>e</sub> (Kozeny)	0.363	tau (Sauerbrei)	1.053
d <sub>e</sub> (Zunker)	0.371	d <sub>geometric mean</sub>	1.387
d <sub>e</sub> (Zamarin)	0.380	σ <sub>φ</sub>	1.775
lo (Alyameni)	-0.514		
mm	0	% in sample	
>64	Boulder		
16 - 64	coarse gravel		
8 - 16	medium gravel		
2 - 8	fine gravel		49.66101695
0.5 - 2	coarse sand		17.37288136
0.25 - 0.5	medium sand		31.52542373
0.063 - 0.25	fine sand		6.355932203
0.016 - 0.063	coarse silt		
0.008 - 0.016	medium silt		
0.002 - 0.008	fine silt		
<0.002	clay		



Grain Size Analysis Report

Date:

25 June 2015

Sample Name:

Core 5- 5

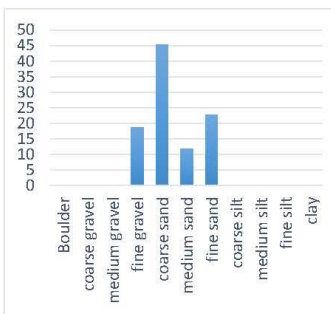
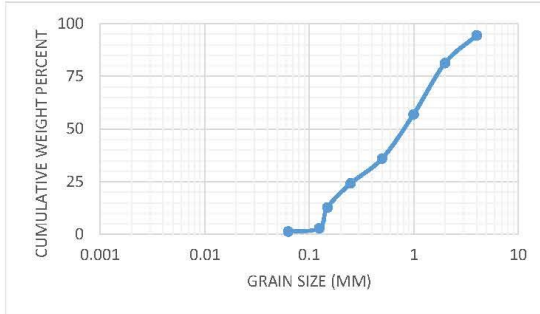
Mass Sample (g):

58.4

T (oC)

20

Poorly sorted gravelly sand low in fines



Sieve opening (ps) d <sub>i</sub> (mm)	Mass of retained (mr) (g)	mass fraction (mf)	Percent Passing (pp)
4	3.283891	0.056231	94.3769
2	7.632827	0.130699	81.30699
1	14.20061	0.243161	56.99088
0.5	12.24802	0.209726	36.01824
0.25	6.922796	0.118541	24.16413
0.15	6.656535	0.113982	12.76596
0.125	5.768997	0.098784	2.887538
0.063	0.887538	0.015198	1.367781
	0.9		0

Effective Grain Diameters (mm)		Other Useful Parameters	
d <sub>10</sub>	0.143	Uniformity Coef.	7.86
d <sub>17</sub>	0.187	n computed	0.31
d <sub>20</sub>	0.213	g (cm/s <sup>2</sup> )	980.00
d <sub>50</sub>	0.833	ρ (g/cm <sup>3</sup> )	0.9981
d <sub>60</sub>	1.124	μ (g/cm s)	0.0098
de (Kruzer)	0.289	ρg/μ (1/cm s)	9.9327E+04
de (Kozeny)	0.266	tau (Sauerbrei)	1.053
de (Zunker)	0.273	d <sub>geometric mean</sub>	0.710
de (Zamarin)	0.281	σ <sub>φ</sub>	1.689
lo (Alyameni)	-0.047		
mm		0	% in sample
>64		Boulder	
16 - 64		coarse gravel	
8 - 16		medium gravel	
2 - 8		fine gravel	18.69300912
0.5 - 2		coarse sand	45.2887538
0.25 - 0.5		medium sand	11.85410334
0.063 - 0.25		fine sand	22.79635258
0.016 - 0.063		coarse silt	
0.008 - 0.016		medium silt	
0.002 - 0.008		fine silt	
<0.002		clay	



Grain Size Analysis Report

Date:

25 June 2015

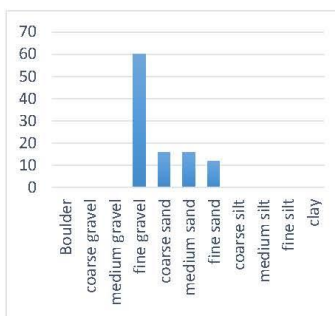
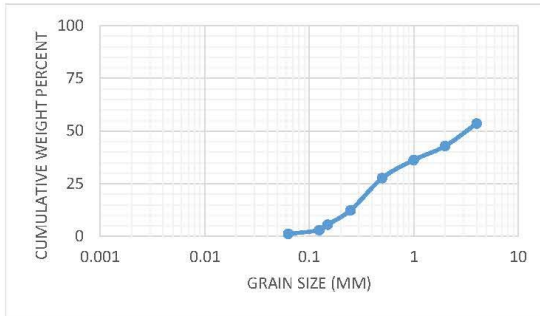
Sample Name:

Core 5- 6

Mass Sample (g): 146.1

T (oC) 20

Poorly sorted sandy gravel low in fines



Sieve opening (ps) d <sub>i</sub> (mm)	Mass of retained (mr) (g)	mass fraction (mf)	Percent Passing (pp)
4	71.3	0.488022	53.48989
2	16.3	0.111567	42.85714
1	10.2	0.069815	36.20352
0.5	13.2	0.090349	27.59295
0.25	23.2	0.158795	12.45923
0.15	10.6	0.072553	5.544684
0.125	4	0.027379	2.935421
0.063	2.7	0.01848	1.174168
	1.8		0

Effective Grain Diameters (mm)		Other Useful Parameters	
d <sub>10</sub>	0.214	Uniformity Coef.	20.92
d <sub>17</sub>	0.325	n computed	0.26
d <sub>20</sub>	0.375	g (cm/s <sup>2</sup> )	980.00
d <sub>50</sub>	3.344	ρ (g/cm <sup>3</sup> )	0.9981
d <sub>60</sub>	4.487	μ (g/cm s)	0.0098
de (Kruzer)	0.458	ρg/μ (1/cm s)	9.9327E+04
de (Kozeny)	0.426	tau (Sauerbrei)	1.053
de (Zunker)	0.435	d <sub>geometric mean</sub>	1.864
de (Zamarin)	0.444	σ <sub>φ</sub>	1.938
lo (Alyameni)	-0.715		
mm		0	% in sample
>64		Boulder	
16 - 64		coarse gravel	
8 - 16		medium gravel	
2 - 8		fine gravel	59.95893224
0.5 - 2		coarse sand	16.0164271
0.25 - 0.5		medium sand	15.87953457
0.063 - 0.25		fine sand	11.84120465
0.016 - 0.063		coarse silt	
0.008 - 0.016		medium silt	
0.002 - 0.008		fine silt	
<0.002		clay	



Grain Size Analysis Report

Date:

25 June 2015

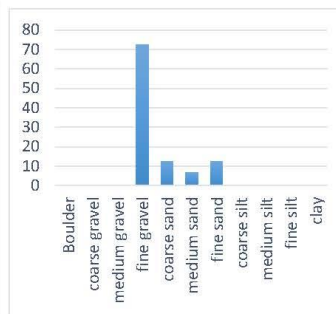
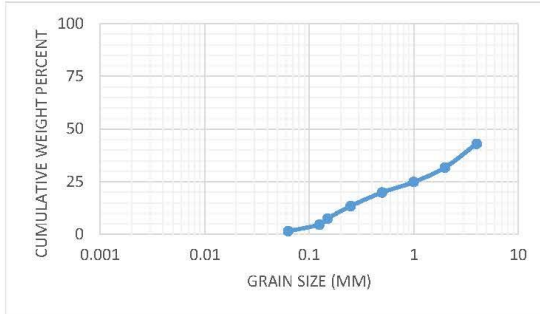
Sample Name:

Core 5- 7

Mass Sample (g): 110.7

T (oC) 20

Poorly sorted sandy gravel low in fines



Sieve opening (ps) di (mm)	Mass of retained (mr) (g)	mass fraction (mf)	Percent Passing (pp)
4	67.1	0.606143	42.99065
2	13.2	0.119241	31.7757
1	8.2	0.074074	24.80884
0.5	5.8	0.052394	19.88105
0.25	7.6	0.068654	13.42396
0.15	7	0.063234	7.476636
0.125	3.4	0.030714	4.587935
0.063	3.6	0.03252	1.529312
1.8			0

Effective Grain Diameters (mm)		Other Useful Parameters	
d10	0.192	Uniformity Coef.	29.01
d17	0.388	n computed	0.26
d20	0.512	g (cm/s <sup>2</sup> )	980.00
d50	4.652	ρ (g/cm <sup>3</sup> )	0.9981
d60	5.583	μ (g/cm s)	0.0098
de (Kruger)	0.606	ρg/μ (1/cm s)	9.9327E+04
de (Kozeny)	0.561	tau (Sauerbrei)	1.053
de (Zunker)	0.573	d <sub>geometric mean</sub>	2.333
de (Zamarin)	0.585	σ <sub>φ</sub>	2.045
lo (Alyameni)	-0.910		
mm		0	% in sample
>64		Boulder	
16 - 64		coarse gravel	
8 - 16		medium gravel	
2 - 8		fine gravel	72.53839205
0.5 - 2		coarse sand	12.64679313
0.25 - 0.5		medium sand	6.865401987
0.063 - 0.25		fine sand	12.64679313
0.016 - 0.063		coarse silt	
0.008 - 0.016		medium silt	
0.002 - 0.008		fine silt	
<0.002		clay	



Grain Size Analysis Report

Date:

25 June 2015

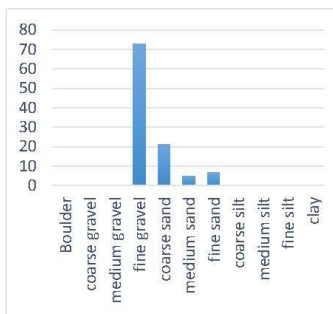
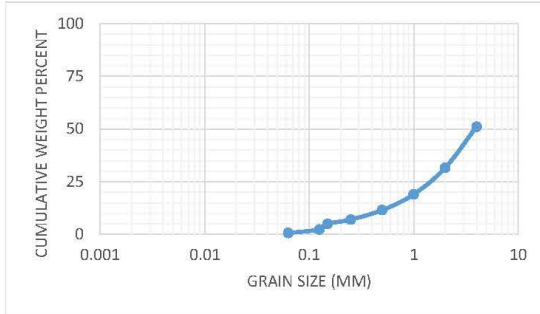
Sample Name:

Core 5- 8

Mass Sample (g): 115.3

T (oC) 20

Poorly sorted sandy gravel low in fines



Sieve opening (ps) d <sub>i</sub> (mm)	Mass of retained (mr) (g)	mass fraction (mf)	Percent Passing (pp)
4	59.9	0.519514	51.06209
2	23.9	0.207285	31.53595
1	15.4	0.133565	18.95425
0.5	9.1	0.078925	11.51961
0.25	5.5	0.047702	7.026144
0.15	2.5	0.021683	4.98366
0.125	3.3	0.028621	2.287582
0.063	2	0.017346	0.653595
	0.8		0

Effective Grain Diameters (mm)		Other Useful Parameters	
d <sub>10</sub>	0.415	Uniformity Coef.	11.31
d <sub>17</sub>	0.869	n computed	0.29
d <sub>20</sub>	1.083	g (cm/s <sup>2</sup> )	980.00
d <sub>50</sub>	3.891	ρ (g/cm <sup>3</sup> )	0.9981
d <sub>60</sub>	4.700	μ (g/cm s)	0.0098
de (Kruger)	0.714	ρg/μ (1/cm s)	9.9327E+04
de (Kozeny)	0.648	tau (Sauerbrei)	1.053
de (Zunker)	0.666	d <sub>geometric mean</sub>	2.737
de (Zamarin)	0.685	σ <sub>φ</sub>	1.612
lo (Alyameni)	-0.089		
mm		0	% in sample
>64		Boulder	
16 - 64		coarse gravel	
8 - 16		medium gravel	
2 - 8		fine gravel	72.67996531
0.5 - 2		coarse sand	21.24891587
0.25 - 0.5		medium sand	4.770164788
0.063 - 0.25		fine sand	6.764960971
0.016 - 0.063		coarse silt	
0.008 - 0.016		medium silt	
0.002 - 0.008		fine silt	
<0.002		clay	



K from Grain Size Analysis Report

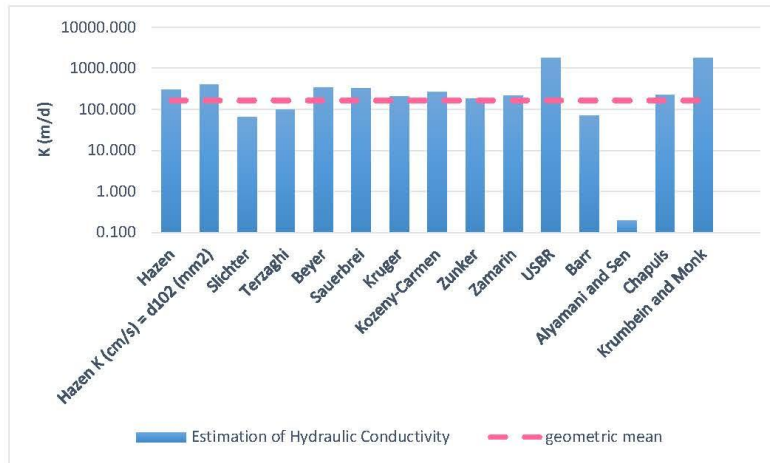
Date: 25 June 2015

Sample Name: Core 5-9

Mass Sample (g): 148.1

T (oC) 20

Poorly sorted sandy gravel low in fines



Estimation of Hydraulic Conductivity	cm/s	m/s	m/d
Hazen	.344E+00	.344E-02	297.55
Hazen K (cm/s) = d <sub>10</sub> (mm)	.469E+00	.469E-02	405.27
Slichter	.737E-01	.737E-03	63.65
Terzaghi	.115E+00	.115E-02	99.08
Beyer	.394E+00	.394E-02	340.45
Sauerbrei	.384E+00	.384E-02	331.64
Kruger	.238E+00	.238E-02	206.00
Kozeny-Carmen	.301E+00	.301E-02	260.17
Zunker	.208E+00	.208E-02	179.30
Zamarin	.248E+00	.248E-02	214.16
USBR	.210E+01	.210E-01	1816.63
Barr	.828E-01	.828E-03	71.53
Alyamani and Sen	.221E-03	.221E-05	0.19
Chapuis	.263E+00	.263E-02	227.07
Krumbain and Monk	.204E+01	.204E-01	1764.42
geometric mean	.190E+00	.190E-02	164.55

## **Appendix D: Permeameter Tests (Missori, 2015)**



**FALLING HEAD PERMEAMETER TESTS - WOODSTOCK (ON)**

SAMPLE	Initial He	Final Head	Dh (mm)	Time (s)	N° burette	Diameter B	Height S	Date	k (mm/s)	K (cm/s)
Core 4 - 5	2000	1000	1000	55	2	15.75	45	23 Jul	0.095904	0.00959
	2000	1000	1000	54	2	15.75	45	24 Jul	0.09768	0.009768
	2000	1000	1000	52	2	15.75	45	24 Jul	0.101437	0.010144
Core 5 - 2	2000	1000	1000	29	2	15.75	30	24 Jul	0.121259	0.012126
	2000	1000	1000	26	2	15.75	30	24 Jul	0.13525	0.013525
	2000	1000	1000	25	2	15.75	30	24 Jul	0.14066	0.014066
	800	200	600	63	1	31.46	30	28 Jul	0.445406	0.044541
	800	200	600	60	1	31.46	30	28 Jul	0.467676	0.046768
	800	200	600	57	1	31.46	30	28 Jul	0.492291	0.049229
Core 5 - 3	800	200	600	141	1	31.46	23	28 Jul	0.152575	0.015258
	800	200	600	95	1	31.46	23	28 Jul	0.226454	0.022645
	800	200	600	113	1	31.46	23	28 Jul	0.190381	0.019038
Core 4 - 3	2000	1000	1000	79	2	15.75	30	28 Jul	0.044513	0.004451
	2000	1000	1000	69	2	15.75	30	28 Jul	0.050964	0.005096
	2000	1000	1000	61	2	15.75	30	28 Jul	0.057647	0.005765
Core 4 - 8	800	200	600	53	1	31.46	47	28 Jul	0.829464	0.082946
	800	200	600	60	1	31.46	47	28 Jul	0.732693	0.073269
	800	200	600	56	1	31.46	47	28 Jul	0.785028	0.078503
Core 4 - 4	2000	1000	1000	47	2	15.75	40	28 Jul	0.099759	0.009976
	2000	1000	1000	46	2	15.75	40	28 Jul	0.101927	0.010193
	2000	1000	1000	44	2	15.75	40	28 Jul	0.106561	0.010656
Core 4 - 2	2000	1000	1000	161	4	3.74	47	28 Jul	0.001929	0.000193
	2000	1000	1000	174	4	3.74	47	28 Jul	0.001785	0.000179
	2000	1000	1000	184	4	3.74	47	28 Jul	0.001688	0.000169

## **Appendix E: Survey Data**

			Distance m	Elevation		
1216	4770300.263	519945.9328	0	303.07466	Grnd TST4 West end of Transect	West end of topographic survey transect through Ehsan's station 4 (TST4). Ground elevation
1217	4770303.139	519947.1594	3.1	302.49854	Grnd TST4	Ground
1218	4770305.945	519948.4123	6.2	301.93667	Grnd TST4	Ground
1219	4770308.844	519949.8446	9.4	301.45069	Grnd TST4	Ground
1220	4770311.777	519951.4395	12.8	300.9507	Grnd TST4	Ground
1221	4770314.837	519953.03	16.2	300.51471	Grnd TST4	Ground
1222	4770317.601	519954.5332	19.4	300.23372	Grnd TST4	Ground
1223	4770320.221	519955.931	22.3	300.07473	Grnd TST4	Ground
1224	4770322.79	519957.1919	25.2	299.96274	Grnd TST4	Ground
1225	4770324.2	519957.8864	26.8	299.84675	Grnd TST4	Ground
1226	4770325.695	519958.8628	28.6	299.78676	Grnd TST4	Ground
1227	4770326.684	519959.6495	29.8	299.80976	Grnd TST4 at station 4	Ground at Ehsan station 4
1228	4770327.777	519960.6231	31.3	299.78877	Grnd TST4 at station 4	Ground at soil temperature probes at Ehsan Station 4
1229	4770329.691	519961.544	33.4	299.81678	Grnd TST4	Ground
1230	4770331.311	519962.9257	35.5	299.86679	Grnd TST4	Ground
1231	4770333.149	519964.049	37.7	299.9238	Grnd TST4	Ground
1232	4770334.886	519964.9949	39.7	299.97381	Grnd TST4	Ground
1233	4770336.747	519966.2213	41.9	300.00182	Grnd TST4	Ground
1234	4770338.828	519967.0753	44.1	300.02583	Grnd TST4	Ground
1235	4770341.195	519968.7736	47.1	300.05884	Grnd TST4	Ground
1236	4770343.776	519970.3804	50.1	300.19986	Grnd TST4	Ground
1237	4770346.22	519971.7936	52.9	300.25387	Grnd TST4	Ground
1238	4770348.885	519973.7041	56.2	300.34788	Grnd TST4	Ground
1239	4770351.501	519975.1358	59.2	300.5189	Grnd TST4	Ground
1240	4770354.034	519976.8987	62.3	300.66591	Grnd TST4	Ground
1241	4770356.932	519978.6931	65.7	300.85893	Grnd TST4	Ground
1242	4770359.917	519980.3286	69.1	300.97194	Grnd TST4	Ground
1243	4770362.651	519981.8712	72.2	301.09795	Grnd TST4	Ground
1244	4770364.899	519983.4554	75.0	301.20659	Grnd TST4 East end of Transect	East end of topographic survey transect through Ehsan's station 4 (TST4). Ground elevation
1280	4770295.861	519963.5573	0	302.92861	Grnd TST5 West end of Transect	West end of topographic survey transect through Ehsan's station 5 (TST5). Ground elevation
1281	4770298.517	519964.6848	2.9	302.35587	Grnd TST5	Ground
1282	4770301.433	519966.0003	6.1	301.79488	Grnd TST5	Ground
1283	4770304.377	519967.3022	9.3	301.22889	Grnd TST5	Ground
1284	4770306.946	519968.6228	12.2	300.8689	Grnd TST5	Ground
1285	4770309.786	519969.9318	15.3	300.48591	Grnd TST5	Ground
1286	4770312.584	519971.2314	18.4	300.09392	Grnd TST5	Ground
1287	4770315.088	519972.4423	21.2	299.82893	Grnd TST5	Ground
1288	4770317.214	519973.5037	23.6	299.79794	Grnd TST5	Ground
1289	4770319.014	519974.326	25.5	299.71495	Grnd TST5	Ground
1290	4770320.924	519975.4057	27.7	299.69695	Grnd TST5	Ground
1291	4770322.392	519976.3917	29.5	299.73396	Grnd TST5 near P-5	Ground near P-5
1292	4770324.197	519977.5517	31.6	299.77397	Grnd TST5	Ground
1293	4770325.88	519978.6714	33.7	299.83998	Grnd TST5	Ground
1294	4770327.613	519979.9741	35.8	299.85099	Grnd TST5	Ground
1295	4770329.493	519981.1421	38.1	299.852	Grnd TST5 near BML-5	Ground near BML-5
1296	4770331.389	519982.5175	40.4	299.87402	Grnd TST5	Ground
1297	4770333.136	519983.8256	42.6	299.88003	Grnd TST5	Ground
1298	4770335.024	519984.9569	44.8	299.88004	Grnd TST5	Ground
1299	4770337.142	519986.1106	47.2	299.88905	Grnd TST5	Ground
1300	4770339.142	519986.916	49.3	300.03205	Grnd TST5	Ground
1301	4770340.996	519987.8751	51.4	300.14206	Grnd TST5	Ground
1302	4770343.939	519989.257	54.7	300.32707	Grnd TST5	Ground

1307	4770359.879	519997.0406	72.5	301.33513	Grnd TST5	Ground
1308	4770363.021	519998.7556	76.1	301.56714	Grnd TST5	Ground
1309	4770366.09	520000.4882	79.6	301.84103	Grnd TST5 East end of Transect	East end of topographic survey transect through Ehsan's station 5 (TST5). Ground elevation
1310	4770291.867	519985.6328	0	300.91162	Grnd TST3 West end of Transect	West end of topographic survey transect through Ehsan's station 3 (TST3). Ground elevation
1311	4770294.411	519987.1433	3.0	300.70613	Grnd TST3	Ground
1312	4770297.185	519988.7794	6.2	300.36015	Grnd TST3	Ground
1313	4770299.884	519990.3723	9.3	300.13216	Grnd TST3	Ground
1314	4770302.817	519992.073	12.7	299.83918	Grnd TST3	Ground
1315	4770305.617	519993.8284	16.0	299.68119	Grnd TST3	Ground
1316	4770308.636	519995.7039	19.6	299.57721	Grnd TST3	Ground
1317	4770311.492	519997.649	23.0	299.59622	Grnd TST3	Ground
1318	4770314.23	519999.2703	26.2	299.67024	Grnd TST3	Ground
1319	4770317.019	520000.9755	29.5	299.64625	Grnd TST3	Ground
1320	4770318.838	520001.9849	31.5	299.61126	Grnd TST3	Ground
1321	4770320.444	520003.0573	33.5	299.65327	Grnd TST3	Ground
1322	4770322.081	520004.2287	35.5	299.64628	Grnd TST3 near BML3 and NAT-3	Ground near BML3 and NAT-3
1323	4770324.038	520005.4616	37.8	299.67229	Grnd TST3	Ground
1324	4770326.188	520006.7142	40.3	299.7763	Grnd TST3	Ground
1325	4770328.02	520007.8809	42.5	299.89131	Grnd TST3	Ground
1326	4770330.11	520009.1758	44.9	299.96832	Grnd TST3	Ground
1327	4770332.431	520010.3804	47.5	300.11133	Grnd TST3	Ground
1328	4770335.129	520012.2419	50.8	300.30335	Grnd TST3	Ground
1329	4770338.275	520014.0058	54.4	300.54336	Grnd TST3	Ground
1330	4770340.864	520015.7061	57.5	300.76337	Grnd TST3	Ground
1331	4770343.89	520017.4432	61.0	301.03439	Grnd TST3	Ground
1332	4770346.844	520019.3229	64.5	301.2654	Grnd TST3	Ground
1333	4770349.756	520020.8419	67.8	301.43842	Grnd TST3	Ground
1334	4770353.067	520022.6175	71.6	301.65543	Grnd TST3	Ground
1335	4770356.803	520024.8978	75.9	301.91445	Grnd TST3	Ground
1336	4770360.031	520026.7415	79.6	302.18946	Grnd TST3	Ground
1338	4770362.878	520028.6256	83.1	302.3191	Grnd TST3 East end of Transect	East end of topographic survey transect through Ehsan's station 3 (TST3). Ground elevation
1339	4770257.245	520016.6294		299.86054	Grnd at fence west end	Ground topo survey along southern fence. Start at west end - corner post of fence
1340	4770259.048	520018.936		299.65756	Grnd	
1341	4770260.841	520022.0591		299.50559	Grnd	
1342	4770262.836	520024.6335		299.48562	Grnd	
1343	4770264.526	520027.1573		299.54764	Grnd	
1344	4770266.608	520030.1778		299.36367	Grnd	
1345	4770268.277	520032.6351		299.2877	Grnd	
1346	4770270.33	520035.6883		299.30573	Grnd	
1347	4770272.525	520038.8075		299.31276	Grnd	
1348	4770274.593	520041.6869		299.23579	Grnd	Underneath a small tree. GPS slow to fix
1349	4770276.296	520044.4223		299.19082	Grnd	
1350	4770278.231	520047.1719		299.26484	Grnd	
1351	4770280.134	520049.8158		299.26487	Grnd	
1352	4770282.153	520052.793		299.2769	Grnd	
1353	4770284.04	520055.6404		299.52093	Grnd	
1354	4770286.034	520058.5201		299.51696	Grnd	GPS slow to fix
1355	4770287.83	520061.167		299.59898	Grnd	
1356	4770289.788	520064.0494		299.69001	Grnd	

1361	4770298.588	520076.4013		300.41914	Grnd	road opening in fence
1362	4770300.641	520079.2305		300.61016	Grnd	
1363	4770302.528	520082.1987		300.71119	Grnd	
1364	4770304.2	520084.675		300.81922	Grnd	Under a small tree
1365	4770305.872	520086.9817		300.98724	Grnd	
1366	4770307.647	520089.5595		301.07327	Grnd	
1367	4770309.614	520092.3253		301.2023	Grnd	
1369	4770311.361	520094.7471		301.62532	Grnd	Redo of last survey point (deleted). GPS going in and out of fix
1371	4770315.88	520100.6543		301.68425	Grnd at fence east end	Redo of last survey point (deleted). East end at fence corner post
1372	4770310.042	519937.7863		301.17305	Grnd west end	Ground at west end of topographic transect up (north) of station 4
1373	4770315.336	519938.639		300.53455	Grnd	
1374	4770320.361	519939.8955		300.16655	Grnd	
1375	4770325.436	519941.2346		300.12656	Grnd	
1376	4770332.144	519942.0398		299.95555	Grnd	
1377	4770334.56	519942.4248		299.92955	Grnd	
1378	4770339.494	519944.0206		300.13556	Grnd	
1379	4770343.646	519947.3308		300.36659	Grnd	
1380	4770347.928	519950.779		300.48363	Grnd	
1381	4770352.575	519954.0457		300.67065	Grnd	
1382	4770357.729	519956.893		300.89668	Grnd	
1383	4770362.231	519959.0748		301.01169	Grnd	
1384	4770367.831	519961.4339		301.24771	Grnd	
1385	4770372.982	519963.1159		301.56872	Grnd east end	Ground at east end of transect
1386	4770308.091	519915.128		301.13879	Grnd west end	Ground at west end of transect
1387	4770313.448	519917.2875		300.71231	Grnd	
1388	4770318.17	519920.5337		300.48134	Grnd	
1389	4770323.178	519923.376		300.27636	Grnd	
1390	4770328.668	519925.6147		300.23437	Grnd	
1391	4770334.484	519927.1442		300.21738	Grnd	
1392	4770338.568	519928.744		300.04739	Grnd	
1393	4770341.193	519929.5598		300.0344	Grnd	
1394	4770343.749	519930.2035		300.1644	Grnd	
1395	4770349.81	519932.336		300.40241	Grnd	
1396	4770354.879	519935.4468		300.51544	Grnd	
1397	4770359.182	519937.8802		300.66846	Grnd	
1398	4770364.46	519940.8357		300.95248	Grnd	
1399	4770369.851	519943.2198		301.2425	Grnd	
1400	4770375.497	519945.3602		301.49251	Grnd east end	Ground at east end of transect
1401	4770304.368	519894.1922		301.34481	Grnd west end	Ground at west end of transect
1402	4770309.939	519896.733		301.11508	Grnd	
1403	4770315.66	519899.3902		300.8381	Grnd	
1404	4770321.221	519901.5879		300.62911	Grnd	
1405	4770326.718	519904.22		300.42813	Grnd	
1406	4770332.004	519906.8364		300.32015	Grnd	
1407	4770337.671	519909.9522		300.23018	Grnd	
1408	4770343.161	519912.374		300.2632	Grnd	
1409	4770348.623	519915.0727		300.36822	Grnd	
1410	4770354.235	519917.5592		300.44524	Grnd	
1411	4770359.195	519920.6839		300.61426	Grnd	
1412	4770364.131	519923.7205		300.82329	Grnd	
1413	4770369.362	519926.6002		301.07431	Grnd	
1414	4770374.258	519929.1241		301.42233	Grnd	
1415	4770379.985	519931.5621		301.7601	Grnd east end	Ground at east end of transect
1416	4770305.066	519872.5277		301.80669	Grnd west end	Ground at west end of transect

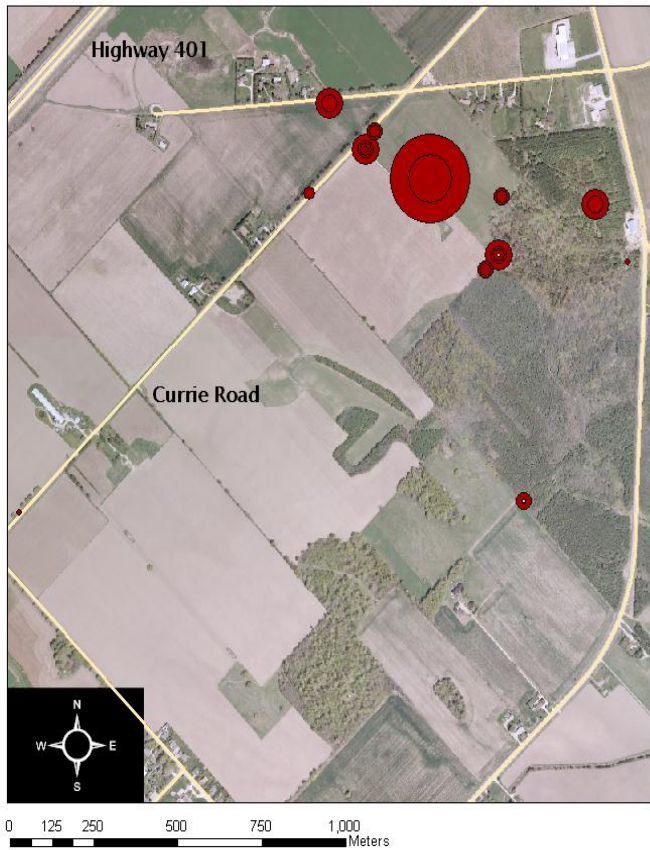
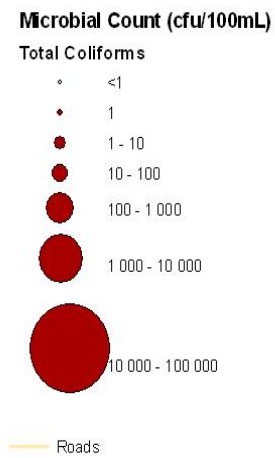
1421	4770332.763	519885.8055		300.56891	Grnd	
1422	4770338.416	519888.627		300.42494	Grnd	
1423	4770343.966	519891.3919		300.39096	Grnd	
1424	4770349.846	519894.1449		300.38598	Grnd	
1425	4770355.325	519896.6129		300.505	Grnd	
1426	4770361.028	519897.9976		300.78	Grnd	
1427	4770366.092	519901.3907		301.10603	Grnd	
1428	4770370.966	519905.4408		301.44307	Grnd	
1429	4770375.721	519909.3597		301.8321	Grnd	
1430	4770381.032	519912.0671		302.21225	Grnd east end	Ground at east end of transect
1431	4770308.236	519854.5315		301.81035	Grnd west end	Ground at west end of transect
1432	4770313.804	519856.9026		301.52762	Grnd	
1433	4770319.682	519859.3613		301.22263	Grnd	
1434	4770325.853	519862.218		301.03466	Grnd	
1435	4770331.764	519865.1609		300.89268	Grnd	
1436	4770337.544	519868.6401		300.72071	Grnd	
1437	4770342.81	519871.536		300.57773	Grnd	
1438	4770347.744	519874.6432		300.56076	Grnd	
1439	4770353.488	519877.2162		300.66378	Grnd	
1440	4770358.58	519879.4221		300.91379	Grnd	
1441	4770363.353	519882.3507		301.21982	Grnd	
1442	4770368.834	519885.2785		301.75284	Grnd	
1443	4770373.904	519887.8223		302.50786	Grnd	
1444	4770379.086	519891.4944		303.1009	Grnd	
1445	4770385.198	519893.7084		303.85453	Grnd east end	Ground at east end of transect
1446	4770316.173	519826.7952		302.11177	Grnd west end	Ground at west end of transect through Jacqueline Brook site
1447	4770322.552	519829.9039		301.73229	Grnd	
1448	4770328.81	519833.1103		301.45932	Grnd	
1449	4770335.568	519836.702		301.20735	Grnd	
1450	4770341.815	519839.9098		301.01337	Grnd	
1451	4770347.555	519842.7474		300.9944	Grnd	
1452	4770352.289	519845.6775		301.00442	Grnd	
1453	4770355.285	519847.4133		300.99243	Grnd	
1454	4770358.93	519849.325		300.78145	Grnd between OW wells	Ground between two monitoring well casings
1455	4770361.598	519851.1812		300.74747	Grnd	
1456	4770365.619	519853.9289		301.15049	Grnd	
1457	4770370.141	519856.5177		301.57351	Grnd	Next to a 1-inch ID PVC pipe
1458	4770374.873	519859.6417		302.32854	Grnd	
1459	4770379.381	519862.4015		303.08956	Grnd	
1460	4770384.123	519865.1443		303.84959	Grnd	
1461	4770388.68	519867.638		304.49361	Grnd east end	Ground at east end of transect through Jacqueline Brook site
1462	4770280.714	519997.6413		300.58453	Grnd west end	Ground at west end of transect south of station 3 and north of fence
1463	4770284.769	520002.0861		299.92432	Grnd	
1464	4770289.591	520007.1592		299.52637	Grnd	
1465	4770293.456	520011.7265		299.56142	Grnd	
1466	4770297.723	520015.6753		299.52545	Grnd	
1467	4770302.686	520019.8391		299.49149	Grnd	
1468	4770306.995	520024.3398		299.52853	Grnd	
1469	4770310.757	520028.6754		299.66158	Grnd	
1470	4770314.727	520032.8543		299.91962	Grnd	
1471	4770318.81	520036.6544		300.22265	Grnd	
1472	4770323.327	520040.7828		300.64769	Grnd	
1473	4770327.72	520045.0649		300.93773	Grnd	
1474	4770332.456	520049.6811		301.16977	Grnd	

## **Appendix F: Geochemistry Data (Christie, 2009)**

Date	Aerobic Endospores	Total Coliforms	E. Coli
01-Apr	>17000	>30000	49
02-Apr	22300	>30000	60
07-Apr	11400	>30000	31

### Microbial Response During Spring Melt

Thornton Well Field Shallow Aquifer





## **Appendix G: Temperature Thermister Casing Design (Brook, 2012)**

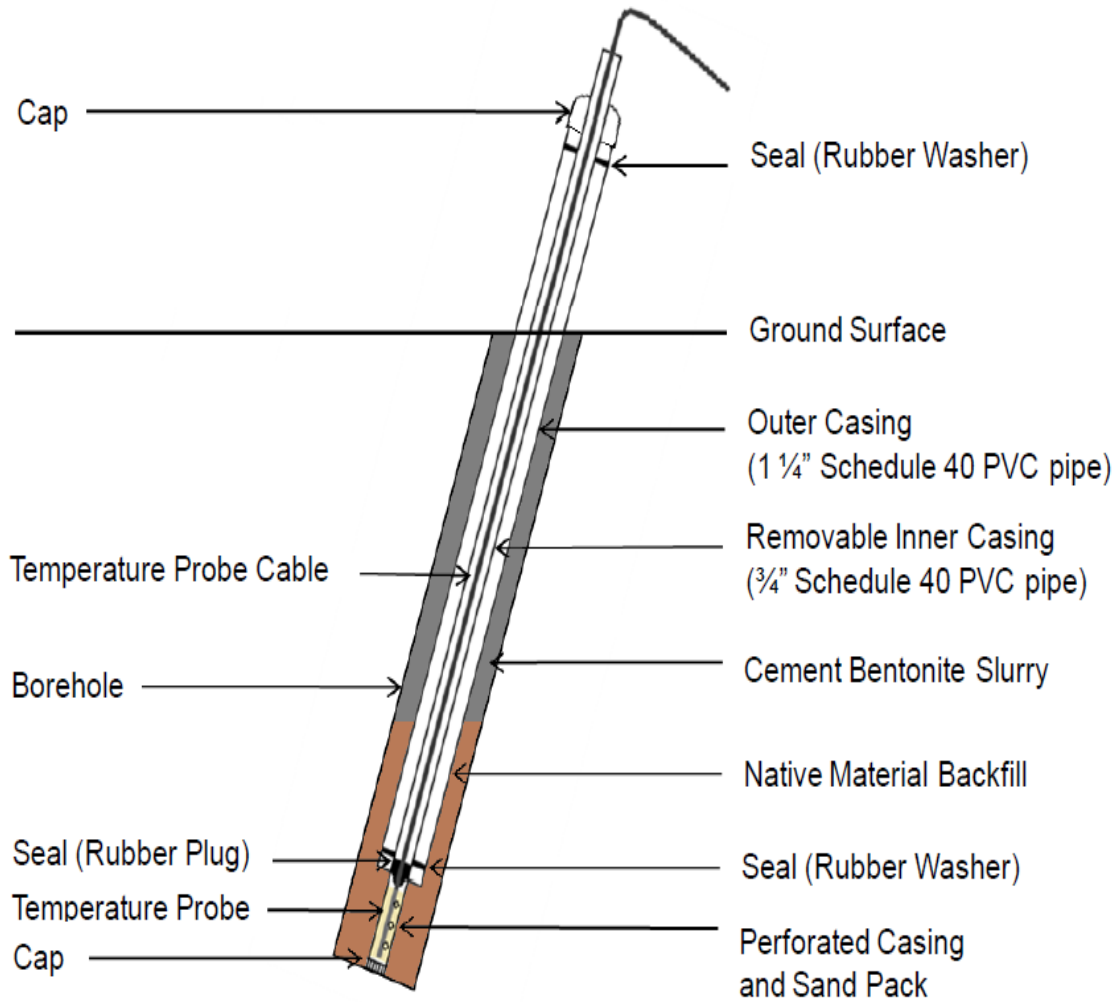


Figure 4.3.3 Schematic of a temperature probe installation showing the protective casing and borehole construction.

## **Appendix H: Monitoring Well Details**

Well	Name		Casing	Ground	Top of	Bottom of	Aquifer
	Northing	Easting	Elevation	Elevation	Screen	Screen	Screen
	(m)	(m)	(masl)	(masl)	(mbgs)	(mbgs)	
WO35*	4770190	519977.8	303	302.52	5.18	6.7	2
WO36*	4770309	520061.9	300.9	300.39	3.35	4.88	2
WO37*	4770359	519848.9	301.22	300.72	3.35	4.88	2
WO40*	4770560	519548.2	305.1	304.19	6.4	7.92	2
WO75S*	4770114	520015.1	303.62	302.68	8.84	10.36	2
WO11-18*	4770437	519657.1	303.18	303.1	17.288	18.05	3
WO63*	4770359	519849.9	301.38	300.71	10.67	13.72	3
WO67*	4770318	519488.2	313.23	312.46	15.24	18.29	3
WO72S*	4770580	519792.7	310.04	309.09	13.41	16.4	3
WO72D*	4770580	519790.6	310.01	309.06	17.87	20.67	3

**Appendix I: Water flow equations (HYDRUS 1D Manual Chapter 7, Simunek et. al, 2013)**

## Space and Time Discretization

The soil profile is first discretized into  $N-1$  adjoining elements, with the ends of the elements located at the nodal points, and  $N$  being the number of nodes. The same spatial discretization is used for water flow, solute transport and heat movement. HYDRUS assumes that the vertical coordinate  $x$  is directed positive upward.

A mass-lumped linear finite elements scheme was used for discretization of the mixed form of the Richards' equation (2.1) (the numerical solution for equation (2.3) is in principle similar to the solution to equation (2.1)). Since the mass-lumped scheme results in an equivalent and somewhat standard finite difference scheme [e.g., *Vogel et al.*, 1996], we omit the detailed finite element development and give immediately the invoked final finite difference scheme:

$$\frac{\theta_i^{j+1,k+1} - \theta_i^j}{\Delta t} = \frac{1}{\Delta x} \left( K_{i+1/2}^{j+1,k} \frac{h_{i+1}^{j+1,k+1} - h_i^{j+1,k+1}}{\Delta x_i} - K_{i-1/2}^{j+1,k} \frac{h_i^{j+1,k+1} - h_{i-1}^{j+1,k+1}}{\Delta x_{i-1}} \right) + \frac{K_{i+1/2}^{j+1,k} - K_{i-1/2}^{j+1,k}}{\Delta x} \cos \alpha - S_i^j \quad (7.1)$$

where

$$\begin{aligned} \Delta t &= t^{j+1} - t^j \\ \Delta x &= \frac{x_{i+1} - x_{i-1}}{2} \quad \Delta x_i = x_{i+1} - x_i \quad \Delta x_{i-1} = x_i - x_{i-1} \\ K_{i+1/2}^{j+1,k} &= \frac{K_{i+1}^{j+1,k} + K_i^{j+1,k}}{2} \quad K_{i-1/2}^{j+1,k} = \frac{K_i^{j+1,k} + K_{i-1}^{j+1,k}}{2} \end{aligned} \quad (7.2)$$

in which subscripts  $i-1$ ,  $i$ , and  $i+1$  indicate the position in the finite difference mesh; superscripts  $k$  and  $k+1$  denote the previous and current iteration levels, respectively; and superscripts  $j$  and  $j+1$  represent the previous and current time levels, respectively. Equation (7.1) is based on a fully implicit discretization of the time derivative, and will be solved with a Picard iterative solution scheme. Notice also that the sink term,  $S$ , is evaluated at the previous time level. The mass-conservative method proposed by *Celia et al.* [1990], in which  $r_{j+1,k+1}$  is expanded in a truncated Taylor series with respect to  $h$  about the expansion point  $J_{i+1,k}$ , is used in the time difference scheme of (7.1):

$$\frac{\theta_i^{j+1,k+1} - \theta_i^j}{\Delta t} = C_i^{j+1,k} \frac{h_i^{j+1,k+1} - h_i^{j+1,k}}{\Delta t} + \frac{\theta_i^{j+1,k} - \theta_i^j}{\Delta t} \quad (7.3)$$

where  $C_i$  represents the nodal value of the soil water capacity [ $L^{-1}$ ]:

$$C_i^{j+1,k} = \left. \frac{d\theta}{dh} \right|^{j+1,k} \quad (7.4)$$

This method has been shown to provide excellent results in terms of minimizing the mass balance error. Notice that the second term on the right hand side of (7.3) is known prior to the current iteration. The first term on the right hand side of (7.3) should vanish at the end of the iteration process if the numerical solution converges. The derivation leads to the following matrix equation with matrix  $[P_w]$  and vectors  $\{h\}$  and  $\{F_w\}$

$$[P_w]^{j+1,k} \{h\}^{j+1,k+1} = \{F_w\} \quad (7.5)$$

The symmetrical tridiagonal matrix  $[P_w]$  in (7.5) has the form

$$[P_w] = \begin{pmatrix} d_1 & e_1 & 0 & & & 0 \\ e_1 & d_2 & e_2 & 0 & & 0 \\ 0 & e_2 & d_3 & e_3 & 0 & 0 \\ & & \cdot & \cdot & \cdot & \\ & & \cdot & \cdot & \cdot & \\ 0 & & 0 & e_{N-3} & d_{N-2} & e_{N-2} & 0 \\ 0 & & & 0 & e_{N-2} & d_{N-1} & e_{N-1} \\ 0 & & & & 0 & e_{N-1} & d_N \end{pmatrix} \quad (7.6)$$

where the diagonal entries  $d$ ; and above-diagonal entries  $e$ ; of the matrix  $[P_w]$ , and the entries/; of vector  $\{F_w\}$ , are given by

$$d_i = \frac{\Delta x}{\Delta t} C_i^{j+1,k} + \frac{K_{i+1}^{j+1,k} + K_i^{j+1,k}}{2\Delta x_i} + \frac{K_i^{j+1,k} + K_{i-1}^{j+1,k}}{2\Delta x_{i-1}} \quad (7.7)$$

$$e_i = -\frac{K_i^{j+1,k} + K_{i+1}^{j+1,k}}{2\Delta x_i} \quad (7.8)$$

$$f_i = \frac{\Delta x}{\Delta t} C_i^{j+1,k} h_i^{j+1,k} - \frac{\Delta x}{\Delta t} (\theta_i^{j+1,k} - \theta_i^j) + \frac{K_{i+1}^{j+1,k} - K_{i-1}^{j+1,k}}{2} \cos \alpha - S_i^j \Delta x \quad (7.9)$$

The tridiagonal matrix [Pw] is symmetric and therefore the below-diagonal entries are equal to the above-diagonal entries. The entries  $dI$ ,  $e_i$ ,  $J_i$ , and  $eN-h$   $dN$ ,  $fN$  are dependent upon the prescribed boundary conditions.

### Treatment of Pressure Head Boundary Condition

If a first-type (Dirichlet) boundary condition is specified at the top or bottom of the soil profile, then the terms  $dI$  or  $dN$  are equal to unity,  $eI$  or  $eN-I$  reduce to zero, and  $J_i$  or  $fN$  equal to the prescribed pressure head,  $h_0$ . Some additional rearrangement of matrix [Pw] is also necessary to preserve its symmetry. The appropriate entries in the second or (N-1)st equations containing the prescribe boundary pressure head  $h_0$  in the left-hand side matrix must then be incorporated into the known vector on the right-hand side of the global matrix equation. When done properly, this rearrangement will restore symmetry in [Pw].

### Treatment of Flux Boundary Condition

If a third-type (Neumann) boundary condition at the bottom of the profile is specified, then the individual entries are obtained by discretization of Darcy's law, i.e.,

$$q = -K \frac{\partial h}{\partial x} - K \quad (7.10)$$

such that  $dI$  and  $J_i$  in [Pw] attain the values



$$d_1 = \frac{K_1^{j+1,k} + K_2^{j+1,k}}{2\Delta x_1} \quad (7.11)$$

$$f_1 = \frac{K_1^{j+1,k} + K_2^{j+1,k}}{2} + q_0^{j+1} \quad (7.12)$$

where  $q_0$  is the prescribed bottom boundary flux and where  $e_1$  is described by (7.8). A similar discretization of Darcy's law is possible to incorporate flux boundary condition at the top of the soil profile. This approach, however, can quickly lead to relatively unstable solutions when the boundary fluxes at the soil surface vary strongly with time (erratic irrigation of rainfall rates). A more stable and mass conservative solution results when the mass balance equation instead of Darcy's law is discretized.

$$\frac{\partial \theta}{\partial t} = -\frac{\partial q}{\partial x} - S \quad (7.13)$$

Discretization of (7.12) gives

$$\frac{\theta_N^{j+1,k+1} - \theta_N^j}{\Delta t} = -\frac{2(q_N^{j+1} - q_{N-1/2}^{j+1,k})}{\Delta x_{N-1}} - S_N^j \quad (7.14)$$

Expanding the time derivative on the left hand side of (7.14) as in (7.3), and using the discretized form of Darcy's law for  $q_{N-1/2}$  leads to

$$d_N = \frac{\Delta x_{N-1}}{2\Delta t} C_N^{j+1,k} + \frac{K_N^{j+1,k} + K_{N-1}^{j+1,k}}{2\Delta x_{N-1}} \quad (7.15)$$

$$f_N = \frac{\Delta x_{N-1}}{2\Delta t} C_N^{j+1,k} h_N^{j+1,k} - \frac{\Delta x}{2\Delta t} (\theta_N^{j+1,k} - \theta_N^j) - \frac{K_N^{j+1,k} + K_{N-1}^{j+1,k}}{2} \cos \alpha - \frac{\Delta x_{N-1}}{2} S_N^j - q_N^{j+1} \quad (7.16)$$

where  $q_N$  is the prescribed soil surface boundary flux. Implementation of a third-type boundary condition always preserves symmetry of the matrix [Pw].

## Numerical Solution Strategy

### *Iterative Process*

Because of the nonlinear nature of (7.5), an iterative process must be used to obtain solutions of the global matrix equation at each new time step. For each iteration a system of linearized algebraic equations is first derived from (7.5), which, after incorporation of the boundary conditions, is solved using Gaussian elimination. The Gaussian elimination process takes advantage of the tridiagonal and symmetric features of the coefficient matrix in (7.5). After solving (7.5) the first time, the coefficients in (7.5) are re-evaluated using this first solution, and the new equations are again solved. The iterative process continues until a satisfactory degree of convergence is obtained, i.e., until at all nodes in the saturated (or unsaturated) region the absolute change in pressure head (or water content) between two successive iterations becomes less than some small value determined by the imposed absolute pressure head (or water content) tolerance. The first estimate (at zero iteration) of the unknown pressure heads at each time step is obtained by extrapolation from the pressure head values at the previous two time levels.

### *Time Control*

Three different time discretizations are introduced in HYDRUS: (1) time discretizations associated with the numerical solution, (2) time discretizations associated with the implementation of boundary conditions, and (3) time discretizations which provide printed output of the simulation results (e.g., nodal values of dependent variables, water, solute mass balance components, and other information about the flow regime).

Discretizations 2 and 3 are mutually independent; they generally involve variable time steps as described in the input data file. Discretization 1 starts with a prescribed initial time increment, *Lit*. This time increment is automatically adjusted at each time level according to the following rules [Mis, 1982; Simunek et al., 1992]:

- a. Discretization 1 must coincide with time values resulting from time discretizations 2 and 3.
- b. Time increments cannot become less than a preselected minimum time step, *Ltmin*, nor exceed a maximum time step, *Ltmax* (i.e.,  $Ltmin \leq \Delta t \leq Ltmax$ ).

- c. If, during a particular time step, the number of iterations necessary to reach convergence is  $i \leq 5$ , the time increment for the next time step is increased by multiplying  $\Delta t$  by a predetermined constant  $>1$  (usually between 1.1 and 1.5). If the number of iterations is  $>7$ ,  $\Delta t$  for the next time level is multiplied by a constant  $<1$  (usually between 0.3 and 0.9).
- d. If, during a particular time step, the number of iterations at any time level becomes greater than a prescribed maximum (usually between 10 and 50), the iterative process for that time level is terminated. The time step is subsequently reset to  $\Delta t/3$ , and the iterative process restarted.

### **Atmospheric Boundary Conditions and Seepage Faces**

Atmospheric boundaries are simulated by applying either prescribed head or prescribed flux boundary conditions depending upon whether equation (2.72) or (2.72) is satisfied [Neuman, 1974]. If (2.72) is not satisfied, boundary node  $n$  becomes a prescribed head boundary. If, at any point in time during the computations, the calculated flux exceeds the specified potential flux in (2.72), the node will be assigned a flux equal to the potential value and treated again as a prescribed flux boundary.

If a seepage face is considered as the lower boundary condition and if during each iteration the lower part of the soil profile is saturated then the last node is treated as a prescribed pressure head boundary with  $h=0$ . However, if this node is unsaturated then a prescribed flux boundary with  $q=0$  is imposed at the lower boundary. Alternatively, a certain non-zero value of  $h_{seep}$  can also be specified as the limiting pressure head.

### **Water Balance Computations**

The HYDRUS code performs water balance computations at prescribed times for several preselected subregions of the flow domain. The water balance information for a subregion consists of the actual volume of water,  $V$ , in that subregion, and the rate,  $O$  [ $LT^{-1}$ ], of inflow or outflow to or from the subregion. These variables  $V$  and  $O$  are evaluated in Hydrus by means of

$$V = \sum_e \Delta x_i \frac{\theta_i + \theta_{i+1}}{2} \quad (7.17)$$

and

$$O = \frac{V_{new} - V_{old}}{\Delta t} \quad (7.18)$$

respectively, where  $\theta_i$  and  $\theta_{i+1}$  are water contents evaluated at the corner nodes of element  $e$ ,  $L_i$  is the size of the element, and  $V_{new}$  and  $V_{old}$  are volumes of water in the subregion computed at the current and previous time levels, respectively. The summation in (7.17) is taken over all elements within the subregion. Similar calculations are carried out for the mobile and immobile regions of the dual-porosity model and for the matrix and fracture regions of the dual-permeability model.

The absolute error in the mass balance of the flow domain is calculated as

$$\mathcal{E}_a^w = V_t - V_0 + \int_0^t T_a dt - \int_0^t (q_0 - q_N) dt \quad (7.19)$$

where  $V_t$  and  $V_0$  are the volumes of water in the flow domain, Eq. (7.17), evaluated at times  $t$  and zero, respectively. The third term on the right-hand side of (7.19) represents the cumulative root water uptake amount, while the fourth term gives the net cumulative flux through both boundaries.

The accuracy of the numerical solution is evaluated by the relative error,  $e_r^w$  [%], in the water mass balance as follows

$$e_r^w = \frac{|\mathcal{E}_a^w|}{\max \left( \sum_e |V_t^e - V_0^e|, \int_0^t T_a dt + \int_0^t (|q_N| + |q_0|) dt \right)} 100 \quad (7.20)$$

absolute changes in water content over all elements, whereas the second quantity is the sum of the absolute values of all fluxes in and out of the flow domain.

## Computation of Nodal Fluxes

Components of the Darcian flux are computed at each time level during the simulation only when the water flow and solute (or heat) transport equations are solved simultaneously. When the flow equation is being solved alone, the flux components are calculated only at selected print times. The x-components of the nodal fluxes are computed for each node  $n$  according to

$$\begin{aligned}
 q_1^{j+1} &= -K_{1+1/2}^{j+1} \left( \frac{h_2^{j+1} - h_1^{j+1}}{\Delta x_i} + 1 \right) \\
 q_i^{j+1} &= \frac{-K_{i+1/2}^{j+1} \left( \frac{h_{i+1}^{j+1} - h_i^{j+1}}{\Delta x_i} + 1 \right) \Delta x_{i-1} - K_{i-1/2}^{j+1} \left( \frac{h_i^{j+1} - h_{i-1}^{j+1}}{\Delta x_{i-1}} + 1 \right) \Delta x_i}{\Delta x_{i-1} + \Delta x_i} \\
 q_N^{j+1} &= -K_{N-1/2}^{j+1} \left( \frac{h_N^{j+1} - h_{N-1}^{j+1}}{\Delta x_{N-1}} + 1 \right) - \frac{\Delta x_{N-1}}{2} \left( \frac{\theta_N^{j+1} - \theta_N^j}{\Delta t} + S_N^j \right)
 \end{aligned} \tag{7.21}$$

## Evaluation of Soil Hydraulic Parameters

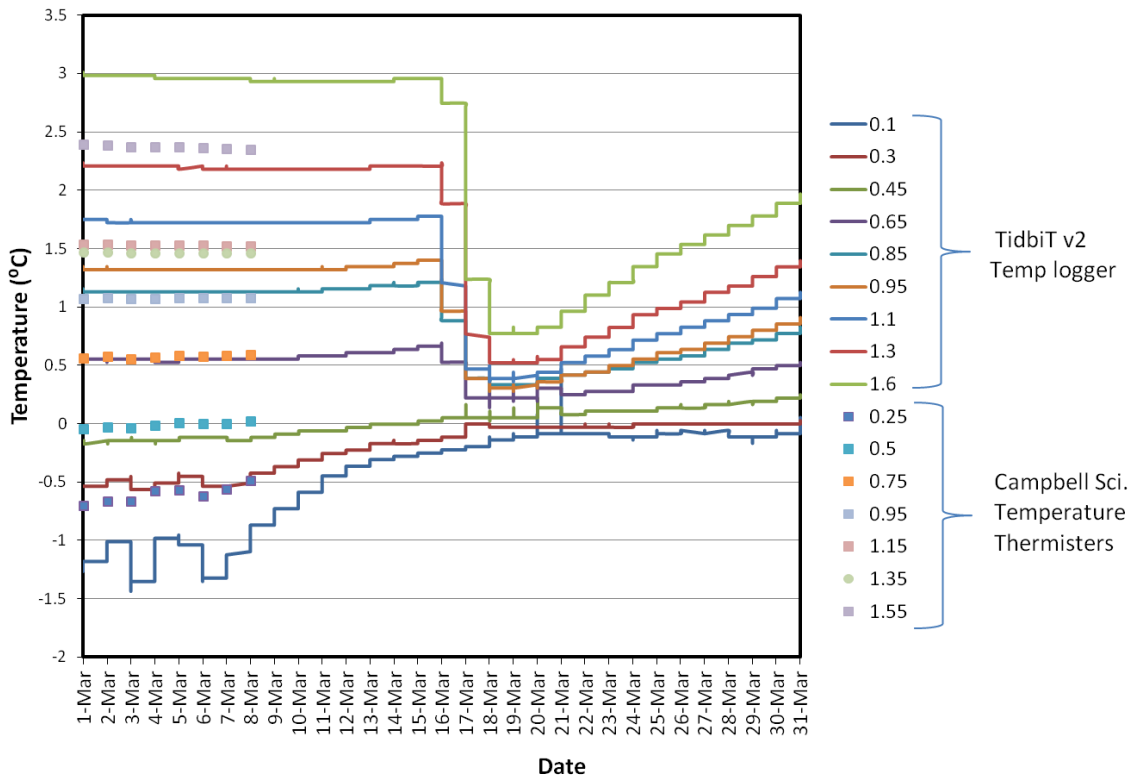
At the beginning of a simulation, HYDRUS generates for each soil type in the flow domain a table of water contents, hydraulic conductivities, and specific water capacities from the specified set of hydraulic parameters [Vogel, 1987]. The values of  $\theta$ ,  $K$ , and  $C$  in the table are evaluated at prescribed pressure heads  $h$ ; within a specified interval  $(h, hb)$ . The entries in the table are generated such that

$$\frac{h_{i+1}}{h_i} = \text{constant} \tag{7.23}$$

which means that the spacing between two consecutive pressure head values increases in a logarithmic fashion. Values for the hydraulic properties,  $\theta(h)$ ,  $K(h)$  and  $C(h)$ , are computed during the iterative solution process using linear interpolation between the entries in the table. If an argument  $h$  falls outside the prescribed interval  $(h, hb)$ , the hydraulic characteristics are evaluated directly from the hydraulic functions, i.e., without interpolation. The above interpolation technique was found to be much faster computationally

than direct evaluation of the hydraulic functions over the entire range of pressure heads, except when very simple hydraulic models are used.

## **Appendix J: Temperature instrumentation calibration**





## **Appendix K: Soil Moisture Content Data (Neutron Probe)**

Core 3						
	13-Mar-15	16-Mar-15	17-Mar-15	20-Mar-15	26-Mar-15	1-Apr-15
0.1	0.370	0.359	0.360	0.362	0.371	0.372
0.2	0.374	0.365	0.358	0.368	0.366	0.369
0.3	0.299	0.309	0.288	0.324	0.313	0.307
0.4	0.167	0.126	0.163	0.187	0.183	0.181
0.5	0.108	0.103	0.101	0.124	0.122	0.118
0.6	0.089	0.104	0.091	0.104	0.096	0.105
0.7	0.094	0.123	0.109	0.106	0.101	0.110
0.8	0.108	0.142	0.151	0.135	0.135	0.126
0.9	0.130	0.170	0.220	0.182	0.167	0.156
1	0.161	0.168	0.268	0.230	0.213	0.208
1.1	0.237	0.201	0.281	0.272	0.269	0.265
1.2	0.262	0.273	0.280	0.284	0.284	0.287

Core 4						
	13-Mar	16-Mar	17-Mar	20-Mar	26-Mar	01-Apr
	0.316	0.317	0.312	0.324	0.316	0.309
0.1	0.208	0.216	0.217	0.217	0.209	0.207
0.2	0.161	0.160	0.198	0.171	0.160	0.155
0.3	0.131	0.126	0.197	0.163	0.154	0.143
0.4	0.099	0.103	0.203	0.151	0.132	0.126
0.5	0.091	0.104	0.197	0.143	0.127	0.125
0.6	0.118	0.123	0.206	0.154	0.148	0.139
0.7	0.126	0.142	0.213	0.209	0.193	0.177
0.8	0.144	0.170	0.243	0.269	0.259	0.252
0.9	0.151	0.168	0.269	0.254	0.236	0.229
1	0.191	0.201	0.290	0.274	0.267	0.248
1.1	0.251	0.273	0.291	0.299	0.298	0.286
1.2	0.267	0.282	0.279	0.293	0.289	0.281
1.3	0.265	0.273	0.260	0.268	0.266	0.272
1.4	0.244	0.249	0.240	0.252	0.253	0.248
1.5	0.295	0.301	0.287	0.297	0.295	0.296
1.6	0.356	0.353	0.353	0.364	0.360	0.367

	Core 5					
	13-Mar-15	16-Mar-15	17-Mar-15	20-Mar-15	26-Mar-15	1-Apr-15
0.1	0.368	0.376	0.357	0.370	0.375	0.375
0.2	0.323	0.323	0.342	0.321	0.312	0.310
0.3	0.177	0.183	0.324	0.191	0.189	0.192
0.4	0.103	0.109	0.373	0.144	0.130	0.132
0.5	0.097	0.100	0.426	0.143	0.132	0.133
0.6	0.095	0.094	0.304	0.146	0.128	0.137
0.7	0.101	0.102	0.271	0.147	0.130	0.126
0.8	0.117	0.122	0.264	0.170	0.144	0.142
0.9	0.149	0.162	0.257	0.206	0.184	0.175
1	0.194	0.207	0.262	0.236	0.220	0.218
1.1	0.256	0.267	0.287	0.273	0.279	0.271
1.2	0.334	0.342	0.320	0.327	0.333	0.330

## **Appendix L: Hydrus 1D parameters**

Core 3: Hydraulic Parameters (L=m, t=min)					
$\theta_r$	$\theta_s$	$\alpha$	$\eta$	Ks	I [-]
0.078	0.43	3.6	1.56	4.86E-05	0.5
0.078	0.35	2	1.56	1.39E-06	0.5
0.078	0.33	7	2.7	0.003472	0.5
0.078	0.3	5	2.5	0.002083	0.5
0.078	0.35	5	3	0.003472	0.5
0.078	0.43	10	9	0.006944	0.5

Core 4: Hydraulic Parameters (L=m, t=min)					
$\theta_r$	$\theta_s$	$\alpha$	$\eta$	Ks	I [-]
0.1	0.35	0.9	1.3	0.00008	0.5
0.05	0.3	3.4	2.1	0.0033	0.5
0.04	0.3	2.2	4	0.0016	0.5
0.12	0.3	2.8	4.2	0.0035	0.5
0.12	0.35	5	3.5	0.004	0.5

Core 5: Hydraulic Parameters (L=m, t=min)					
$\theta_r$	$\theta_s$	$\alpha$	$\eta$	Ks	I [-]
0.08	0.33	0.9	1.3	6.94E-05	0.5
0.05	0.45	2.8	2.5	0.004	0.5
0.05	0.35	4	2.2	0.0008	0.5
0.05	0.35	3	2.3	0.003125	0.5
0.08	0.33	5	2.3	0.003819	0.5

## **Appendix M: Numerical Models Profile Discretization**

Core 3

Core 4

Core 5

